THE ROLE OF LKB1 AND PTEN IN THE DEVELOPMENT OF PAPILLARY SEROUS OVARIAN CANCER

By

Julienne Rose-Louters Brock

A DISSERTATION

Submitted to
Michigan State University
in partial fulfillment of the requirements
for the degree of

Physiology—Doctor of Philosophy

2021

ABSTRACT

THE ROLE OF LKB1 AND PTEN IN THE DEVELOPMENT OF PAPILLARY SEROUS OVARIAN CANCER

By

Julienne Rose-Louters Brock

Ovarian cancer is a devastating disease that affects 22,000 women yearly in the United States. Serous ovarian cancer, which constitutes about 70% of all epithelial ovarian cancer, is the deadliest. Understanding differentiation of ovarian cancer histotypes provides the possibility of subtype-specific treatment for this deadly disease. Tumor suppressor genes upstream of mTORC1, *STK11*, *PTEN*, and *TSC2*, are deleted in 88%, 40%, and 55% of high grade serous ovarian cancer, respectively. In deleting these genes alone and in combinations in the ovarian surface epithelium of mice, we found that papillary serous ovarian cancer histology only developed with deletion of *Stk11* and *Pten*. These tumors are positive for high grade serous ovarian cancer markers including PAX8 in most 15–20-week-old ovaries indicating that PAX8 1) is not an early driver of differentiation and 2) is acquired during transformation of ovarian surface epithelial cells. When isolated and cultured, these cells have higher growth rates *in vitro* than single mutants or controls. RNA sequencing of control, $Stk11^{cko}$, $Pten^{cko}$, and $Stk11^{cko}Pten^{cko}$ mouse ovarian surface epithelial cells reveals that $Stk11^{cko}Pten^{cko}$ cluster away from other groups and have over 3000 differentially expressed genes versus control. Interestingly, *Pten* transcripts are twice as abundant in $Stk11^{cko}$ versus control revealing a compensatory mechanism inhibiting uncontrolled growth. Gene set enrichment analysis of $Stk11^{cko}Pten^{cko}$ versus $Stk11^{cko}$ indicates many DNA repair pathways are dysregulated. Together, these results highlight the important roles that *Pten* and *Stk11* deletion play in papillary serous ovarian cancer and provide evidence to further investigate therapies that target these pathways.

To my family, friends, teachers and mentors

ACKNOWLEDGEMENTS

First, I would like to thank my mentor, Dr. Jose Teixeira for accepting me into his lab and for his mentorship and guidance throughout my graduate career. Sage advice, such as "perfect is the enemy of good" will stick with me well beyond my years here. I would also like to thank each one of my committee members whose kind encouragement, support, and discussions were invaluable to me. The cancer research network was a great way to stay updated on all of the impressive cancer research happening at MSU. Your collective mentorship has brought me a long way when I think back to that nerve-wracking first committee meeting when I literally read my presentation notes and Dr. Kathy Gallo called me out on it. I have gained so much confidence in my presentation skills since then and have truly found joy in teaching and explaining my research to many different audiences since then. Mentors and collaborators outside our lab were instrumental in my research and broadened my interests and knowledge within and outside of the ovarian cancer field.

I would also like to thank the members of the Teixeira lab. Post-docs in the lab like Amanda and Jitu were incredible sources to bounce ideas off of early in the process and their friendship both in and out of the lab were precious to me. The mouse work would not have been possible without the efforts of VAI and MSU vivarium staff and I'd like to especially thank Tyler. His genotyping and help caring for the mice made this research possible. He was always happy to help and was always happy to enjoy a beer with me and other lab mates.

Finally, I would like to thank the people I love, who supported me and encouraged me. To my friends and family, who brought me joy and made my life full. To my dad, thank you for instilling a fiery curiosity and love of science in me from the beginning. To my mom and in-

laws, thank you for your encouragement and all the time you put into taking care of Sydney so I could work on editing my dissertation. I could not have done it without you. Thank you to my dog, Callie, who basically became an emotional support animal during the stress and isolation of a global pandemic and graduate school. Thank you to Sydney Joann, born January 29, for literally (in the womb) kicking me along to the finish line of defending my dissertation and for adding immeasurable hope, joy, and love to our lives. Last, but certainly not least, thank you to my husband, for loving me through this, for picking up the slack when I needed it, and encouraging me every step of the way.

TABLE OF CONTENTS

LIST OF TABLES

LIST OF FIGURES

KEY TO ABBREVIATIONS

ADP	adenosine diphosphate
AKT	AKT Serine/Threonine kinase
AMP	adenosine monophosphate
AMPK	AMP-activated protein kinase
ARID1A	AT-rich interactive domain-containing protein 1A
ATM	ataxia telangiectasia mutated
ATP	adenosine triphosphate
BARD1	BRCA1-associated RING domain protein 1
BRCA1/2	breast cancer type 1/2 susceptibility protein
BRIP1	BRCA1 Interacting Protein C-Terminal Helicase 1
CCC	clear cell carcinoma
CA125	cancer antigen 125
CDKN2A	cyclin-dependent kinase inhibitor 2A
CHEK2	checkpoint kinase 2
CIC	cortical inclusion cyst
CIC	cortical inclusion cyst
CK7	cytokeratin 7
CK8	cytokeratin 8
CNA	copy number alteration
CPM	counts per million
DEPTOR	DEP domain-containing mTOR-interacting protein

DSB	double-strand breaks
EMT	epithelial to mesenchymal transition
EOC	epithelial ovarian cancer
ER	estrogen receptor
FACS	fluorescence activated cell sorting
FIGO	International Federation of Gynecology and Obstetrics
FTE	fallopian tube epithelium
FTSEC	fallopian tube secretory epithelial cells
GAP	GTPase-activating protein
GßL	G protein beta subunit-like
GEMM	genetically engineered mouse model
GSEA	gene set enrichment analysis
HGF	hepatocyte growth factor
HGEC	high grade endometrioid carcinoma
HGSOC	high-grade serous ovarian carcinoma
HOX	homeobox
HPV	human papilloma virus
HR	homologous recombination
IHC	immunohistochemistry
IP	intraperitoneal
KRT17	keratin 17
LGEC	low-grade endometrioid carcinoma
LGSOC	low-grade serous ovarian carcinoma

LMM	linear mixed-effects model
MACC1	MET transcriptional regulator
MAPK	mitogen activated protein kinase
MC	mucinous carcinoma
MIS	Mullerian inhibiting substance
MO25	mouse protein 25
MRE11A	meiotic recombination 11 homolog A
MSX2	msh Homeobox 2
mTOR	mechanistic target of rapamycin
mTORC1	mechanistic target of rapamycin complex 1
NHEJ	non-homologous end joining
NLS	nuclear localization signal
OSE	ovarian surface epithelium
OvCa	ovarian cancer
P53	tumor protein 53
PALB2	partner and localizer of BRCA2
PAP	Papanicolaou
PARP	poly (ADP ribose) polymerase
PAX8	paired box gene 8
PFU	plaque forming units
PI3K	phosphoinositide 3-kinase
PIP2	phosphatidylinositol-4,5-bisphosphate
PIP3	phosphatidylinositol-3,4,5-triphosphate

PLAC1	placental-specific protein 1
PR	progesterone receptor
PTEN	phosphatase and tensin homolog
Raptor	regulatory-associated protein of mTOR
RTCA	real time cell analysis
SC	subcutaneous
SP	signal peptide
SSB	single stranded breaks
STIC	serous tubal intraepithelial carcinoma
STOSE	spontaneously transformed ovarian surface epithelium
STRAD	STE20-related kinase adapter protein alpha
TCGA	the cancer genome atlas
tp53inp1	tumor protein 53 induced nuclear protein 1
TP53	tumor protein 53
TSC2	tuberous sclerosis complex 2
TSG	The Cancer Genome Atlas
WHO	World Health Organization
WT1	Wilms tumor 1

CHAPTER 1. INTRODUCTION

1.1 Background and significance

While ovarian cancer is the second most deadly gynecological cancer in the world behind cervical cancer, ovarian cancer has the highest case-fatality ratio of gynecologic cancers [1]. Worldwide, there are nearly 300,000 cases diagnosed and around 185,000 deaths annually, ranking it as the 7th most common cancer and 8th most fatal cancer for women overall [1]. In the US in 2019, there were 22,530 new cases diagnosed and 13,980 deaths due to ovarian cancer making it the 5th most deadly cancer for US women with a 5-year survival rate of 47.7% [2]. Taken together these statistics highlight the urgency of early detection and improved treatment, which requires a deeper understanding of the disease.

Ovarian cancer incorporates several different malignancies, usually involving the ovary, and all found within the female pelvis. As early as the 1930s, pathologists began to subdivide these based on morphologic/histological characteristics that later evolved into a more formal classification system by the world health organization (WHO) in 1973. The three types of ovarian cancer were germ cell, sex cord, and epithelial. Each type was further subdivided and epithelial ovarian cancer (EOC) could be categorized as serous, mucinous, endometrioid, clear cell, Brenner, mixed epithelial, undifferentiated, and unclassified tumors [3]. While these categories provided a framework for scientific studies, it did little to identify and distinguish cell of origin or inform treatment strategies for the patient.

About 90% of all ovarian cancer diagnoses are epithelial [4]. As we learn more about the etiology of EOC, studies have been able to redefine these subtypes to better reflect our

understanding of cell of origin, risk factors, molecular compositions, and clinical features and treatment. Current subtypes of EOC include high-grade serous ovarian carcinoma (HGSOC), low-grade serous ovarian carcinoma (LGSOC), high grade endometrioid carcinoma (HGEC), low-grade endometrioid carcinoma (LGEC), clear-cell carcinoma (CCC), and mucinous carcinoma (MC) [4]. Despite all being classified as ovarian cancers, EOC is not always thought to be derived from the ovary, and many are thought to be extraovarian in origin. HGSOC can originate from fallopian tube epithelium (FTE) or ovarian surface epithelium (OSE) [5, 6]. Some ovarian cancers may arise from the peritoneum, known as serous peritoneal papillary carcinoma, which upon further analysis may be distinct enough to be reclassified as its own subtype [7]. Endometrioid and clear cell carcinomas can arise from endometriosis [4]. The table below summarizes the current state of the subcategorization of EOCs [4].

Table 1.

Characteristics of ovarian cancer by histology, genomic characteristics, possible cell of origin, and treatment options. (Matulonis et al., Copyright © 2016, Nature Reviews Disease Primers. Used with permission.)

Histological subtype	Clinical findings	Genetic characteristics	Treatment options
High-grade serous carcinoma and high-grade endometrioid carcinoma	• Can present with peritoneal carcinomatosis, ascites and/or pelvic mass • Typically, advanced stage at presentation	• Deficiencies in homologous recombination (50% of tumors) • Associated with *BRCA* and *TP53* mutations	• Platinum-based chemotherapy and poly (ADP-ribose) polymerase inhibitors • Initially sensitive to chemotherapy, but most recur
Low-grade serous carcinoma	• Presents in younger patients (median reported age: 43-55 years) • Early or late stage at presentation	• Associated with *KRAS* and *BRAF* mutations • Tumors have genomic stability	• MEK inhibitors (currently being tested in clinical trials) and hormonal therapies
Low-grade endometrioid carcinoma	• Can be associated with endometriosis	• Associated with *PTEN*, *ARID1A*, and *PIK3CA* mutations • Can have microsatellite instability	• Possible hormonal therapies (not yet established)
Clear-cell carcinoma	• Can be present with parenchymal metastases (in the liver and lungs) • Can be associated with hypercoagulability and hypercalcemia	• Associated with *ARID1A* and *PIK3CA* mutations	• Immunotherapy agents • Can be resistant to platinum-based chemotherapy
Mucinous carcinoma	• Presents in younger patients and is typically early stage at presentation	• Associated with *KRAS* mutations	• Tends to be insensitive to chemotherapy but is still treated initially with cytotoxic chemotherapy

In 2004, Shih and Kurman introduced an alternative dualistic classification, broadly segregating EOCs into type 1 and type 2 [8]. Type 1 EOCs develop from pre-malignant or borderline tumors [9]. Type 1 are usually tumor protein 53 (P53) wild type, and while they have oncogenic mutations or copy number alterations within pathways like Phosphoinositide 3-kinase (PI3K) – AKT and RAS – mitogen activated protein kinase (MAPK), genomic instability is not a usual characteristic of these tumors [9]. Clinically, these tumors are slow growing and if caught early, have a good prognosis when contained to the ovary [9]. Type 1 tumors include LGSOC, CCC, MC, and transitional cell (Brenner) subtypes [9]. Unlike Type 1 tumors, Type 2 EOCs are characterized by P53 mutations and widespread genomic instability [10]. Clinically, these are much more aggressive and have often disseminated throughout the peritoneal cavity at diagnosis, giving these patients a much poorer prognosis [10]. Type 2 tumors include HGSOC and HGEC subtypes [10]. HGSOC is the predominant diagnosis and makes up 70-80% of deaths from all forms of ovarian cancer [10].

1.2 Etiology and current treatment of high grade serous ovarian cancer (HGSOC)

HGSOC is the deadliest subtype of epithelial ovarian cancer constituting about 70% of EOCs and will be the focus of this dissertation [10]. Histologically, these solid tumors are characterized by finger-like projections or papillary architecture that resemble that of normal FTE [11]. Cytologically, HGSOC cells display nuclear pleomorphism with some containing large nuclei and others are multinucleated [11]. HGSOC cells often have prominent nucleoli that appear eosinophilic and their mitotic index is elevated [11]. Immunologically, HGSOC expresses several markers that are used to distinguish it from other subtypes. Most ubiquitous is the tumor protein 53 (*TP53)* mutation that is found in >96% of all HGSOC [12]. This can be

seen as positive staining of the protein if there is a missense mutation or a complete absence of staining due to a nonsense mutation that produces a truncation that is not detected by the p53 antibody [10, 13]. Other immunological markers used diagnostically are positive staining of Wilms tumor 1 (WT1), cyclin-dependent kinase inhibitor 2A (CDKN2A), cytokeratin 7 (CK7), cytokeratin 8 (CK8), AT-rich interactive domain-containing protein 1A (ARID1A), paired box gene 8 (PAX8), estrogen receptor (ER) in about 80% of cases, and progesterone receptor (PR) in about 30% of cases [11]. Since these tumors proliferate faster than LGSOC, they also present with a higher Ki-67 proliferation index [10].

Increasing age is the most common risk factor for HGSOC [14]. It is rarely diagnosed in pre-menopausal women, with 63 being the median age at diagnosis [14]. Most HGSOCs are sporadic, but there is also be a genetic component to some [15]. If a woman has a first degree relative with ovarian cancer, her risk increases 3-fold [15]. Germline breast cancer type 1/2 susceptibility protein (*BRCA1/2)* mutations are responsible for 3.6% and 3.3% of EOCs, respectively [14, 16, 17]. By the age of 70, women with *BRCA1/2* mutations have a 44% and 27% risk of developing EOC, respectively [18]. These women usually develop HGSOC and are diagnosed at a younger age than women who develop sporadic disease [14]. BRCA1 and BRCA2 play a critical role in homologous recombination (HR) for double-strand breaks (DSB) [19]. Unlike non-homologous end joining (NHEJ), HR is less error prone and is able to repair DSB without altering the reading frame [19]. Dependency on NHEJ for DSB repair in patients with *BRCA1* or *BRCA2* mutations may lead to errors in DSB repairs, genomic instability, and even cancer [19]. This is particularly relevant in breast and ovarian tissue where it is hypothesized that estrogen and oxidative stress, respectively, may increase DSB and make women particularly susceptible to breast and ovarian cancer [20, 21]. Poly (ADP ribose)

polymerase (PARP) inhibitors, like Olaparib, have been shown to be effective in treating *BRCA1* or *BRCA2* mutant ovarian cancer [22]. PARP is critical in single stranded breaks (SSB), so PARP inhibitors prevent SSB repair which leads to DSBs upon replication [22]. When these DSBs cannot be efficiently repaired because of mutations in *BRCA1* or *BRCA2*, synthetic lethality of these cancer cells occurs [22]. Other lower penetrance mutations within the homologous recombination (HR)-mediated pathway of DNA repair are thought to also risk factors in developing EOC [23]. Such genes include BRCA1 Interacting Protein C-Terminal Helicase 1 (*BRIP1), RAD1C* and *RAD1D,* which have lifetime risks of developing EOC of 5.8%, 5.2% and 12%, respectively, as well as BRCA1-associated RING domain protein 1 (*BARD1),* checkpoint kinase 2 (*CHEK2),* meiotic recombination 11 homolog A (*MRE11A), RAD50,* Partner And Localizer Of BRCA2 (*PALB2)* and Ataxia Telangiectasia Mutated (*ATM)* [24-26].

Another risk factor is ovulation [10]. The association between more ovulatory cycles and greater risk of EOC has been shown through various studies [27-29]. There appears to be a protective affect for women who have late first menarche, early menopause, given birth (with each additional birth showing a 10-20% risk reduction), breastfed, and had taken birth control [14, 30-33]. Compared to women who have never taken hormonal birth control, women who are former hormonal birth control users have a 30% lower risk of developing EOC [33]. Through analysis of 45 epidemiological studies, one group estimated that the use of hormonal birth control has prevented up to 200,000 cases of EOC globally [33]. Smoking, diabetes, obesity, and usage of perineal talc are other potential risk factors for EOC [14].

A majority of women diagnosed with HGSOC are found to have late stage disease when metastasis has already occurred and the 10-year survival rate plummets to 15% [34]. There are several reasons why an early diagnosis, where the 10-year survival rate is 55%, poses such a

challenge in HGSOC [34]. First, there are currently no effective screening strategies [4]. The anatomical placement of the fallopian tubes and ovaries within the peritoneal cavity make finding a lump through self-examination impossible. The combination of transvaginal sonography with serum cancer antigen 125 (CA125) levels was a potential screening option, but patient outcomes did not improve [35, 36]. One effective strategy, specifically for patients with BRCA mutations, is the prophylactic oophorectomy and salpingectomy prior to the age of 40. This prevented an estimated 85-90% of EOCs [37]. In 2018, Wang and colleagues published their evaluation of liquid biopsies from the Papanicolaou (PAP) test with blood samples for earlier detection of EOCs and demonstrated the promising potential of using genetic mutations to detect up to 54% of early-stage disease [38]. Second, the most common symptoms of HGSOC often are misdiagnosed as gastrointestinal issues. Symptoms of HGSOC can include: abdominal pain, bloating, nausea, acid reflux, lower back pain, fatigue, constipation or diarrhea, weight loss, tenesmus, increased urinary frequency, vaginal discharge, and sometimes dyspnea in more advanced disease [4, 11]. More than a third of women with EOC will present with ascites upon diagnosis [39]. Ascites is pro-inflammatory fluid in the peritoneal cavity containing cellular components and soluble factors that aids in the dissemination and growth of EOC [39].

If these symptoms are suspected to be EOC, a pelvic exam and imaging are done and CA125 levels are taken [4]. CA125 levels are elevated in patients with EOC but there is a large range within that population of 500-1000 U/mL [4]. Once baseline CA125 is measured, it can be used to track the disease severity throughout treatment [4]. Laparoscopic surgery may then be performed to get a biopsy of the tumor as well as stage the disease [4].

According to the latest International Federation of Gynecology and Obstetrics (FIGO) staging system, stage I disease is contained to the ovary and fallopian tube, stage II has

disseminated locally to organs like the uterus, stage III involves other organs or lymph nodes within the peritoneal cavity, stage IV has spread to organs beyond the peritoneal cavity like the lungs [40]. In end stage HGSOC, there is often malignant bowel obstruction because of adhesions of the bowel to the tumors [40]. This obstructs the absorption of life-sustaining nutrients and can lead to death [40].

In 2011 the cancer genome atlas (TCGA) network performed a large-scale genetic analysis on 316 HGSOC patients by whole exome sequencing [12]. HGSOC is characterized by very few mutations, one exception being the ubiquitous *TP53* mutation, and widespread copy number alteration [12]. The TCGA study found more than 96% of samples had *TP53* mutations, and later analysis postulates those remaining 4% may have been misdiagnosed as HGSOC [41]. It is thought to be an early, potentially initiating event as they were observed in serous tubal intraepithelial carcinoma (STIC)s, the FTE precancerous lesion [5]. This may also help to explain the widespread genomic instability characteristic of HGSOC since the p53 protein is considered the guardian of the genome as it plays a critical role in genetic stability [42]. Since p53 is a tetramer, any single mutant P53 protein may act as in a dominant negative fashion and can inhibit tetramerization and functionality even with wild type p53 [43]. Mutant p53 is also more stable since it lacks the ability to bind to HDM2, its inhibitor that would normally ensure appropriate degradation through the proteasome [44]. *BRCA1* and *2* germline mutations were found in 9% and 8% of patients, respectively, and somatic mutations were found in an additional 3% of patients for both [12]. Only 6 other genes were found to be mutated recurrently in 6% or less of samples: *CSMD3*, *FAT3*, *NF1*, *CDK12*, *GABRA6*, and *RB1* [12].

Far greater than the number of mutations in a HGSOC sample are the number of copy-number alterations. In over 20% of samples, *CCNE1*, *MYC* and *MECOM* were found to be

amplified [12]. By combining analysis of mutations, copy number alterations, and gene expression data, important pathways to the etiology of HGSOC were revealed. In 51% of cases, the HR DNA repair pathway was defective [12]. *BRCA1/2* was lost in 33% of patients through germline and somatic mutation as well as epigenetic silencing by hypermethylation [12]. Additionally, altered within the HR pathway are *ATM* (1% mutated), *ATR* (<1% mutated), *EMSY* (8% amplified/mutated), *FA core complex* (5% mutated), *FANCD2* (<1% mutated), *RAD51C* (3% hypermethylated), and *PTEN* (7% deleted) [12].

RB signaling, which plays an important role in cell cycle progression, is altered in 67% of cases [12]. RAS/PI3K signaling, which is involved in proliferation and cell survival, is altered in 45% of cases [12]. NOTCH signaling, also important in proliferation, is altered in 22% of cases [12]. And in 84% of cases there were alterations in FOXM1 signaling, which is affects cell cycle progression and DNA repair [12]. It is important to note that p53 is a direct inhibitor of FOXM1 so mutations in *TP53* are is likely responsible for the over activation of this pathway [12].

This better understanding of the underlying genetics of HGSOC led to the establishment of molecular subtypes of HGSOC: immunoreactive, differentiated, proliferative and mesenchymal [45, 46]. Patient outcome varies between these groups with proliferative and mesenchymal subtypes bearing the worst prognosis to immunoreactive having the best patient outcomes [47]. The differentiated subtype is the most heterogeneous and so there have been efforts to add a 5^{th} subtype: anti-mesenchymal, which has a better prognosis than differentiated [48]. These efforts to better understand the genetics and molecular subtyping hope to develop more specific treatment plans for women with HGSOC [49].

1.3 High grade serous ovarian cancer: an origin story

The cell of origin for HGSOC has long remained a crucial gap in knowledge. Historically, the OSE was hypothesized to be the source of HGSOC [50]. There was and is evidence to support this. Even at early stages, tumors involved the ovary and the OSE was the first proposed cell of origin [10]. The OSE is a cuboidal, meso-epithelial single cell layer that surrounds the ovary that undergoes rupture and repair each month ovulation occurs [10]. In 1971, Fathalla proposed the "incessant ovulation" hypothesis that would garner support within the field [47]. This theory argues that the constant rupture and repair of this layer could leave these cells particularly vulnerable to transformation [47]. A pro-inflammatory and pro-oxidative environment accompanies the physical damage to the tissue, and the subsequent inability to repair that damage could lead to HGSOC [27]. Mutations in DNA-repair genes such as BRCA1/2 increase women's risk of developing ovarian cancer [26]. Further supporting this theory is the evidence that women who have fewer cycles of ovulation either through oral contraception, pregnancy, or breastfeeding are at lower risk for ovarian cancer [10].

Through study of the rupture and repair process during ovulation, cortical inclusion cysts (CICs) were observed [10, 28]. Invaginations of the OSE can occur during post-ovulation repair and form CICs under the surface where they are exposed to hormones that promote growth and differentiation, again providing an ideal environment in which transformation can occur [10, 28].

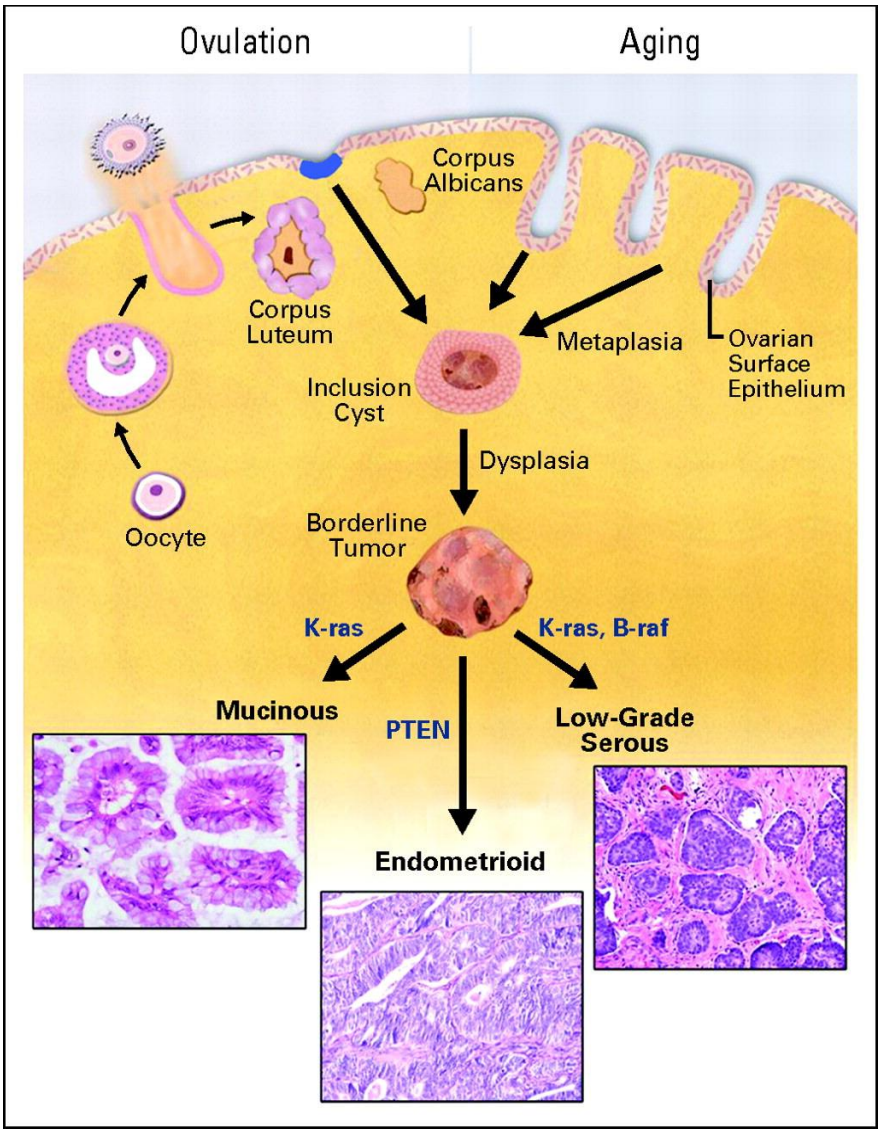

Figure 1

Transformation of ovarian surface epithelium (OSE). The OSE undergoes cyclic ovulation-induced rupture, leading to formation of cortical inclusion cysts (CICs). Entrapped within the ovarian cortex, the OSE undergoes Müllerian metaplasia, and is exposed to hormone and inflammatory stimuli that induce replicative stress and DNA damage which can lead to defined mutations and transformation into mucinous, endometrioid, and low-grade serous carcinomas. (Levanon *et al.*, Copyright © 2008, American Society of Clinical Oncology. Used with permission.)

By 1999, Dubeau and colleagues suggested an alternate site of origin: Mullerian duct derived tissue [6]. The Mullerian duct is derived from primitive coelomic epithelium that invaginates caudally from the fetal kidney and runs alongside the Wolffian duct during embryonic development [51]. In males with a Y chromosome, the bipotential gonad develops into testes that produce Mullerian inhibiting substance (MIS), which degrades the Mullerian duct [51]. In females, the absence of MIS allows the Mullerian duct to remain and develop into the fallopian tubes, endometrium, and endocervix of the female reproductive tract under control of HOXA9, 10, and 11, respectively [51]. Since HGSOC more closely resembles Mullerian duct-derived FTE than it does normal OSE, he argued that metaplastic transformation of the OSE was unproven and may be less likely than transformed Mullerian duct derived cells seeding tumors on the ovary [6].

This alternate theory gained traction soon after when women with BRCA mutations had prophylactic surgery to remove the ovary and fallopian tube [52]. Upon careful examination of serial sections of this tissue, Piek and colleagues described the presence of dysplastic changes in the secretory cells of the fallopian tube that showed histologic similarity to HGSOC [53]. These were later named STICs and diagnosed if they fit the criteria of morphologic characteristics (nuclear enlargement, hyperchromasia, irregularly distributed chromatin, nucleolar prominence, mitotic activity, apoptosis, loss of polarity, and epithelial tufting), have diffused moderate to strong expression of p53 in >75% of the cells in the lesion or complete absence of staining indicating *TP53* mutations and Ki-67 labeling index of >10% [54]. Crum's lab studied a cohort of women with BRCA1/2 mutations and found that 38% displayed STICs without evidence of ovarian involvement and advanced the theory that secretory cells of the distal fallopian tube were a cell of origin for HGSOC [55]. Kuhn and colleagues also found clonal mutations present in

STICs and established HGSOC within the same patient [42]. Looking beyond women with BRCA1/2 mutations, 52% of women with sporadic cases of HGSOC have also shown evidence of STICs [56]. Recent studies show corresponding genetic alterations of HGSOC and STICs within the same patients including one study that established that, within the same patient, amplification of CCNE1 was found in both HGSOC and STICs [17, 57].

Telomere length has also been assessed in normal adjacent tubal epithelium, STICs, and HGSOC by Kuhn and colleagues in 2010 [58]. They found that a majority of STICs had shortened telomeres compared to normal tissue and that HGSOC had longer telomeres than STICs [58]. Telomere shortening has been reported in preneoplastic cells in breast, lung, pancreatic, prostate, cervical, and biliary tract carcinomas and is a hallmark of early stage carcinogenesis [9, 59-62]. Oxidative stress-induced cellular damage from the exposure to reactive oxygen species released from antral follicles during ovulation is a mechanistic theory of telomere shortening in the secretory cells of the FTE [63-65].

All of this evidence builds a strong case that a significant portion of HGSOC originate from the FTE. This has been important in shaping medical decisions to perform salpingectomies in risk-reducing surgeries for women with BRCA1/2 mutations [10]. However, there still remain HGSOC cases in which no FTE involvement can be found leading researchers to believe that some cases arise from FTE while others arise from OSE [66].

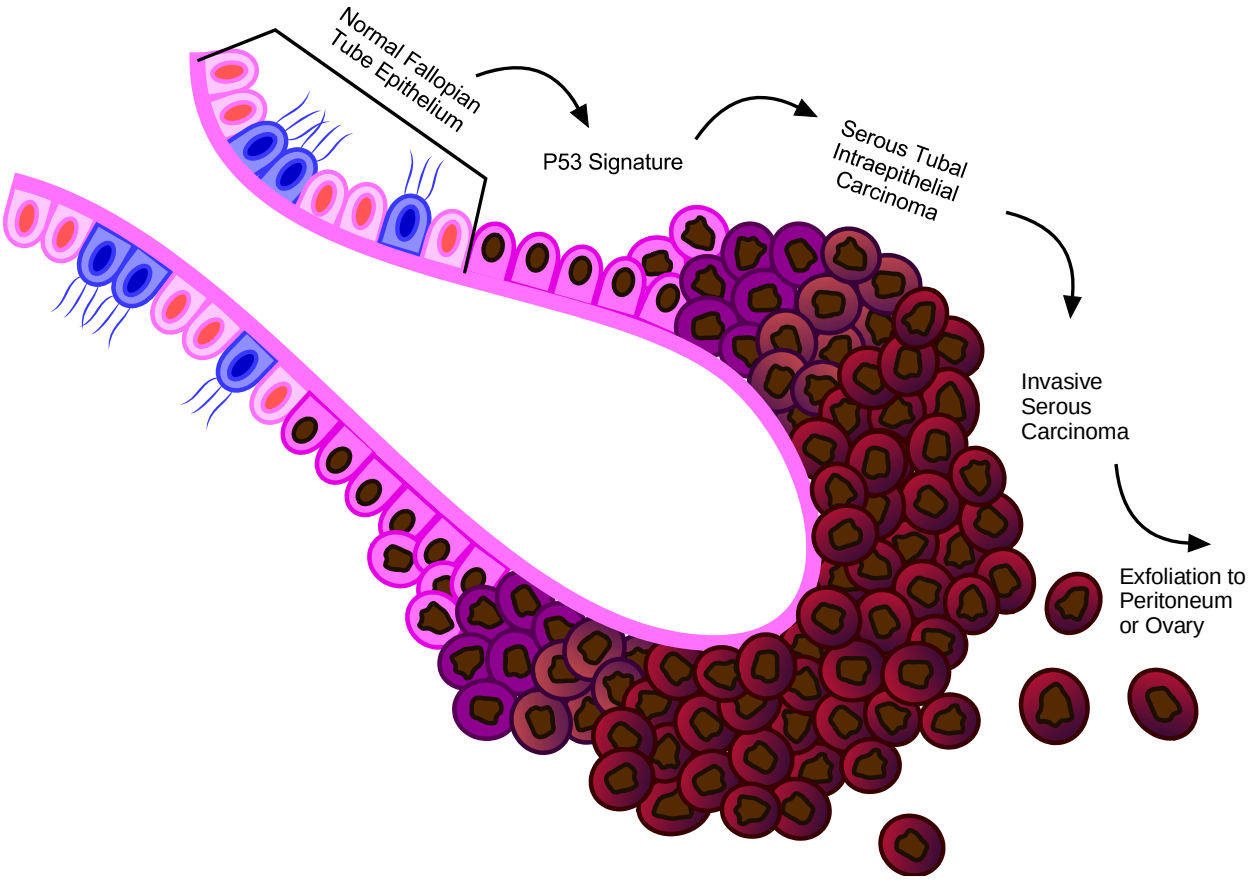

Figure 2

Transformation of the fallopian tube epithelium (FTE) into HGSOC. Secretory FTE cells that appear benign can acquire 'p53 signatures,' a preneoplastic lesion. Following mutation of the TP53 tumor suppressor gene, a known early event in the development of HGSOC, greater proliferative capacity and neoplasticity results in the development of STICs. Once these cells lose cell to cell adhesion and apical-basal polarity, they're able to disseminate to the ovary and/or peritoneal cavity presenting as HGSOC, characterized by TP53 mutations and widespread copy number alterations. (Adapted from Jones et al., 2013, Frontiers in Oncology. Open access.)

1.4 Models of high grade serous ovarian cancer

Cell lines derived from ovarian cancer patients are often used in *in-vitro* studies for HGSOC Mitra and colleagues assessed 11 of these lines *in vivo*: CAOV3, COV362, KURAMOCHI, NIH-OVCAR3, OVCAR4, OVCAR5, OVCAR8, OVSAHO, OVKATE, SNU119, UWB1.289to determine which were most representative of HGSOC [67]. Kuramochi, SNU1119 and UWB1.289 were unable to form tumors in mice; OVKATE and COV362 were only capable of forming sub-cutaneous tumors; OVCAR3, OVCAR4, OVCAR5, OVCAR8, CAOV3, and OVSAHO formed intraperitoneal tumors with HGSOC histology [67]. OVCAR3, OVCAR5, and OVCAR8 were the most aggressive, but OVCAR8 most often presented with ascites [67]. Other popular cell lines, SK-OV-3 and A2780 were determined by Domcke and colleagues to be very poor models of HGSOC since they neither matched the histology nor harbored any *TP53* mutations [68]. This group found that Kuramochi, OVSAHO, SNU119, COV362, and OVCA4 cell lines best represent HGSOC [68]. While cell lines can be a useful tool for *in vitro* research, it is important to recognize their limitations and consider that some are worse than others at modeling HGSOC. More recently, three-dimensional, organoid culturing techniques allow for a more realistic growth environment compared to growth on a plastic dish [17].

McCloskey and colleagues cultured mouse OSE cells and found that eventually they spontaneously transformed (STOSE) [69]. Unlike their parental cells, STOSE cells proliferated faster, formed colonies, formed tumors *in vivo* that mimic HGSOC by histology and presence of HGSOC markers, and have aberrant Wnt/β-catenin and Nf-κB signaling as well as upregulation of *Ccnd1* and loss of *Cdkn2a* consistent with TCGA findings of HGSOC [69]. This model

provides evidence for *in vitro* transformation of normal OSE to HGSOC without additional manipulation [69].

Genetically engineered mouse models (GEMMs), while a larger investment in time and resources, allow us to study the disease progression in the context of whole-body physiology. Ever more important in the context of HGSOC, which is often diagnosed late stage, GEMMs can act as a time machine, allowing study of early disease and progression to later stages. It is also important in identifying key genes that are sufficient in driving HGSOC in mice. Since the origins of HGSOC are both OSE and FTE, GEMMs have been bred where the genetic manipulation occurs in both the OSE and FTE. These GEMMs are summarized in the table below.

Table 2

Genetically Engineered Mouse Models of HGSOC.

Cell of Origin	Cre promoter	Genes altered	Description	Reference
FT stromal cells	*Amhr2*	Deletion of *Dicer* and *Pten*	• HGSOC cytology and histology • STICs from stromal cells of the FT • Positive epithelial markers: KRT14, KRT8, CDH1, KRT17, • Positive HGSOC markers: Ki67 and CA125 • No mention of PAX8 • Low p53 (the group explains that because p53 is upstream of DICER, the deletion of *Dicer* may substitute for *Trp53* mutation) • AKT pathway activation • Ascites	Kim et al, 2012 [70]
OSE	*Amhr2*	Deletion of *Stk11* and *Pten*	• HGSC histology • Positive HGSOC markers: CK8, WT1, PAX8, ERα, TP53 • MTORC1 pathway activation • Ascites	Tanwar et al, 2014 [71]
FTE	*Pax8*	Deletion of Brca, Tp53, and Pten	• HGSC histology • STICs • Positive HGSOC markers: TP53, PAX8, Ki-67, STMN-1, Pan-Keratin, PAX2, WT1, CA125 (serum) • Pathways altered: DNA damage, DNA repair and HR-mediated repair, FOXM1, NOTCH, RB, and PI3K/MYC	Perets et al, 2013 [5]

Table 2 (cont'd)

FTE	*Ovgp-1*	Expression of SV40 large T-antigen (inactivates p53 and Rb)	• STICs and invasive serous adenocarcinoma in the ovary (56%) • Positive HGSOCs markers: p53, Ki-67, PAX8, γ-H2AX, TOPO2 • Pathways altered: p53 signaling, cell cycle control of chromosomal replication, DNA damage response	Sherman-Baust et al, 2014 [72]
FTE	*Ovgp-1*	Deletion of Brca1, Trp53, Rb1, Nf1, Pten	• STICs, HGSOC, malignant mixed Mullerian tumors, and ascites were found in varying degrees in different genetic deletion combinations • Positive HGSOCs markers: CK8, p53, Ki-67, PAX8 • Mice with conditional deletion of *Brca1*, *Trp53*, and *Pten* also display mucinous metaplasia	Zhai et al, 2017 [73]
OSE	Adenovirus-Cre injection into intrabursal space targeting OSE	Deletion of *Trp53*, *Rb*, *Brca1 or 2*	• HGSOC histology, oviduct adenocarcinoma, peritoneal mesothelioma, and ascites • Positive HGSOCs markers: ER, and PR • HGSOC tumors did not express PAX8 • Pathways altered: RB, p53, DNA damage signaling and repair, FOXM1	Szabova et al, 2012 [74]

1.5 mTORC1 pathway overview

The mechanistic target of rapamycin (mTOR) is serine/threonine kinase that, when in complex with DEP domain-containing mTOR-interacting protein (DEPTOR), G protein beta subunit-like (GßL), and Regulatory-associated protein of mTOR (Raptor), forms mTOR complex 1 (mTORC1), which can be suppressed through Rapamycin [75, 76]. mTORC1 is considered the master regulator of proliferation as it receives inputs from various environmental cues from the cell like energy status, growth factors, amino acids, and cell stress and activates downstream signaling that controls cell survival, growth, and proliferation. [76, 77]

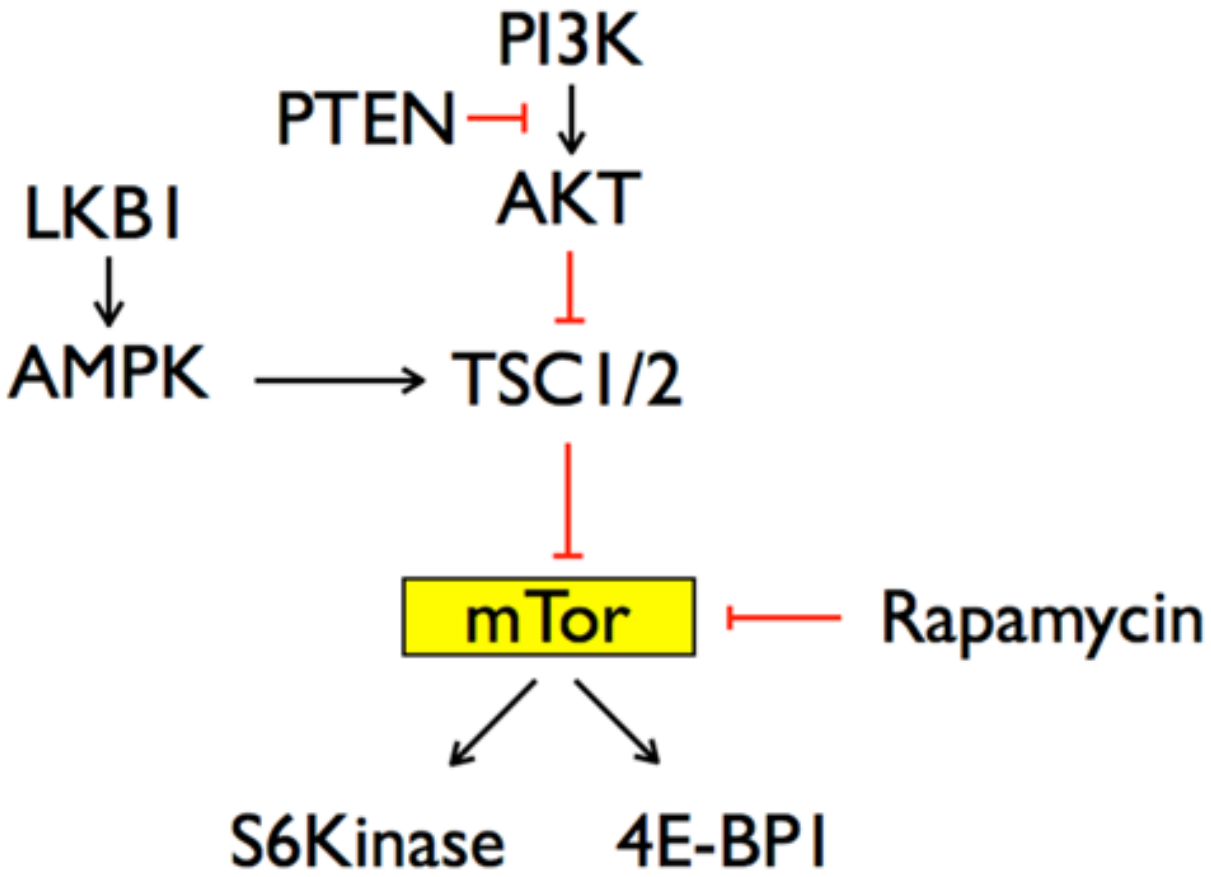

Figure 3

mTORC1 pathway overview.

1.5.1 *Serine/threonine kinase 11 (STK11)*

STK11 encodes for the protein, LKB1, a serine-threonine kinase that directly phosphorylates and activates AMP-activated protein kinase (AMPK), a key switch in cell metabolism [78]. Under low energy conditions where there is a high adenosine monophosphate (AMP) or adenosine diphosphate (ADP) to adenosine triphosphate (ATP) ratio, LKB1, in complex with subunits STE20-related kinase adapter protein alpha (STRAD) and Mouse protein-25 (MO25), is activated) [79, 80]. Once activated, it phosphorylates and activates AMPK which leads to inhibition of mTORC1 [81]. Outside of AMPK, LKB1 can phosphorylate and activate 14 related kinases that can, in turn, phosphorylate and activate downstream substrates that affect cell polarity, transcriptional control of metabolism, acute metabolic changes, and cell growth [82].

STK11 was originally identified as the gene responsible for Peutz-Jeghers Syndrome [83]. These patients have a germline mutation in *STK11* and often suffer from polyps in the gastrointestinal tract and pigmented macules on the skin around the mouth [84]. These patients also have an increased risk of developing cancer reaching a cumulative risk of 85% for all cancers by the age of 70 [84].

STK11 is commonly mutated or downregulated across many cancers [78]. It is the most mutated gene in sporadic lung cancer and 20% of cervical cancers (somatically mutated by human papilloma virus (HPV)) [78]. It has also been found to be somatically mutated in breast, intestinal, cervical, pancreatic, testicular and skin cancers [78]. In HGSOC, deletions in at least one allele of *STK11* can be found in 88% of cases [12].

1.5.2 Tuberous Sclerosis complex 2 (TSC2)

TSC2, bound to its partner TSC1, is the negative regulator of mTORC1 [85, 86]. It does this through TSC2's a GTPase-activating protein (GAP) domain that stimulates the conversion of Rheb-GTP to its inactive Rheb-GDP form [86]. Since the active Rheb-GTP is needed to activate mTORC1, TSC2's inactivation of Rheb directly inhibits mTORC1 activity [86].

TSC1/TSC2 is activated by AMPK and suppressed by AKT [85]. Activated AMPK can directly phosphorylate TSC2 on Ser^{1387} and Thr^{1271} [85]. AKT also directly phosphorylates TSC2, but this phosphorylation inhibits its ability to form a complex with TSC1 [85]. Without the GAP function of TSC1/TSC2, active Rheb-GTP accumulates and activates mTORC1 [85].

Mutations in *TSC1* or *TSC2* cause Tubular Sclerosis complex disorder [86]. Patients with this autosomal dominant disorder may have tumors in multiple organs, primarily within the central nervous system where they can cause epilepsy and mental retardation [86]. Adenoma sebaceum, clinically presenting as raised red papules on the face are also common [86].

1.5.3 Phosphatase and tensin homolog (PTEN)

PTEN is a tumor suppressor that is often lost in many different cancers, both heritable and spontaneous [87]. It has a phosphatase function and dephosphorylates phosphatidylinositol-3,4,5-triphosphate (PIP3), converting it to phosphatidylinositol-4,5-bisphosphate (PIP2) and acting in direct opposition to phosphoinositide 3 kinase (PI3K) [87]. In this particular phosphatase role within the cytoplasm, PTEN acts as a potent tumor suppressor to the PI3K/AKT/mTORC1 pathway [88].

In addition to its role counteracting PI3K in the cytoplasm, PTEN can also translocate to the nucleus. Throughout the cell, it has been found to play critical roles in genomic stability

[89], cellular senescence [90], cell migration and metastasis [91], stem cell self-renewal [92], and the tumor microenvironment [93].

1.5.4 Tumor protein 53 (P53)

P53 is another tumor suppressor protein that is found to be altered in most cancers [8, 17]. It is considered to be the guardian of the genome for its role in maintaining genetic integrity and preventing genetic mutations [94]. Since p53 can induce cell-cycle-arrest and apoptosis, cells need mechanisms to inactivate p53 unless there is a specific stress signal like DNA damage [94]. MDM2 is a ubiquitin ligase that binds to p53 and inactivates it [94]. Under conditions of stress in the cell (DNA damage, oncogene activation, nutrient deprivation, hypoxia, ribosomal stress, and telomere erosion), activated p53 plays a key role in integrating those stresses with the appropriate response (DNA repair, Senescence, Apoptosis, survival, genomic stability, and cell-cycle arrest) [94]. Important for the purposes of this dissertation, p53 mutation is ubiquitous in HGSOC and is thought to be a precursor to the widespread copy number alterations (CNA) and subsequent carcinogenesis that occurs in the disease [12].

1.5.5 Paired box 8 (PAX8)

PAX8 is a lineage specific transcription factor that plays a critical role during both development and tumorigenesis [95]. Infants with mutations or deletions in the *PAX8* gene presented with hypothyroidism due to dysgenesis or agenesis [96]. This led to the discovery of PAX8's developmental function. Scientists further elucidated its role through studying *Pax8*$^{-/-}$ mice. These mice did not survive past weaning, also presented with hypothyroidism, and were severely underdeveloped [97]. In both male and female mice, survival was possible through thyroid hormone replacement, but they were infertile due to malformations of Mullerian duct or absence of some Wolffian duct tissues [98-100]. Adult PAX8 expression is found in the thyroid

gland and kidney in addition to the cervix, endometrium, and fallopian tube in females or the seminal vesicle and epididymis in males [98].

Ubiquitous PAX8 expression in HGSOC has implications in cell of origin: PAX8 expression is maintained from FTE origin or is acquired from OSE origin, as has been shown to occur in our mouse model that will be described in chapter 2. PAX8 is found to be overexpressed in reproductive malignancies including ovarian cancer where higher expression is associated with lower 5-year survival rate and higher reoccurrence rate [101]. *In vitro* analysis of Pax8 overexpression in thyroid epithelial cells shows increased proliferation and colony-forming efficiency [102]. To better understand the functional role of PAX8 in HGSOC, RNAsequencing was performed on fallopian tube secretory epithelial cell lines (FTSEC) and HGSOC cell lines before and after PAX8 knockdown [103]. While PAX8 knockdown had negligible effects in benign FTSEC cell lines, genes related to angiogenesis and morphogenesis were significantly altered in malignant HGSOC cell lines with higher baseline levels of PAX8 [103].

CHAPTER 2. DELETION OF LKB1 AND PTEN SYNERGISTICALLY TRANSFORM MOUSE OVARIAN EPITHELIAL CELLS TO PAPILLARY SEROUS OVARIAN CANCER

2.1 Abstract

Understanding differentiation of ovarian cancer histotypes provides the possibility of subtype-specific treatment for this deadly disease. Tumor suppressor genes upstream of mTORC1, *STK11*, *PTEN*, and *TSC2*, are deleted in 88%, 40%, and 55% of high grade serous ovarian cancer, respectively. In deleting these genes alone and in combinations in the ovarian surface epithelium of mice, we found that papillary serous ovarian cancer histology only developed with deletion of *Stk11* and *Pten*. These tumors are positive for high grade serous ovarian cancer markers including PAX8 in most 15–20-week-old ovaries indicating that PAX8 1) is not an early driver of differentiation and 2) is acquired during transformation of ovarian surface epithelial cells. When isolated and cultured, these cells have higher growth rates *in vitro* than single mutants or controls. RNA sequencing of control, $Stk11^{cko}$, $Pten^{cko}$, and $Stk11^{cko}Pten^{cko}$ mouse ovarian surface epithelial cells reveals that $Stk11^{cko}Pten^{cko}$ cluster away from other groups and have over 3000 differentially expressed genes versus control. Interestingly, *Pten* transcripts are twice as abundant in $Stk11^{cko}$ versus control revealing a compensatory mechanism inhibiting uncontrolled growth. Gene set enrichment analysis (GSEA) of $Stk11^{cko}Pten^{cko}$ versus $Stk11^{cko}$ indicates many DNA repair pathways are dysregulated. Together, these results highlight the important roles that *Pten* and *Stk11* deletion play in high grade serous ovarian cancer and provide evidence to further investigate therapies that target these pathways.

2.2 Introduction

Ovarian cancer (OvCa) is the 5th leading cause of cancer deaths for women and ranks as the most lethal gynecological cancer in the United States [1]. In 2019, there were 22,530 new cases diagnosed and 13,980 deaths due to ovarian cancer making it the 5th most deadly cancer for women with a 5-year survival rate is 47.7% in the US [2]. The high-grade serous histotype of ovarian cancer (HGSOC), which accounts for 90% of epithelial OvCa, is the deadliest [10]. Due to lack of reliable early screening and absence of symptoms until later stages, HGSOC is often only diagnosed when advanced, leading to decreased treatment options and survival rates for patients [10]. At diagnosis, 70% of patients have already progressed to stage III or IV and have less than a 30% chance at 5-year survival [10]. For the few patients whose disease is caught in stage I, the 5-year survival rate is greater than 90% providing hope and promoting urgency for better screening and biomarker discovery [4, 7, 10]. Since HGSOC is usually diagnosed in the late stages, the etiology of the disease has been difficult to study.

The possible molecular mechanisms underlying HGSOC development have mostly been studied in mouse models and cell culture [5, 17, 67, 68, 71-74]. Genetically engineered mouse models (GEMMs) have shown loss of which genes can cause mice to develop a HGSOC phenotype in mouse OSE or FTE highlighting the importance of loss of *Trp53*, *Dicer*, *Pten*, *Stk11*, *Brca*, *Rb1*, and *Nf1* in the initiation of disease [5, 17, 67, 68, 71-74]. One particular milestone in the HGSOC studies has been the collection and analyses of tumors through the Cancer Genome Atlas (TCGA) [12]. This study gave a The TCGA study found more than 96% of samples had *TP53* mutations, and later analysis postulates those remaining 4% may have been misdiagnosed as HGSOC and helps to explain the widespread genomic instability characteristic

of HGSOC since the p53 protein plays a critical role in genetic stability [41]. Although many important copy number alterations and altered pathways have been discovered, a clear progression of the disease from its origin has not been well established; also, over 80% of patient tissue sampled in the TCGA was from late stage (stage III-IV) patients that are likely to be missing many important features of early tumorigenesis [12]. Even the cell of origin itself is debated, which has significant implications in prevention and treatment [6]. It was traditionally thought that the ovarian surface epithelium (OSE) is the cell of origin for all epithelial OvCa subtypes [47], but another theory that serous ovarian cancer develops from the fallopian tube epithelium (FTE) has emerged [68]. One line of evidence for this is that PAX8 is found to be ubiquitously expressed in both HGSOC and normal FTE while absent from normal OSE [101]. PAX8 expression is therefore either maintained in the transformation of normal FTE to HGSOC or acquired in the transformation of normal OSE to HGSOC, which is demonstrated in our mouse model. Although there is no consensus, many researchers in the field argue that HGSOC arises from either the FTE or the OSE [71]. The discovery of the FTE origin of HGSOC has likely been life saving for preventing ovarian cancer in women harboring BRCA1/2 mutations [10]. Prophylactic removal of the fallopian tubes along with the uterus is now standard practice [10]. However, limiting all HGSOC research to FTE origin does a disservice to the field because breakthroughs for treatment may not be efficacious for HGSOC patients whose tumors originated from OSE. Our mouse model uses the Cre Lox system to knock out genes specifically in the OSE, not FTE, under the *Amhr-2* promoter.

According to the Cancer Genome Atlas Nature data accessed through cbioportal (N=316), 84% of HGSOC tumors had loss of one or both alleles of *Stk11;* 39% had loss of one

or both alleles of *Pten* and 53% had loss of one or both alleles of *Tsc2* [12, 104]. 34% of tumors had loss of both *Stk11* and *Pten*, and 20% had loss of all three genes [12, 104]. Our lab has developed OvCa mouse models in which upstream regulators of mTOR signal transduction pathway are conditionally deleted in the OSE. We have previously shown that these transgenic mice develop epithelial OvCa with serous histology with 100% penetrance around 15 weeks of age [71]. While other models, both in vitro and in vivo, focus on other commonly mutated genes like *BRCA1/2* and *KRAS* [5, 72, 73], our models provide a unique view into the role of *STK11* and *PTEN* deletions in HGSOC [10]. For example, since *STK11* and *PTEN* are both tumor suppressor genes (TSGs) upstream of mTORC1 that are frequently deleted in HGSOC, we hypothesized that combining deletion of other key modulators of mTORC1 activity would also give rise to HGSOC in novel mouse models. However, only *Stk11*^{cko}*Pten*^{cko} mice develop serous ovarian tumors. These results suggest that LKB1 and PTEN have a critical tumor suppressor role outside of suppressing growth through the mTORC1 pathway in this setting.

2.3 Results

To determine whether deleting different combinations of key TSGs in the mTORC1 pathway could phenocopy the papillary serous ovarian cancer histology we have previously observed in our *Stk11*^{cko};*Pten*^{cko} mice, we bred and analyzed mice with combined *Stk11*^{cko};*Tsc2*^{cko} deletions and *Tsc2*^{cko};*Pten*^{cko}deletions (Fig 4). Since *Amhr2* drives CRE expression in the stromal cells of Mullerian duct-derived tissues, deletion of genes occurs throughout the female reproductive tract stroma, in addition to the ovarian surface epithelial (OSE) cells. *Stk11*^{cko};*Tsc2*^{cko} mice present with large fluid-filled uterine cysts as early as 10

weeks of age (n=3/7 mice collected) and all 7 mice examined had tumors throughout the reproductive tract (Fig 4C). Ovaries appear predominately normal upon histological examination other than microscopic papillae formation (Fig 4D) with the exception of 2 unspecified solid tumors, even in mice aged out to 6 months (data not shown). 2 of 3 3 month old *Tsc2*^{cko};*Pten*^{cko} mice examined also had uterine tumors (Fig 4E). After 6 months, 1 of 7 had cysts and 3 of 7 had very large tumors throughout the reproductive tract. However, histological examination of ovaries shows microscopic papillae formation (Fig 4F) by 6 months. *Stk11*^{cko};*Pten*^{cko} mice at 15-20 weeks of age develop invasive papillary ovarian cancer (N = 10/10 ovaries examined) (Fig 4H) and many develop cervical (Fig 4G) and uterine tumors, which we have previously reported [71]. Representative images of control, normal reproductive tract (Fig 4A) and histology of ovaries, surrounded by a single layer of cuboidal epithelium, (Fig 4B) are shown for comparison.

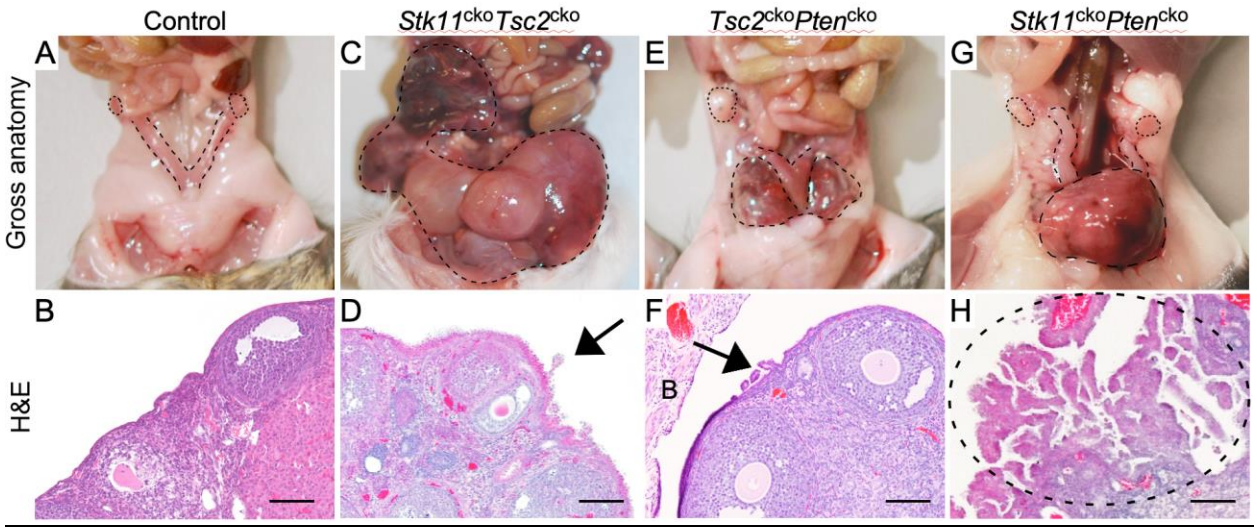

Figure 4

Phenotypic analyses of reproductive tracts and ovaries of adult mice, >12 weeks, with combinations of conditional knockout of tumor suppressor genes upstream of mTORC1.

(A) Representative image of a control reproductive tract. (B) Histology shows a normal phenotype in the ovarian surface epithelium. (C) Representative image of a *Stk11*^{cko}*Tsc2*^{cko} reproductive tract shows large fluid-filled cysts and tumors throughout the reproductive tract. (D) Histology shows that papillae formation, marked by a black arrow, is the extent of abnormality in the ovarian surface epithelium. (E) *Tsc2*^{cko}*Pten*^{cko} mice have uterine tumors. (F) Representative histology shows papillae formation, marked by a black arrow, is the extent of abnormality in the ovarian surface epithelium. (G) Representative image showing *Stk11*^{cko}*Pten*^{cko} mice reproductive tract tumors, outlined in the large dashed line. (H) Histology shows a papillary serous tumor phenotype in the ovarian surface epithelium. Medium dashed lines outline the reproductive tracts (A, C, E, G) and small dashed lines outline the ovaries when visible (A, E, G). B marks the bursa. (Scale bars, 100 um).

To understand how deletions of these tumor suppressor genes affect downstream signaling cascades, we performed immunohistochemistry on ovarian tissue from *Stk11*^{cko};*Tsc2*^{cko} (n=2), *Tsc2*^{cko};*Pten*^{cko} (n=2), *Stk11*^{cko};*Pten*^{cko} (n=2) mice for pAKT, pAMPK, and pS6 (Fig 2). Loss of *Pten* leads to the over-activation of AKT [105]; while positive staining for pAKT is seen in the OSE of all three mouse genotypes, staining appears stronger in *Tsc2*^{cko};*Pten*^{cko}(Fig 5D) and *Stk11*^{cko};*Pten*^{cko} (Fig 5G) compared to *Stk11*^{cko};*Tsc2*^{cko} (Fig 5A) OSE. LKB1, encoded by *Stk11*, directly phosphorylates and activates AMPK; OSE of *Stk11*^{cko};*Tsc2*^{cko} mice have weak staining of pAMPK (Fig 5B), *Tsc2*^{cko};*Pten*^{cko} OSE stain positively for pAMPK (Fig 5E), and *Stk11*^{cko};*Pten*^{cko} tumors are absent of pAMPK (Fig 5H). Positive pS6 staining is seen in all three mouse models and confirms that mTORC1 is activated. Deleting both *Stk11*^{cko} and *Pten*^{cko} together uniquely gives rise to papillary serous ovarian cancer histology in our mice. Beyond affecting proliferation through activation of mTORC1, both arms of the mTORC1 pathway - loss of *Stk11* and the resulting decrease in pAMPK as well as loss of PTEN and the resulting increase in pAKT - appear to be associated with producing the papillary serous ovarian cancer phenotype.

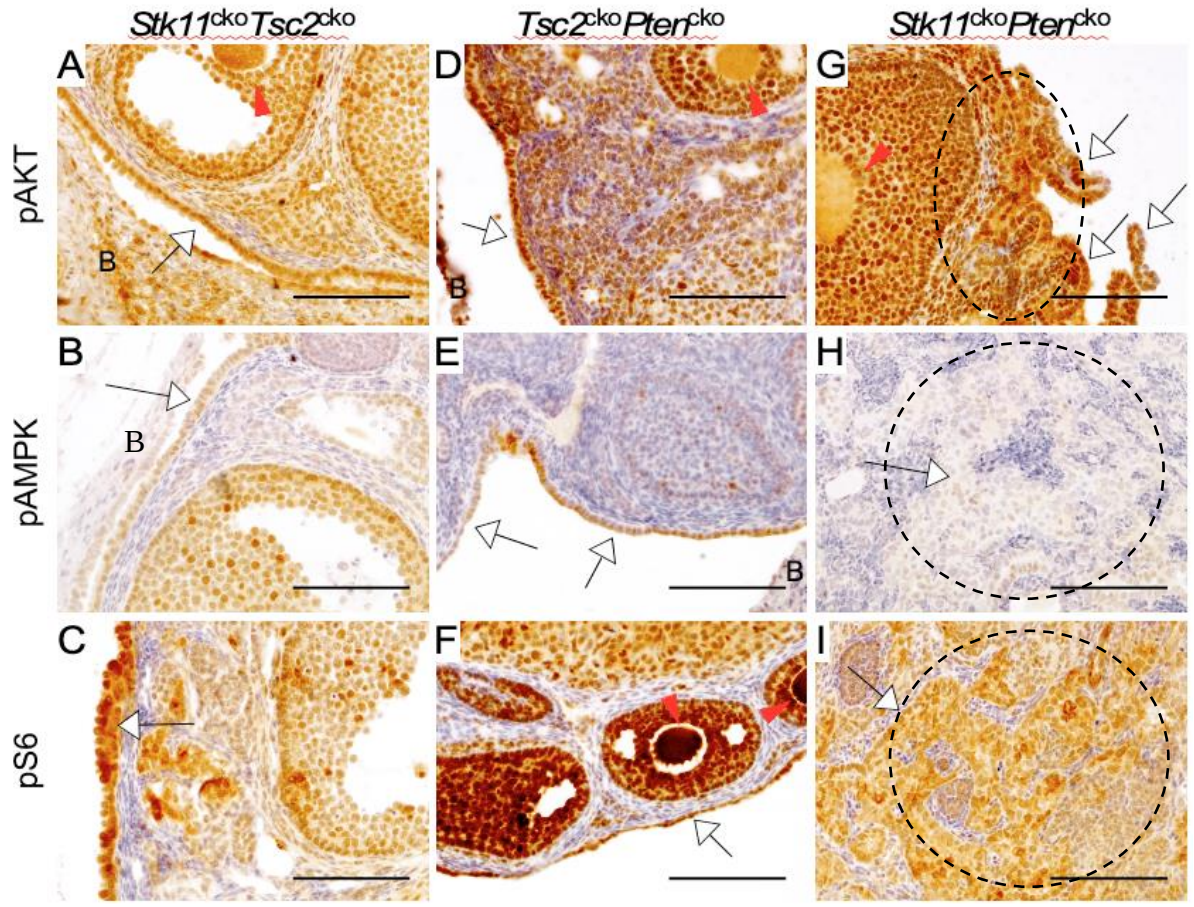

Figure 5

AKT, AMPK, and mTORC1 phosphorylation in *Stk11*^{cko}*Tsc2*^{cko}, *Tsc2*^{cko}*Pten*^{cko}, and *Stk11*^{cko}*Tsc2*^{cko} mouse ovaries. Immunohistochemistry was performed and representative images (n=2 ovaries) are shown for pAKT (A, D, G), pAMPK (B, E, H), and pS6 (C, F, I). White arrows point to ovarian surface epithelium, dashed circles surround the invading serous tumor, and nonspecific staining can be seen in oocytes indicated with red arrows. pAKT can be observed in all mice (A). pAMPK staining is observed in *Skt11*^{cko}*Tsc2*^{cko} and *Tsc2*^{cko}*Pten*^{cko} (B, E), with variability in staining of *Tsc2*^{cko}*Pten*^{cko} shown by the 2 arrows in panel E, but no staining was observed in *Stk11*^{cko}*Pten*^{cko} (H) ovaries. All Cre-expressing cells examined have positive staining of pS6. B marks the bursa. (Scale bars, 100 μm).

Stk11^{cko};*Pten*^{cko} develop ovarian cancer with a papillary serous histotype by 15 weeks of age (Fig 6) and stain positive for the HGSOC markers: CK8, WT1, ERα, and PAX8 [71]. To understand the development of the disease with more granularity, we examined the histology and expression of HGSOC markers at 4, 6, 8-12, and 15-20 weeks by IHC. At 4 weeks old, 3 of 8 ovaries were normal (Figure 6A-B) and 5 of 8 had papillae or cell shedding, and negative for PAX8 (Figure 6C). At 6 weeks old, 2 of 8 ovaries were normal and 6 of 8 had papillae or cell shedding (Figure 6D-E), and negative for PAX8 (Figure 6F). At 8-12 weeks old, 0 of 16 ovaries were normal, 12 of 16 had papillae or cell shedding (Figure 6G-H), and 4 of 16 had developed a papillary serous ovarian histology, and negative for PAX8 (Figure 6I). By 15-20 weeks old, all 10 of 10 ovaries had developed a papillary serous ovarian cancer histology (Figure 6J-K) and, positive for CK8, WT1, and ERα (Supplementary Figure), and 80% were positive for PAX8 (Figure 6L).

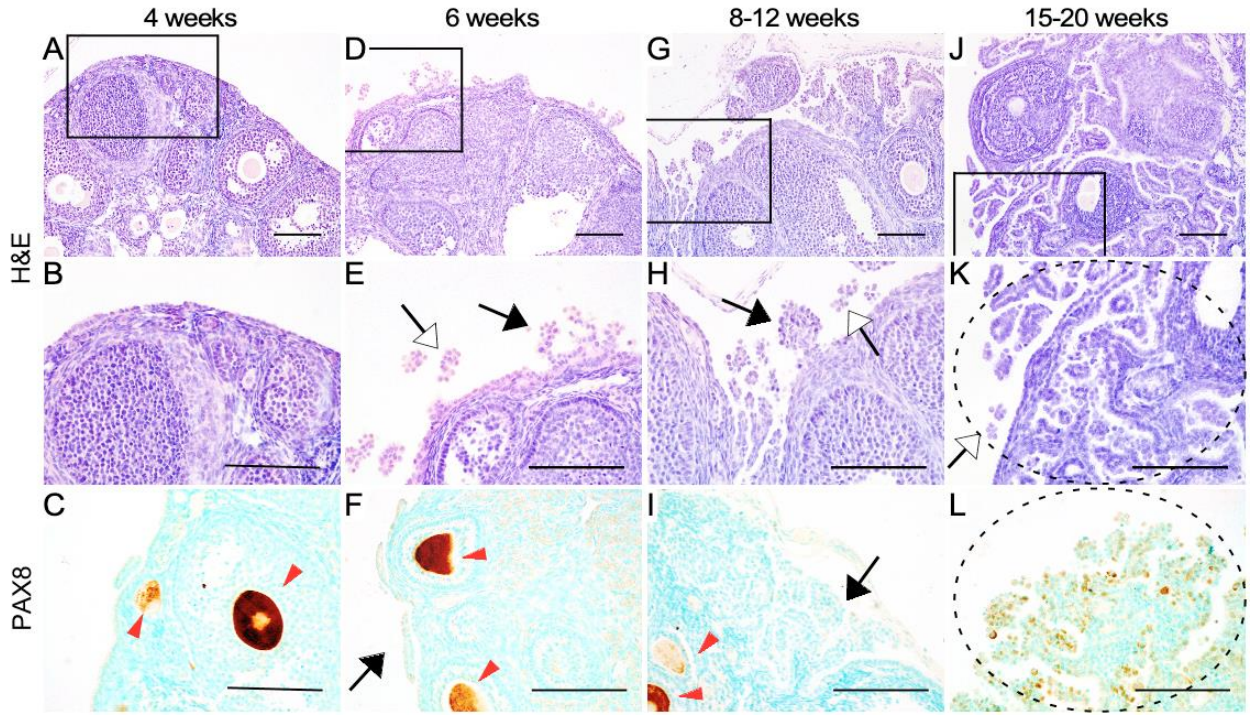

Figure 6

Timeline of tumorigenesis of *Stk11*^{cko}*Pten*^{cko} ovaries. PAX8 expression is observed in 15–20-week-old *Stk11*^{cko}*Pten*^{cko} ovaries. *Stk11*^{cko}*Pten*^{cko} ovaries were collected at (A-C) 4 (n=8), (D-F) 6 (n=8), (G-I) 8-12 (n=16), and (J-L) 15-20 (n=10) weeks of age and analyzed by H&E and PAX8 IHC, as indicated. Representative H&E staining shows evidence of shedding (white arrows) and papillae formation (black arrows) by 6 weeks, postnatal (A-K). Invading papillary serous tumors (surrounded by a dashed circle (K, L)) are observed in 4 of 16 mice at 8-12 weeks postnatal and in 10 of 10 mice at 15-20 weeks postnatal. B, E, H, and K are higher magnification images of outlined areas in A, D, G, and J, respectively. PAX8 expression was not observed by IHC in ovaries 12 weeks and younger, but was observed in ovaries at 8 of 10 15-20 weeks (I-L). Nonspecific staining of oocytes is marked by red arrowheads (C, F, I). (Scale bars, 100 um).

Given that *Stk11*^{cko};*Pten*^{cko} MOSE have activated mTORC1 and unchecked proliferation of MOSE cells *in vivo*, we isolated the cells for primary culture to assay their proliferation rate compared to controls. *Stk11*^{cko};*Pten*^{cko} MOSE proliferate 5 fold faster over 115 hours than *Stk11*^{cko}, *Pten*^{cko}, or controls (Fig 7A and B) showing increased proliferative signaling, characteristic of cancer cells *in vivo*. To characterize these tumor cells further, we performed RNA sequencing. MOSE cells were isolated through a light digestion of ovaries such that MOSE cells would slough off the surface of the ovary with as little digestion of the underlying stromal cells as possible. Only samples with 70-90% epithelial to stromal cell ratios were selected.

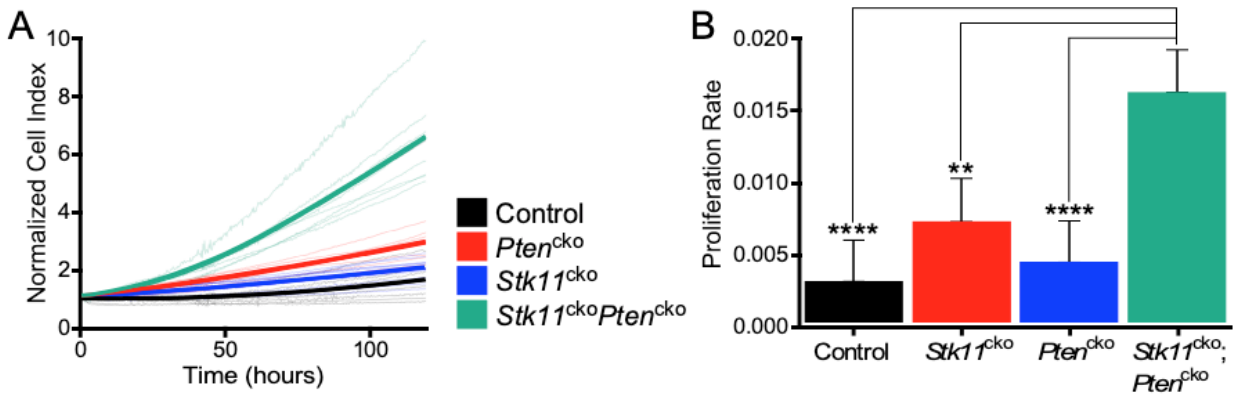

Figure 7

***In vitro* proliferation of *Stk11*^{cko}*Pten*^{cko} , single knockouts, and controls.** *Stk11*^{cko}*Pten*^{cko} MOSE cells proliferate faster *in vitro* compared to controls and single knockouts. Proliferation over 115 hours are shown for control, *Stk11*^{cko}, *Pten*^{cko}, and *Stk11*^{cko}*Pten*^{cko} primary MOSE cells isolated from adult mice; bold lines are the averages of replicates, which can be seen as individual faint lines (A). Proliferation rates were calculated from slopes on a square root scale; data shown with 95% confidence interval upper bound (B). The proliferation rate of *Stk11*^{cko}*Pten*^{cko} MOSE was ~5.6 fold higher than control (95% false coverage interval (FCI) 1.8 – 23.8), 2.3 fold higher than *Stk11*^{cko} (95% FCI 1.3 – 4.3), and 3.8 fold higher than *Pten*^{cko} (95% FCI 1.6 – 10.4); estimated via a hierarchical linear mixed-effects model and Fieller's theorem. *FCI*: false coverage interval, *p<0.001, **p<0.00001.

To confirm knockdown of *Stk11* and *Pten* in our samples, we looked at counts per million and found that while *Stk11* is knocked down in *Stk11*^{cko} and *Stk11*^{cko}*Pten*^{cko} MOSE cells (Fig 8A). *Pten* transcript counts per million are elevated in *Stk11*^{cko} and *Stk11*^{cko}*Pten*^{cko} MOSE cells equivalent to control in *Pten*^{cko} (Fig 8B). These take into account the read pileups for the entire gene. Since only exons 3-6 are knocked out in *Stk11* and exon 5 of *Pten* to cause loss of protein [71], we looked at the read pileups for the entire gene focusing on the knocked out exons. The exons knocked out in our mice are enclosed in boxes in Figure 8 C-D. In exons 3-6 of *Stk11,* transcript counts per million is knocked down in *Stk11*^{cko} and *Stk11*^{cko}*Pten*^{cko} MOSE cells (Fig 8C). In the knocked-out exon 5 of *Pten,* transcript counts per million are elevated in *Stk11*^{cko} and knocked down in *Pten*^{cko} and *Stk11*^{cko}*Pten*^{cko} MOSE cells (Fig 8D).

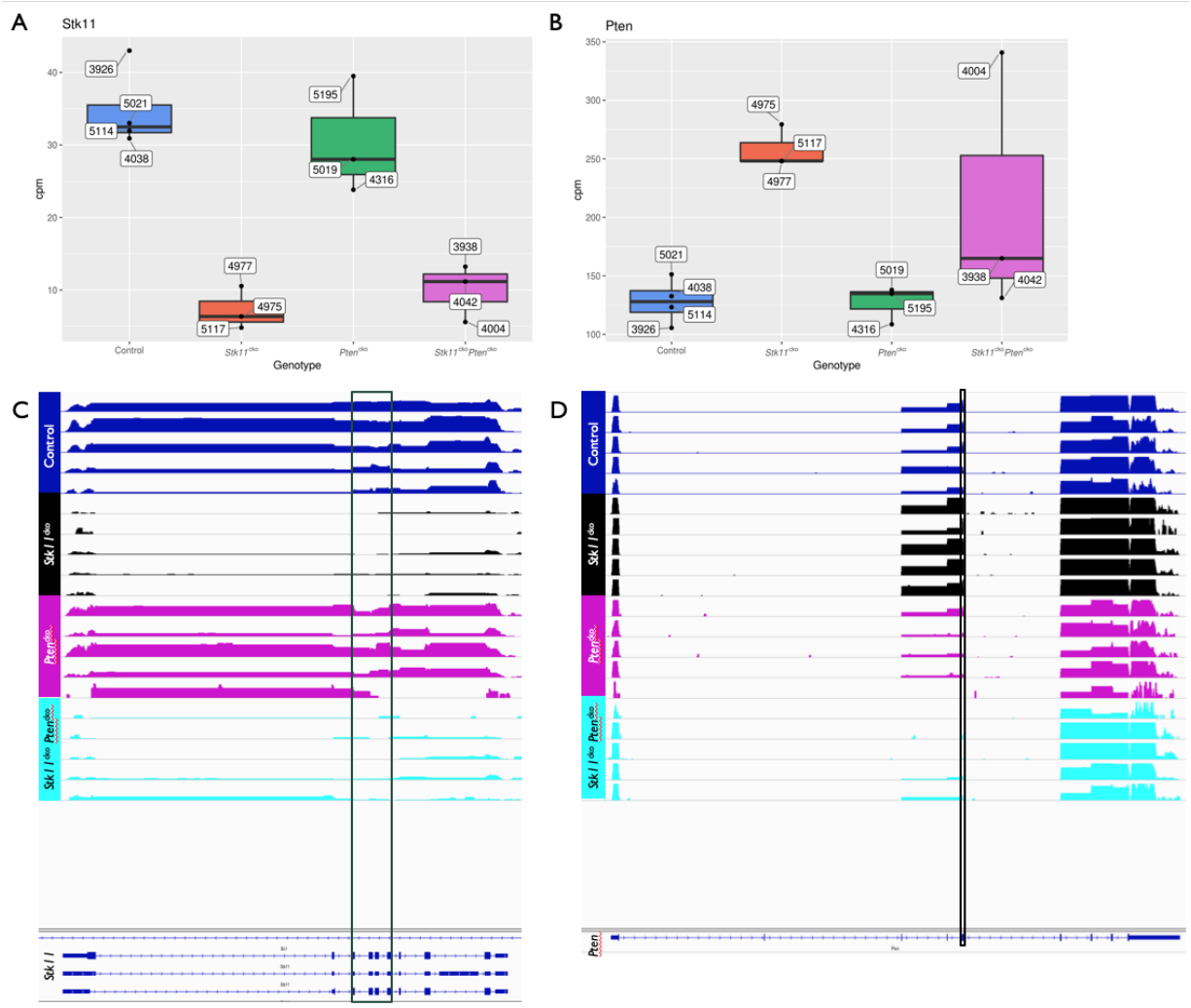

Figure 8

Confirmation of knockdown of *Stk11* and *Pten*. *Stk11* transcript counts per million is knocked down in *Stk11*^{cko} and *Stk11*^{cko}*Pten*^{cko} MOSE cells (A). *Pten* transcript counts per million are elevated in *Stk11*^{cko} and *Stk11*^{cko}*Pten*^{cko} MOSE cells equivalent to control in *Pten*^{cko} (B). These take into account the read pileups for the entire gene. The exons knocked out in our mice are enclosed in boxes in C-D. In the knocked-out exons 3-6 of *Stk11*, transcript counts per million is knocked down in *Stk11*^{cko} and *Stk11*^{cko}*Pten*^{cko} MOSE cells (C). In the knocked-out exon 5 of *Pten*, transcript counts per million are elevated in *Stk11*^{cko} and knocked down in *Pten*^{cko} and *Stk11*^{cko}*Pten*^{cko} MOSE cells (D).

Stk11^{cko};*Pten*^{cko} cells cluster together and away from the 3 controls by principle component analysis (Fig 9A). There are over 3000 genes that are differentially expressed between *Stk11*^{cko};*Pten*^{cko} and control while there are very few differences between *Pten*^{cko} and control (Figure 9B). The highest fold change differentially expressed genes between *Stk11*^{cko} and control (Figure 9C), *Stk11*^{cko};*Pten*^{cko} and control (Figure 9D), and *Pten*^{cko} and control (Figure 9E) are shown in heat maps where blue represents downregulated genes and red represents upregulated genes. Unsupervised hierarchal cluster analysis of the top 500 and 1000 differentially expressed genes for all comparisons (Anova like) can be found in appendix A (Figures 12-13). GSEA were performed for all comparisons (Figures 15-20). Since there were not significant differences between left and right ovaries from the same animal, those ovaries were treated as technical replicates in the analysis. placental-specific protein 1 (Plac1), keratin 17 (Krt17), metastasis associated in colon cancer (Macc1), and msh homeobox 2 (Msx2) are all significantly upregulated in *Stk11*^{cko};*Pten*^{cko} compared to control (Figure 9F-I) and are found in the upper right quadrant of the volcano plot in appendix A (Figure 14). Macc1, Msx2, and Plac1 are amplified or upregulated in 5-10% of cases of HGSOC according to the TCGA database, but did not exclusively cooccur with *STK11* and/or *PTEN* deletion. All four genes are implicated in playing a pro-tumorigenic role in the literature [106-119]. Additional data analysis can be found in appendix A

*

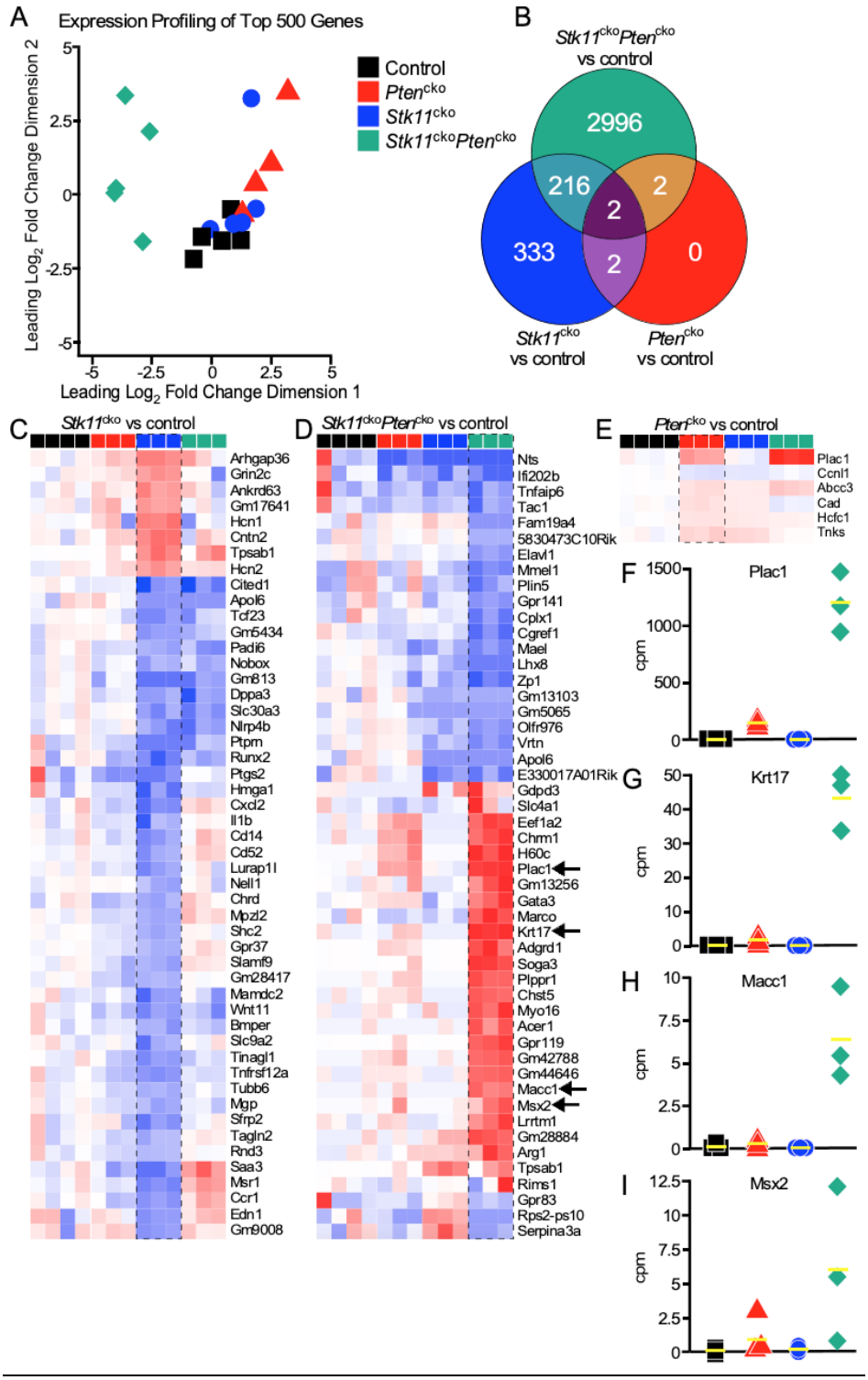

Figure 9

***Stk11*^{cko}*Pten*^{cko} MOSE cells and have vastly different gene expression profiles compared to controls and single knockouts.** RNA sequencing was performed on primary MOSE cells

Figure 9 (cont'd)

isolated from 15+ week old Control (n=5), *Stk11*^{cko}(n=5), *Pten*^{cko} (n=5), and *Stk11*^{cko}*Pten*^{cko} (n=5) mice. *Stk11*^{cko}*Pten*^{cko} MOSE cluster together and away from other groups in a principal component analysis (A). Venn diagram shows that there are over 3000 significant ($q<0.05$), differentially expressed genes (DEGs) between *Stk11*^{cko}*Pten*^{cko} and control and 551 DEGs between *Stk11*^{cko} and control, but only 6 DEGs between *Pten*^{cko} and control (B). Upregulated genes are shown in red and downregulated genes are shown in blue in the heat map of the top 50 significant ($q<0.05$), DEGs between *Stk11*^{cko} and control (C), *Stk11*^{cko}*Pten*^{cko} and control (D), and all of the significant ($p<0.05$) DEGs in *Pten*^{cko} compared to control are shown in (E). Genes of interest are marked by an arrow and CPM values for each are plotted (F-I).

Examination of the RNA-sequencing data, we found that the levels of *Pten* mRNA reads are two-fold higher in *Stk11*^{cko} ovaries compared to controls (Fig 10A). Immunohistochemical analysis of PTEN in *Stk11*^{cko} and control ovaries (N=3) confirmed that PTEN expression is induced when *Stk11* is deleted from the OSE (Fig 10B-E). PTEN was first found to be a potent tumor suppressor of the PI3K/AKT pathway through its dephosphorylation of PIP3 to PIP2 acting in direct opposition to the activation of AKT [87]. Downstream signaling pathways from activated AKT prevent apoptosis signaling and promotes cell growth, so loss of PTEN activated AKT signaling pathways and promotes tumorigenesis [91, 120]. Recent studies have shown that in addition to its tumor suppressor role at the cell membrane, it may also play a role in maintaining the stability of the genome through physical interaction with centromeres and regulation of DNA repair [89]. Without PTEN, cells were found to have a greater frequency of DSBs and less genomic stability[89, 121]. We used Gene Set Enrichment Analysis (GSEA) to investigate PTEN's nuclear DNA repair role and found a significant correlation between the gene set of *Stk11*^{cko}*Pten*^{cko} and *Stk11*^{cko} RNA-seq results and several pathways associated with DNA repair (Fig 10F). These results suggest that induced PTEN expression has a tumor suppressor effect in the Stk11-deleted OSE, perhaps by inducing its DNA repair activity.

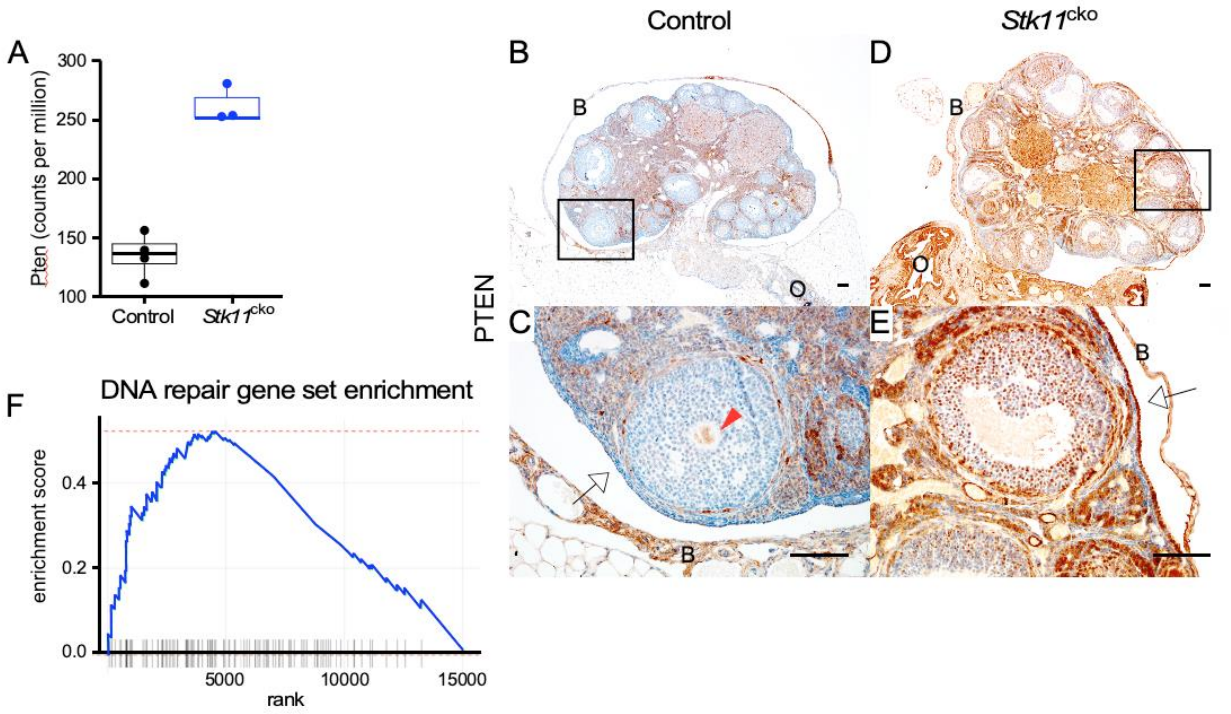

Figure 10

PTEN expression is induced when *Stk11* is deleted, which may play a role in maintenance of genome integrity. *Pten* transcript levels in the RNA-seq analyses are 1.01 log fold higher in *Stk11*^{cko} compared to control (A). The box encapsulates the first and third quartiles, the band is the median and the end of the whiskers represent the minimum and maximum. Representative ovaries are shown of control (B,C) and *Stk11*^{cko} (D,E) stained for PTEN expression. Panels C and E are higher magnification images of boxed areas in B and D, respectively. White arrows point to OSE. B marks the bursa and O marks the oviduct. (Scale bars, 100 um). Gene Set Enrichment Analysis shows that the DNA Repair reactome pathway significantly correlates with DEGs between *Stk11*^{cko}*Pten*^{cko} and *Stk11*^{cko} (F).

2.4 Discussion

Both the identification of the origins of ovarian cancer as well as the modeling of those origins through genetically engineered mouse models (GEMMs) have been hurdles to the advancement of the ovarian cancer field. Most often, serous ovarian cancer is diagnosed in women after metastasis throughout the peritoneal cavity has occurred. The origin of the disease had traditionally been thought to be the OSE and there have been many GEMMs, including ours [71], that have recapitulated that through the deletion of key tumor suppressor genes in the OSE. Using a Cytokeratin 18 promoter driven Cre, Szabova *et al.* showed that loss of *Tp53, Rb, Brca1* or *Brca2* in OSE cells causes development of metastatic ovarian serous carcinomas [74]. Unlike 99% of human ovarian serous carcinomas, most of those murine tumors did not express PAX8 [74, 122].

PAX8 is a marker normally expressed in FTE. This is one of the reasons the FTE was proposed to be another cell of origin for HGSOC. Discovery of serous tubal intracellular carcinomas (STICs) in the FTE of Brca1 positive patients with induced p53 expression further strengthened this hypothesis. GEMMs with FTE origin were subsequently developed. Various groups have successfully modeled the disease in mice by deleting *Brca*, *Tp53*, and *Pten* in the FTE [5, 73]. Strong evidence supporting both origins suggests that both FTE and OSE may give rise to serous ovarian tumors [66, 123]. Deciphering the difference between tumors originating from these two origins has been a recent topic of interest that will lead to better treatment and prevention strategies for patients. Through the development of *Trp53*$^{R172H/Fl}$;T121 OSE and FTE orthotopic allografted organoids, Zhang and colleagues were able to study the effects of origin on the development of tumors [124]. Even though the driving mutations were identical, OSE origin led to a more proliferative subtype, enhanced DNA damage pathway, longer survival, and

more resistance to standard in-vitro chemotherapy whereas, FTE origin led to a more mesenchymal subtype with enhanced P53 signaling, shorter survival, and greater sensitivity to chemotherapy [124]. These tumors continue to express PAX8 since they originate from FTE [124].

Our *Stk11*^{cko};*Pten*^{cko} mouse model shows us that PAX8 expression can be induced in OSE cells (since Amhr2 is not expressed in FTE) and that PAX8 does not appear to be a driver of early disease. Since early disease is difficult to detect in women, we often don't see the progression or know the origin. Our mouse model acts like a time machine and shows us that there is clear development over time in the OSE with PAX8 expression getting turned on once the cells have already invaded into the parenchyma of the ovary, suggesting that PAX8 expression could be the result of metaplasia. Further investigation of models using the OSE origin are important for illuminating possible treatment options for women whose ovarian cancer has originated there.

Widespread copy number alterations are a hallmark of serous ovarian cancer and is often attributed to the loss of DNA repair mechanisms, therefore making the loss or gain of genes a passenger effect [10]. We have shown that *Pten* loss, when combined with the deletion of *Stk11*, induces cancer progression and severity indicating that the loss of multiple tumor suppressor genes in the same pathway may have cumulative tumorigenic effects. We hypothesized that different combinations of loss of tumor suppressor genes upstream of mTORC1 would recapitulate our *Stk11*^{cko}*;Pten*^{cko} OSE GEMM. However, deleting other combinations of these genes (*Stk11*^{cko}*;Tsc2*^{cko} and *Tsc2*^{cko}*;Pten*^{cko}) is not sufficient to drive transformation in our mice. Both decrease of pAMPK with deletion of *Stk11* and increase of pAKT with deletion of *Pten* are necessary to drive the development of serous ovarian cancer. Because all three mouse

models show mTORC1 activity though the increase of pS6, the development of serous ovarian cancer in our mice does not solely depend on mTORC1 activity.

Beyond the differences we see in phenotype in the mice, *Stk11*^{cko}*;Pten*^{cko} cells proliferate faster than single mutants and control cells and also have a unique expression profile. Genes that are significantly upregulated in the double mutant cells have also found to be upregulated in other carcinomas. Placental-specific protein 1 (Plac1) is a gene that encodes a microvillous membrane protein that is normally only found in trophoblast cells of the placenta of the pregnant female as well as the adult testis of the male [125]. Under malignant conditions, it is found to be re-expressed in biopsies of ovary [109], endometrium [109], breast [113, 126, 127], colon [127-129], stomach [130], prostate [112], liver [110], and lung [131, 132] cancers. It may play a role in maintaining an immune-tolerant microenvironment through inflammatory and immunoregulatory chemokines in the stromal microenvironment [125]. Plac1 was highly upregulated in both *Pten*^{cko} versus control as well as *Stk11*^{cko};*Pten*^{cko} versus control. It is a microvillous membrane protein that is highly expressed in placental trophoblasts and, besides low expression in testis, is not present in adult tissue [111]. It has been reported to be expressed in over 50% of human cancer cell lines and had been found to be expressed in EOC [131, 133]. P53 has been found to repress PLAC1 transcription *in vitro* by binding to a putative p53 binding site in the PLAC1 promoter [134]. Mutant P53 is associated with PLAC1 expression in serous OvCa and may allow for PLAC1 transcription because it is no longer able to bind to the PLAC1 promoter [108]. In breast cancer, Plac1 is capable of suppressing PTEN activity and inducing AKT activity [114, 125]. Interestingly in our data, we show that knocking out PTEN induces the expression of PLAC1. Keratin 17 (Krt17) encodes a type 1 intermediate filament chain keratin

17 normally expressed mostly in basal epithelial cells. As an intermediate filament, it an regulate cell growth and proliferation and its aberrant expression can be found in cervical, breast, squamous, gastric, and oral cancers [106]. MET transcriptional regulator (Macc1) is transcriptional activator of hepatocyte growth factor receptor (MET) and activates the hepatocyte growth factor (HGF)-MET pathway. It was identified in 2009 as being significantly upregulated in colon cancer and has since been shown to and since been shown to be involved in pro-malignant pathways of cell growth, epithelial to mesenchymal transition (EMT), angiogenesis, cell motility, invasiveness, and metastasis in an array of cancers including ovarian cancer [116-119]. Msh Homeobox 2 (Msx2) is a homeobox (HOX) gene whose expression pattern is pivotal in normal development of organs, thought to be a downstream target of RAS signaling, and its overexpression has been found in many epithelial cancer cell lines [135]. In Pancreatic cancer, it is associated with EMT through Twist1 expression [115].

Pten transcripts and protein expression were found to be more abundant in $Stk11^{cko}$, which could point to a compensatory mechanism within the mTORC1 pathway. When both are deleted, the brakes are completely removed and invasion into the ovary occurs. While $Pten^{cko}$ mice never developed papillary serous OvCa and the proliferation rate of $Pten^{cko}$ MOSE cells were similar to that of control MOSE cells, we were surprised to find only 6 genes differentially expressed between $Pten^{cko}$ MOSE cells and control. Loss of PTEN in mouse oviductal epithelium resulted in much greater gene expression changes including upregulation of non-canonical WNT pathway genes [136]. However, $Pten^{cko}$ clearly contributes significantly to gene expression in the context of $Stk11^{cko}$ as there are nearly ten times more altered genes in $Stk11^{cko}Pten^{cko}$ versus control compared to $Stk11^{cko}$ versus control. In addition to its established

tumor suppressor role through PI3K in the cytoplasm, PTEN can also maintain genomic stability in the nucleus [121, 137]. In PTEN-null endometrial adenocarcinoma (EndoCA) cells, higher levels of DNA damage response were observed through positive γH2AX expression [138]. Investigators in our lab then set out to determine whether adding nuclear PTEN could protect against DNA damage in PTEN-null EndoCA cells. Cells were first transfected with GFP fusion constructs with either control, PTEN wild type, PTEN with a nuclear localization signal, or PTEN with a nuclear export signal. These cell models were then treated with Zeocin, which causes DSB [139]. After a 24-hour recovery, they found that cells with nuclear PTEN present had significantly less DNA damage than controls [138]. Hypothesizing that the loss of PTEN in our mouse model would also contribute to greater DNA damage, we investigated gene sets significantly altered between *Stk11*^{cko}*Pten*^{cko} and *Stk11*^{cko} (isolating changes in gene expression because of *Pten* deletion). Within this comparison, we found several DNA repair pathways that were significantly altered. If PTEN loss was only contributing to mTORC1 activation through AKT, we would expect *Stk11*^{cko};*Tsc2*^{cko} mice to develop papillary serous OvCa. This finding of altered DNA repair pathways indicates that PTEN's nuclear role as a guardian of the genome is fundamental to the tumorigenesis in these mice. The development of papillary serous ovarian cancer in our *Stk11*^{cko};*Pten*^{cko} mouse model but not in any single deletion, *Stk11*^{cko};*Tsc2*^{cko}, or *Tsc2*^{cko};*Pten*^{cko} mice or in *Stk11*^{cko};*Tsc2*^{cko} double mutant mice highlights the synergistic effect of loss of *Stk11* and *Pten* and PTEN's important DNA repair role.

2.5 Methods

Mouse genetics and animal husbandry

All animal experimentation protocols used in this study were approved by the Michigan State University Institutional Animal Care and Use Committee and are in compliance with the NIH Guide for the Care and Use of Laboratory Animals. Mice used in this study were kept in standard housing conditions and were maintained on a mixed genetic background (C57BL/6;129/SvEv). These mice strains: *Amhr2-cre* [140], $Stk11^{tm1Rdp}/Stk11^{fl/fl}$ [141], $Tsc2^{fl/fl}$ [142] and $Pten^{fl/fl}$ [143] were mated to produce *Cre*-null controls, $Amhr2\text{-}cre/+;Stk11^{\Delta/\Delta}$ (referred to as $Stk11^{cko}$), $Amhr2\text{-}cre/+;Pten^{\Delta/\Delta}$, (referred to as $Pten^{cko}$), $Amhr2\text{-}cre/+;Stk11^{\Delta/\Delta};Pten^{\Delta/\Delta}$, (referred to as $Stk11^{cko}Pten^{cko}$). $Amhr2\text{-}cre/+;Stk11^{\Delta/\Delta};Tsc2^{\Delta/\Delta}$ (referred to as $Stk11^{cko}Tsc2^{cko}$), $Amhr2\text{-}cre/+;Tsc2^{\Delta/\Delta};Pten^{\Delta/\Delta}$ (referred to as $Tsc2^{cko}Pten^{cko}$). Tail biopsies were collected for genotyping, and PCR conditions for *Stk11*, *Tsc1*, *Tsc2* and *Pten* alleles have been described [141, 143-145] and deletion was confirmed in the RNA-seq analyses by pileup of the reads. Ovaries were collected postmortem for histological examination. Gross images of the tumors were taken using a Nikon D60 digital camera and macro lens.

Histology and immunohistochemistry

Tissues were fixed, processed and sectioned as previously described [144, 146]. 7-micron sections were cut from paraffin-embedded blocks for standard histological analysis with hematoxylin and eosin staining and for immunohistochemistry. The following primary and secondary antibodies were used for immunohistochemistry (IHC): cytokeratin 8 (TROMA-I AB_531826, Developmental Studies HybridomaBank, IA), PAX8 (10336-1-AP Proteintech group, Chicago, IL), and ɣ-H2AX (ab11174 abcam, Cambridge, MA). AlexaFluor secondary

antibodies (Invitrogen, Carlsbad, CA) or biotinylated donkey anti-mouse or anti-rabbit F_{ab2} (Jackson ImmunoResearch Laboratories, West Grove, PA). Images were taken with a Nikon Eclipse Ni microscope fitted with Nikon DSF12/DS-Q1MC cameras.

Primary ovarian surface epithelial cell isolation from mouse ovaries

Mouse OSE (MOSE) cells were collected from whole ovaries using a method developed by Gamwell et. Al. [147]. Briefly, ovaries were collected from mice of the indicated genotype postmortem, washed 3 times with HBSS, digested at 37˚C for 40 min in collagenase/dispase digestion media, lightly agitated to release MOSE cells. For xCELLigence proliferation studies, MOSE cells were pooled and plated. For RNA-seq transcriptome analyses, ovaries were collected individually and 10% of each sample was plated for epithelial to stromal cell ratio analysis, 10% was counted, and 80% was stored in RNAlater.

xCELLigence proliferation

4,500 cells/well were plated on electronic microtiter plates (E-Plates®) and cell proliferation index was measured through impedance using the real time cell analysis (RTCA) software every 15 min for 5 days. Proliferation rates were modelled using R v3.6.0 (https://cran.r-project.org/) and a hierarchical linear mixed-effects model (LMM) with technical replicate random intercepts nested within biological replicates [148]. The between group variance was assumed to be non-constant [148, 149]. The dependent variable, normalized cell index, was square-root transformed to improve the normality of the residuals. Benjamini-Hochberg adjusted linear contrasts were used to test for group differences in proliferation rates and Fieller's theorem was used to estimate the ratio of proliferation rates between groups [150]. All hypotheses were two-sided with false discovery rate <5% considered significant.

RNAsequencing and Bioinformatic Analysis

Samples were selected that had 70-90% epithelial to stromal cell ratios. RNA was isolated using the Qiagen RNAmicro kit. (details of RNA-seq to be filled in yet) PolyA tails were clipped off using cutadapt and TrimGalore! There was only a small fraction of reads (<5%) that were trimmed. However, the notable gains made are in the overall alignment rates. Alignments to the standard mm10 reference genome and transcript quantification was done using a two-pass approach using STAR, whereby reads were aligned first using known annotations/splice junctions and second using known and learned splice junctions from the first pass, yielding a more specific alignment. Overall alignment rates were high (>80%) for most samples. Uniquely aligned reads were analyzed for a range of metrics prior to differential expression with the edgeR and limma/voom packages in R. Library sizes were normalized using the trimmed mean of M-values (TMM) prior to voom transformation and plotting. Further, low counts were filtered using the following criteria: >1 count per million (CPM) in at 5 samples (corresponds to at least the animals found in one biological condition). Since there were not significant differences between left and right ovaries from the same animal, those ovaries were treated as technical replicates in the analysis.

CHAPTER 3: SUMMARY AND CONCLUSIONS

The information presented in this dissertation explores various mouse models of papillary serous OvCa and more specific treatment options for women diagnosed with HGSOC. In this body of work, I bred and examined many mice of different conditional knockout genetic combinations (*Stk11*^{cko}, *Pten*^{cko}, *Stk11*^{cko}*Pten*^{cko}, *Stk11*^{cko}*Tsc2*^{cko}, *Tsc2*^{cko}*Pten*^{cko}, *Tsc2*^{cko}*Pten*^{cko}*Tp53*^{cko}, and *Stk11*^{cko}*Pten*^{cko} through IP Ad-*Cre* injection) most of which were novel GEMMs. Through collaborations outside the ovarian cancer field, we tested the feasibility and efficacy of MIS and DNaseX as novel treatment options for HGSOC.

In our first study, papillary serous OvCa histology only developed with deletion of *Stk11* and *Pten*. These tumors turn on expression of PAX8 in most 15-20WOA ovaries indicating that PAX8 is acquired during transformation of OSE cells. This is a significant finding that provides evidence for the OSE origin of HGSOC. Because PAX8 is expressed in normal FTE but not normal OSE, this is one line of evidence used to lineage trace HGSOC to FTE [101]. We use *Amhr2* to drive *Cre* expression in our tissue specific knockout mouse model, and *Amhr2* is turned on in OSE but not FTE, so we have shown that OSE can turn on expression of PAX8 in HGSOC progression. The fact that PAX8 gets turned on only after 15 WOA shows us that it is not an early driver of differentiation. However, PAX8 may also play a pro-oncogenic role. Forcing PAX8 expression in MOSE cells drives proliferation, migration, cell survival [151, 152]. In a proteomic analysis of PAX8 overexpression in MOSE cells, Hardy and coworkers found that PAX8 expression drove a migratory phenotype in MOSE cells [153]. They observed upregulation of N-Cadherin (CDH2), implicated in EMT, and actin filaments ACTN1 and ACTN4, drivers of adherens junctions in MOSE cells with forced PAX8 expression [153]. In our RNAsequening data set of *Stk11*^{cko};*Pten*^{cko} MOSE versus control MOSE, CDH2, ACTN4

and several other drivers of adherens junction are significantly upregulated. Table 3 lists these genes from our data set that overlap with upregulated genes found in both the transcriptome and proteome data sets of MOSE-PAX8 cells[153]. Because PAX8 is expressed in HGSOC regardless of FTE origin (where it is natively expressed) or OSE origin (where PAX8 is turned on in malignant transformation), it could be an effective drug target for all HGSOC [69, 71, 154].

Table 3

Drivers of adherens junctions in LP vs C MOSE and PAX8-MOSE

Gene name	**logFC**	**Pvalue**
CDH2	1.32816274	0.00035895
ACTN4	0.70408419	0.00467889
IQGAP1	0.7057243	0.00222438
VCL	1.0347401	0.00768384
SMAD2	0.51700118	0.04849562
TJP1	1.36991308	0.00012615
CTNND1	1.32816274	0.00035895
CTNNA1	0.83924128	0.0005317
ACTG1	0.72693142	0.01336671
CDC42	0.5814476	0.01242422
WASF2	1.480227	2.37E-05

When we performed RNA sequencing, one interesting piece of information was that *Pten* transcripts are twice as abundant in *Stk11*^{cko} versus control suggesting a compensatory mechanism inhibiting uncontrolled growth. GSEA of *Stk11*^{cko}*Pten*^{cko} versus *Stk11*^{cko} indicates many DNA repair pathways are dysregulated. Together, these results highlight the important roles that *Pten* and *Stk11* deletion play in HGSOC and provide evidence to further investigate therapies that target these pathways. The RNA sequencing data provides a rich environment to delve deeper into. Any genes of interest including Plac1, Krt17, Macc1, and Msx2 should be confirmed to be upregulated in *Stk11*^{cko}*Pten*^{cko} MOSE versus control through RT-PCR. Then functional studies could be performed to knockdown those genes *in vitro* to determine if they have any effect on cell proliferation.

In the second investigation in appendix B, we created 2 additional novel GEMMs for HGSOC that may more closely mimic HGSOC in women. *Tsc2*^{cko}*Pten*^{cko}*Tp53*^{cko} importantly includes a deletion of *Tp53* early in development. Ad-*Cre Stk11*^{cko}*Pten*^{cko} mice are a very promising model of HGSOC since it presented with the classic cauliflower appearance of tumors, metastasis throughout the peritoneal cavity, and accumulation of ascites fluid [10]. Another feature that makes this model more realistic is that deletions occur after sexual maturity and not during fetal development when Cre is expressed under the Amhr2 promoter in our first HGSOC GEMM. What makes these models less feasible for studying HGSOC is the time and money investment to create them. Selectively breeding mice to get a triple conditional knockout takes many generations and rounds of genotyping to establish a breeding pair that, at best, gives you your desired genotype 1/8 of the time. The Ad-*Cre Stk11*^{cko}*Pten*^{cko} require less selective breeding but take over a year to develop the HGSOC phenotype observed. Future investigation into the HGSOC marker status and *in vivo* and *in vitro* tumorigenic potential of these cells would

better establish these novel mice as HGSOC GEMMs as well as increasing the number of mice examined.

In the last study in appendix C, we investigated the treatment potential of MIS and DNaseX. While neither showed robust results in our *Stk11*^{cko}*Pten*^{cko} mice or OVCAR3 xenografts *in vivo*, respectively, those concepts are worth further exploration due to limitations in our studies. Importantly, we developed an effective live in vivo imaging model to track metastasis in mice. This method widely applies to any transducible metastatic human cancer cell line and can be used to track the efficacy of any treatment over time.

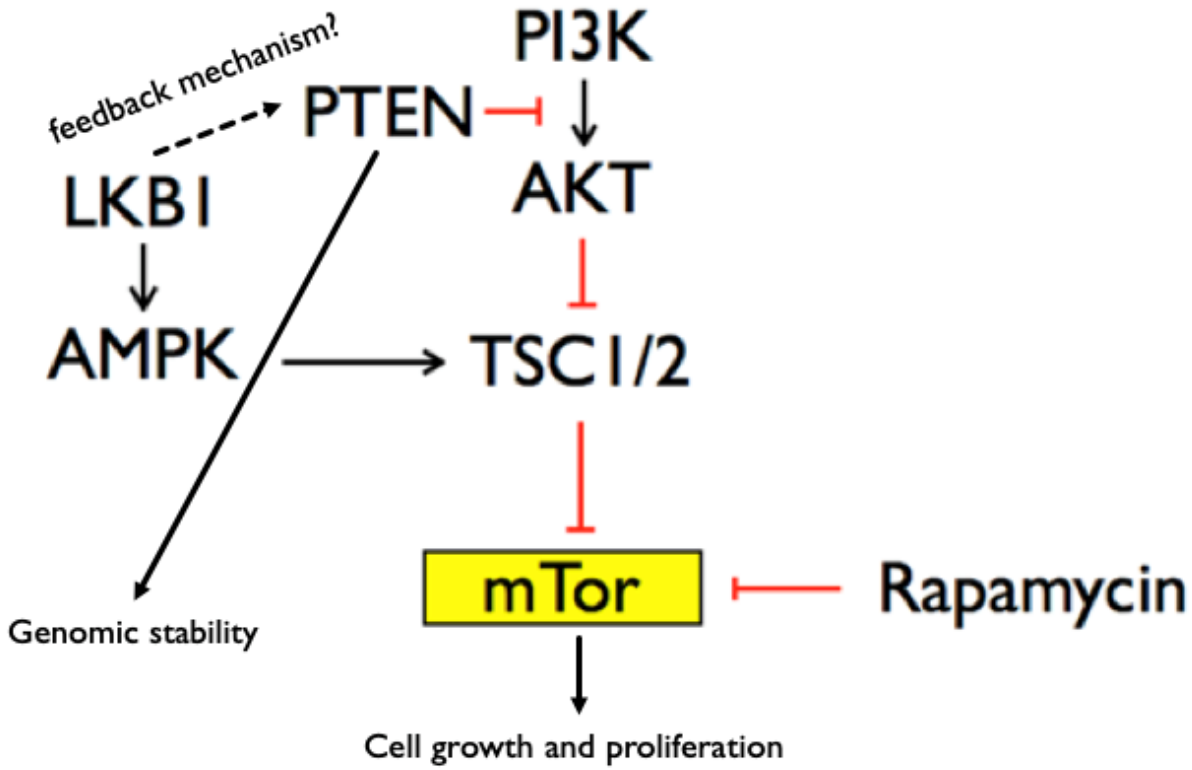

Figure 11

LKB1 and PTEN pathway to papillary serous ovarain cancer. Both LKB1 and PTEN play a role in development of papillary serous OvCa in our mice. Loss of *Stk11* causes upregulation of *Pten*, but when both are lost, papillary serous OvCa develops. PTEN is also playing an important role in genomic stability.

Through activation of mTORC1 and by disrupting DNA repair pathways either through the deletion *Tp53* or *Pten*, we have established several mouse models of papillary serous ovarian cancer. These insights suggest that combination therapy with Rapamycin, an mTORC1 inhibitor, or Olaparib, a PARP inhibitor may be advised for women whose tumors have activated mTORC1 or deletion of *Pten*. Thiostrepton, a chemical inhibitor of PAX8 protein stability, could be used to therapeutically inhibit PAX8 and holds promise to inhibit the aggressiveness of the HGSOC tumor [153]. To find better targeted therapies for women with HGSOC, we must find and exploit what is unique about HGSOC cells. This allows us to more specifically and effectively kill HGSOC cells while preserving surrounding healthy cells to reduce adverse side effects. While treatments like MIS and DNaseX need further study to test efficacy, both apply this concept well. MIS specifically target HGSOCs by binding to Amhr2 receptors on HGSOC cells. DNaseX would use a *Pax8* promoter to drive its expression in HGSOC cells. Better understanding of the disease is vital for providing evidence to explore novel, more effective, and more specific treatment options for women facing a diagnosis of ovarian cancer.

APPENDICES

APPENDIX A

Deletion of LKB1 and PTEN synergistically transform mouse ovarian epithelial cells to papillary serous ovarian cancer additional figures

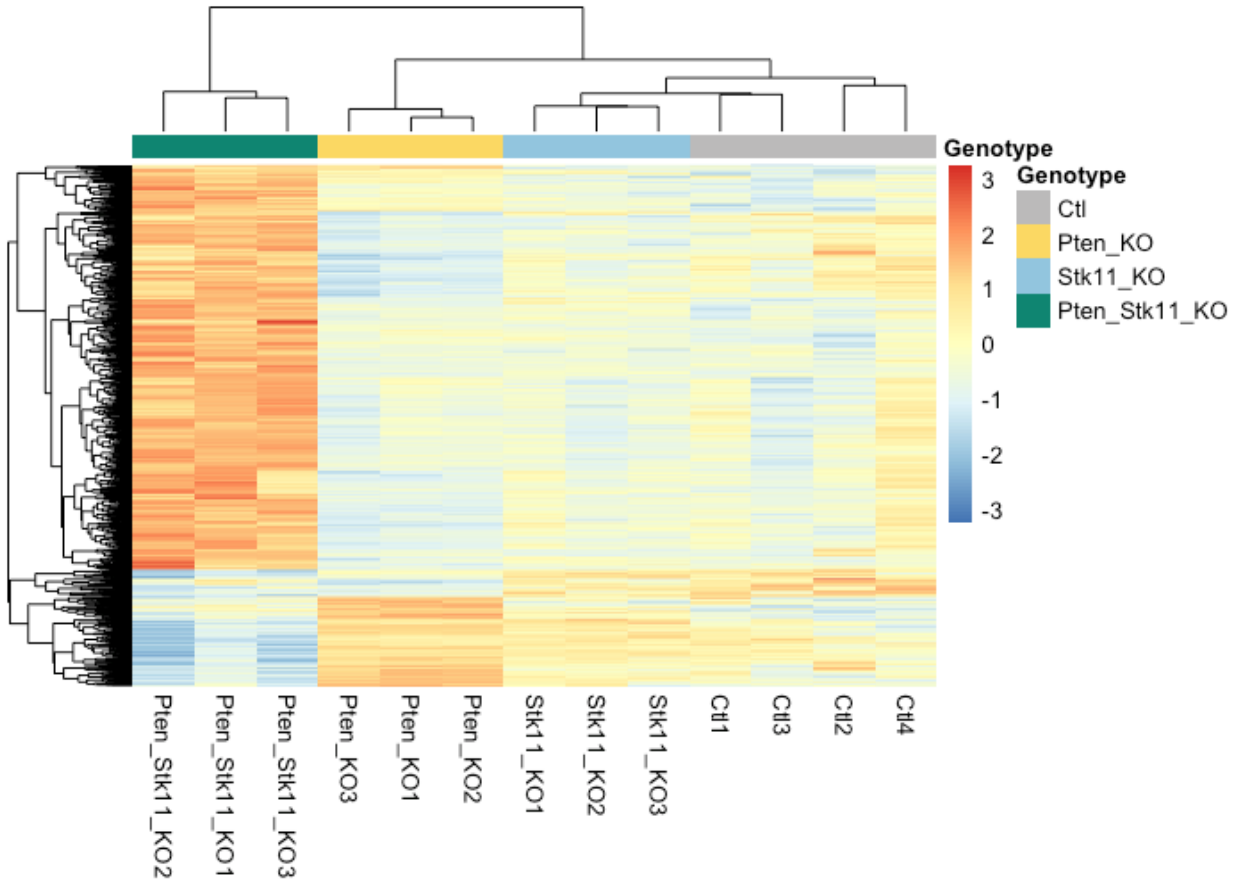

Figure 12

Unsupervised hierarchal cluster analysis of the top 500 differentially expressed genes for all comparisons (Anova like).

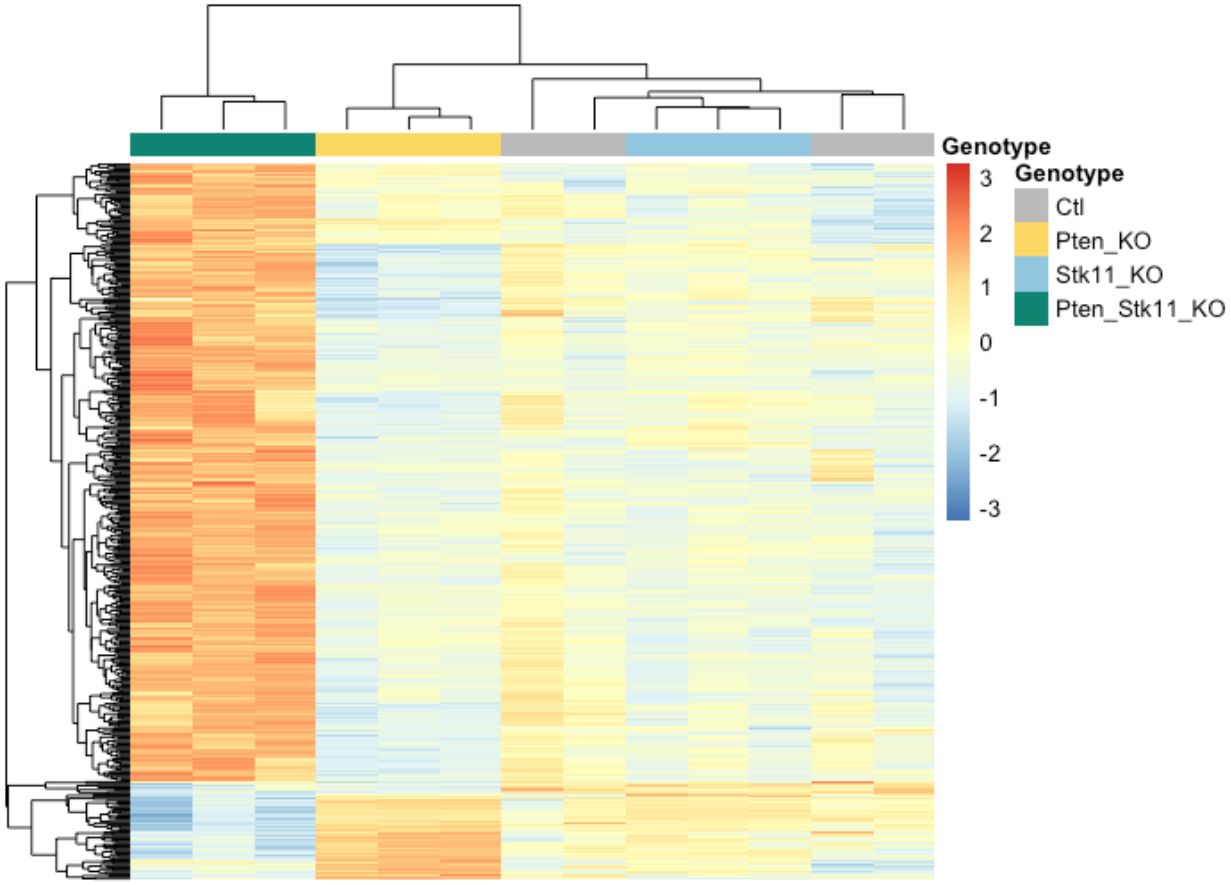

Figure 13

Unsupervised hierarchal cluster analysis of the top 1000 differentially expressed genes for all comparisons (Anova like).

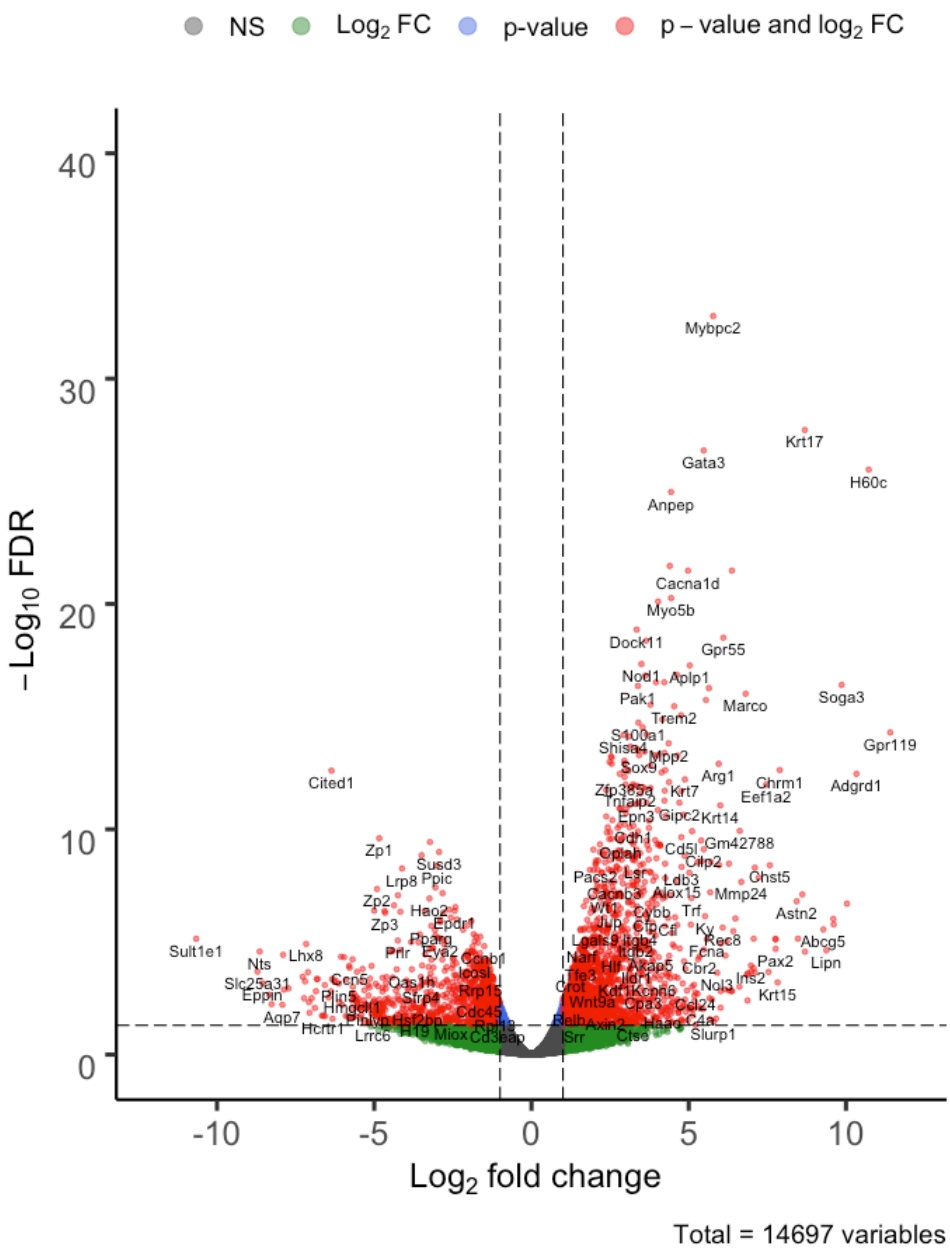

Figure 14

Volcano plot of *Stk11*^{cko}*Pten*^{cko} vs Control. Genes in red are significantly ($p<0.05$) up or down regulated by $\log_2$fold change of <-1 or >1.

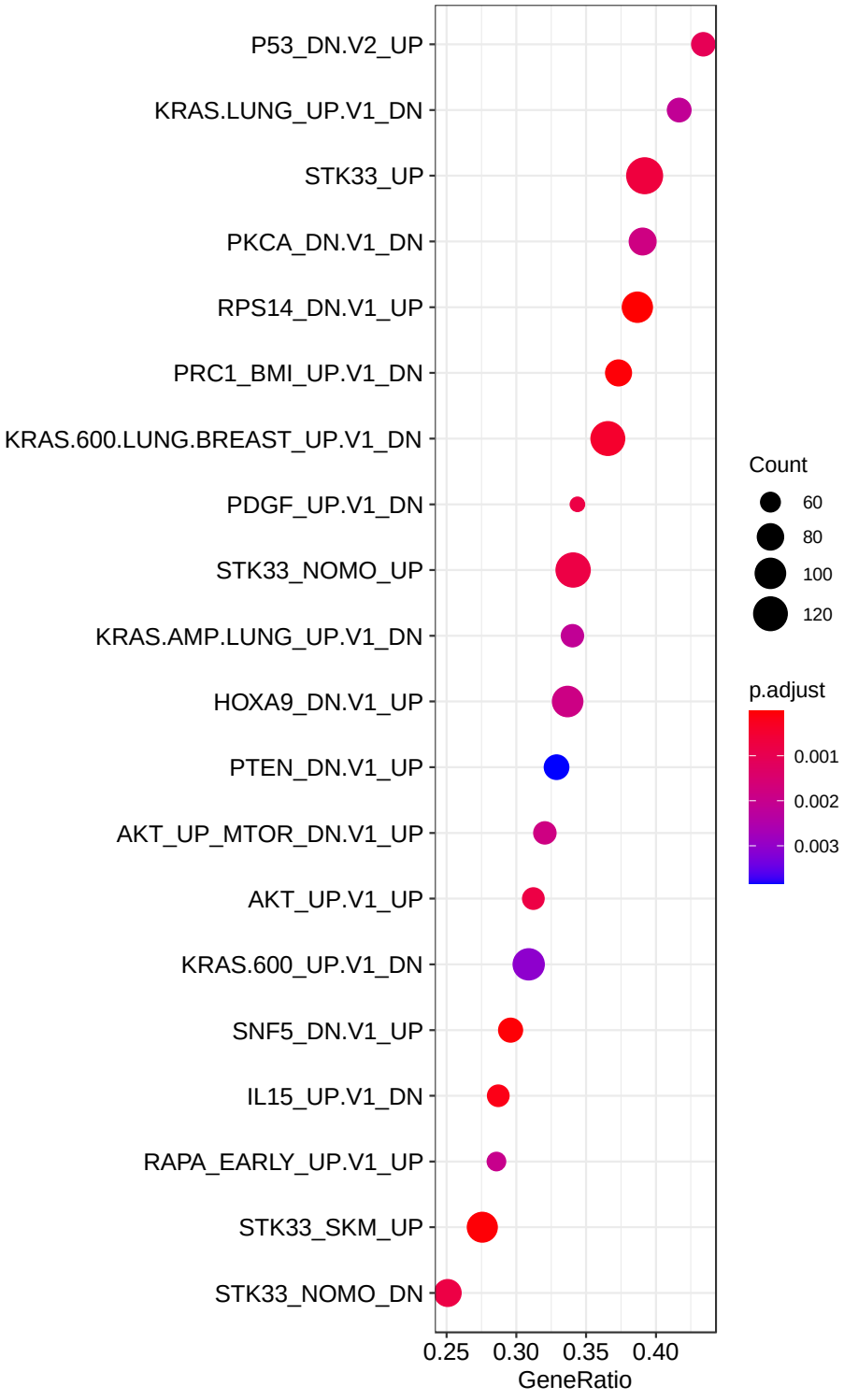

Figure 15

GSEA *Stk11*^{cko}*Pten*^{cko} vs Control.

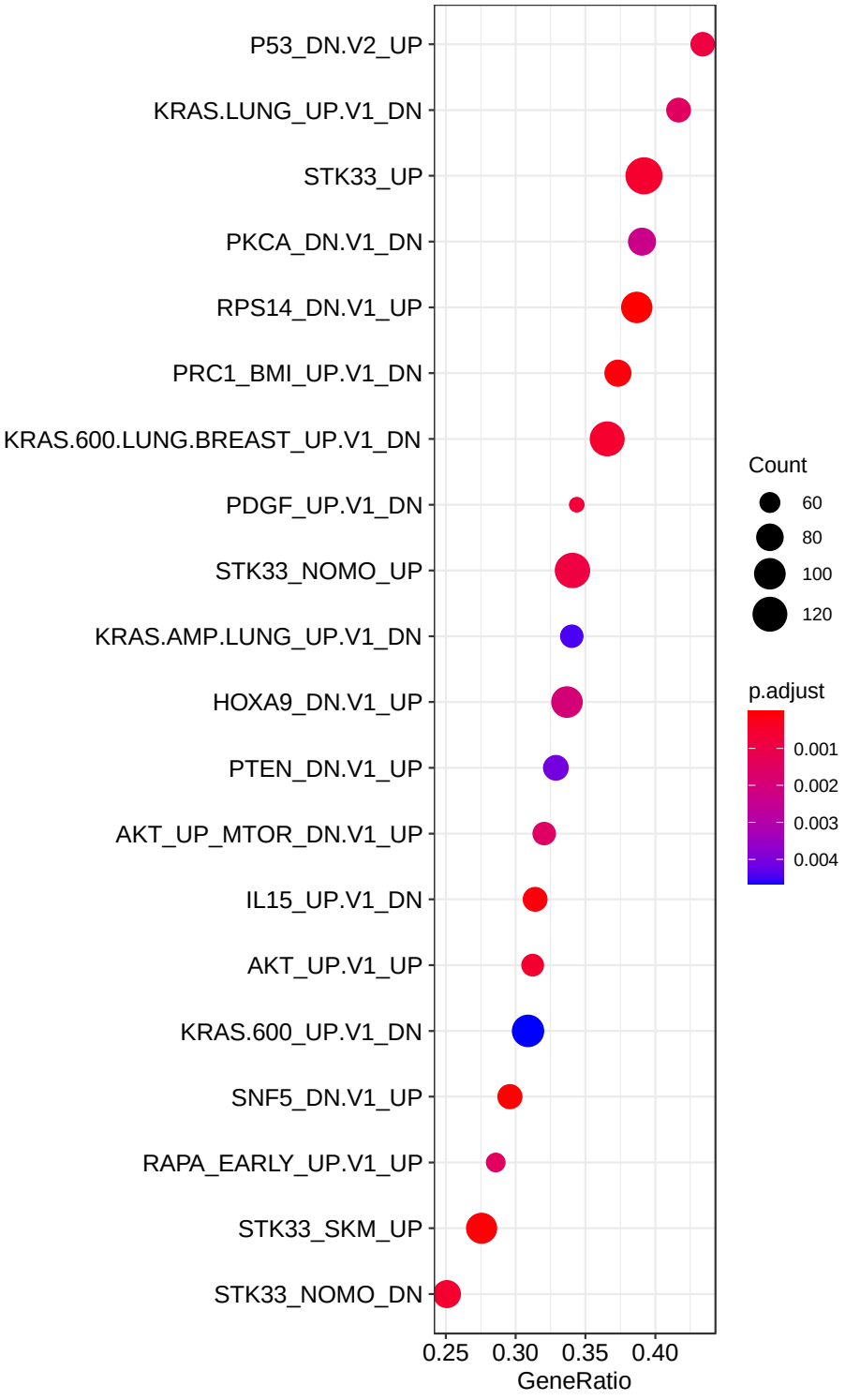

Figure 16

GSEA Control vs *Stk11*^{cko}*Pten*^{cko}.

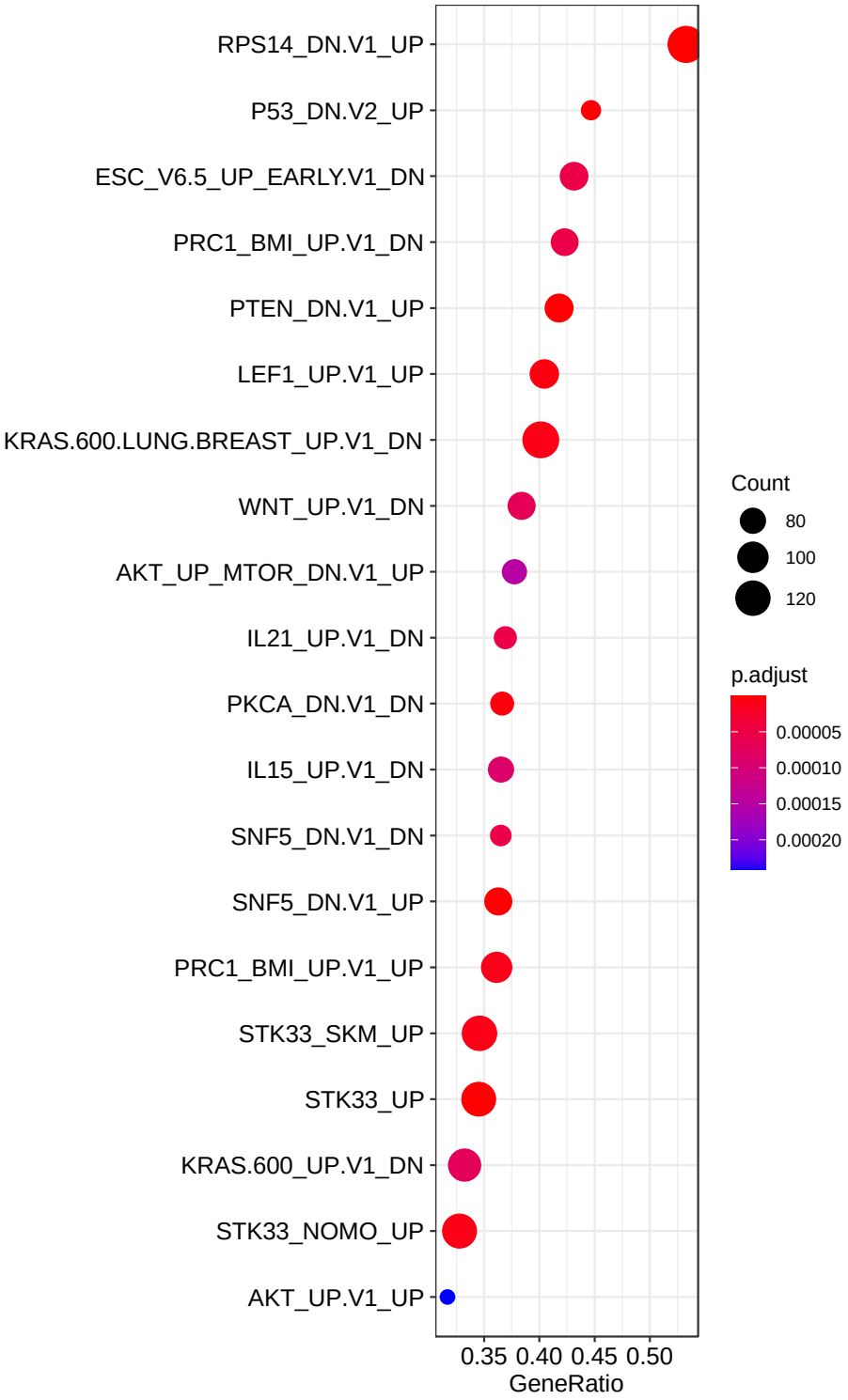

Figure 17

GSEA *Stk11*^{cko} vs *Stk11*^{cko}*Pten*^{cko}.

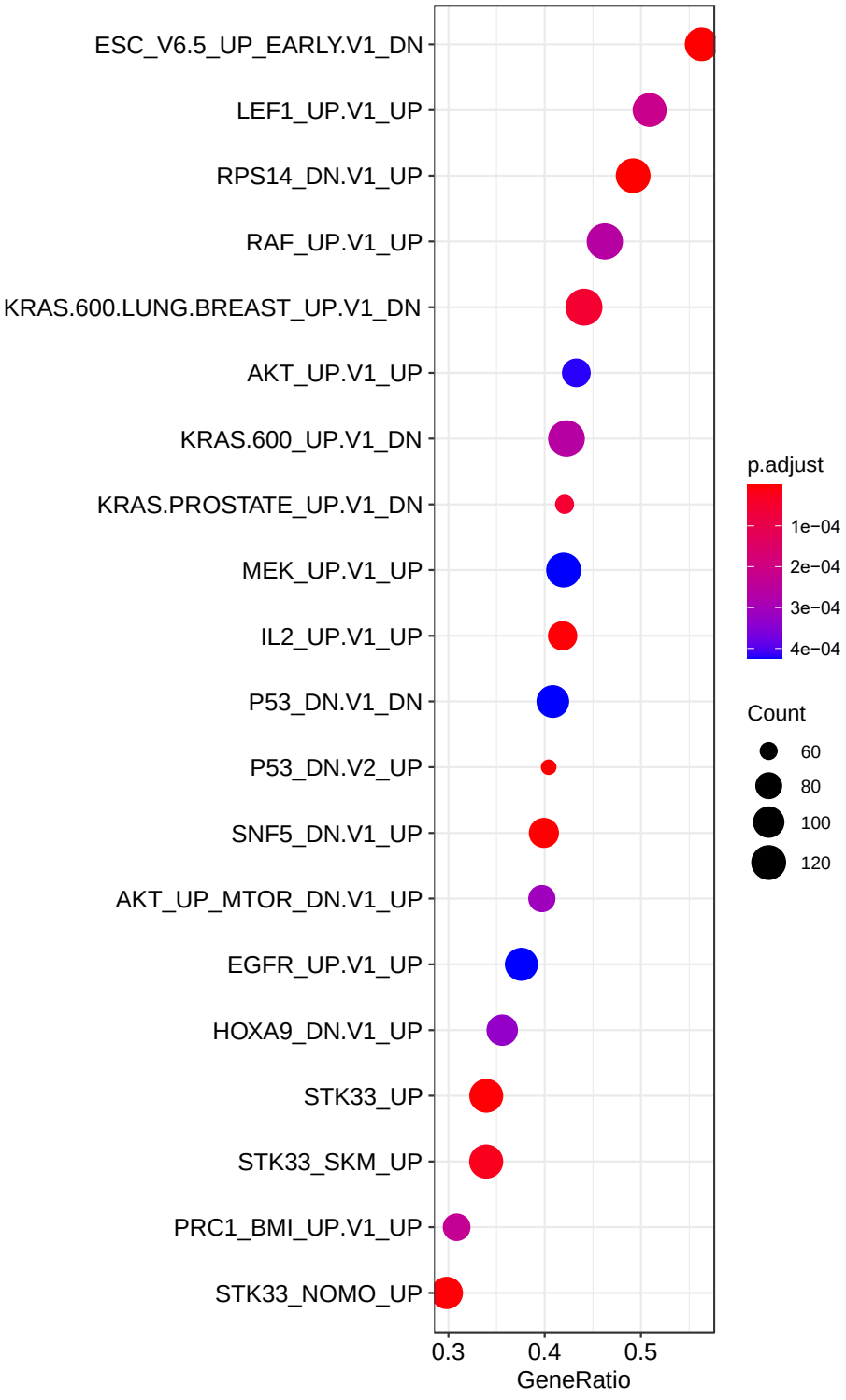

Figure 18

GSEA *Pten*^{cko} vs *Stk11*^{cko}*Pten*^{cko}.

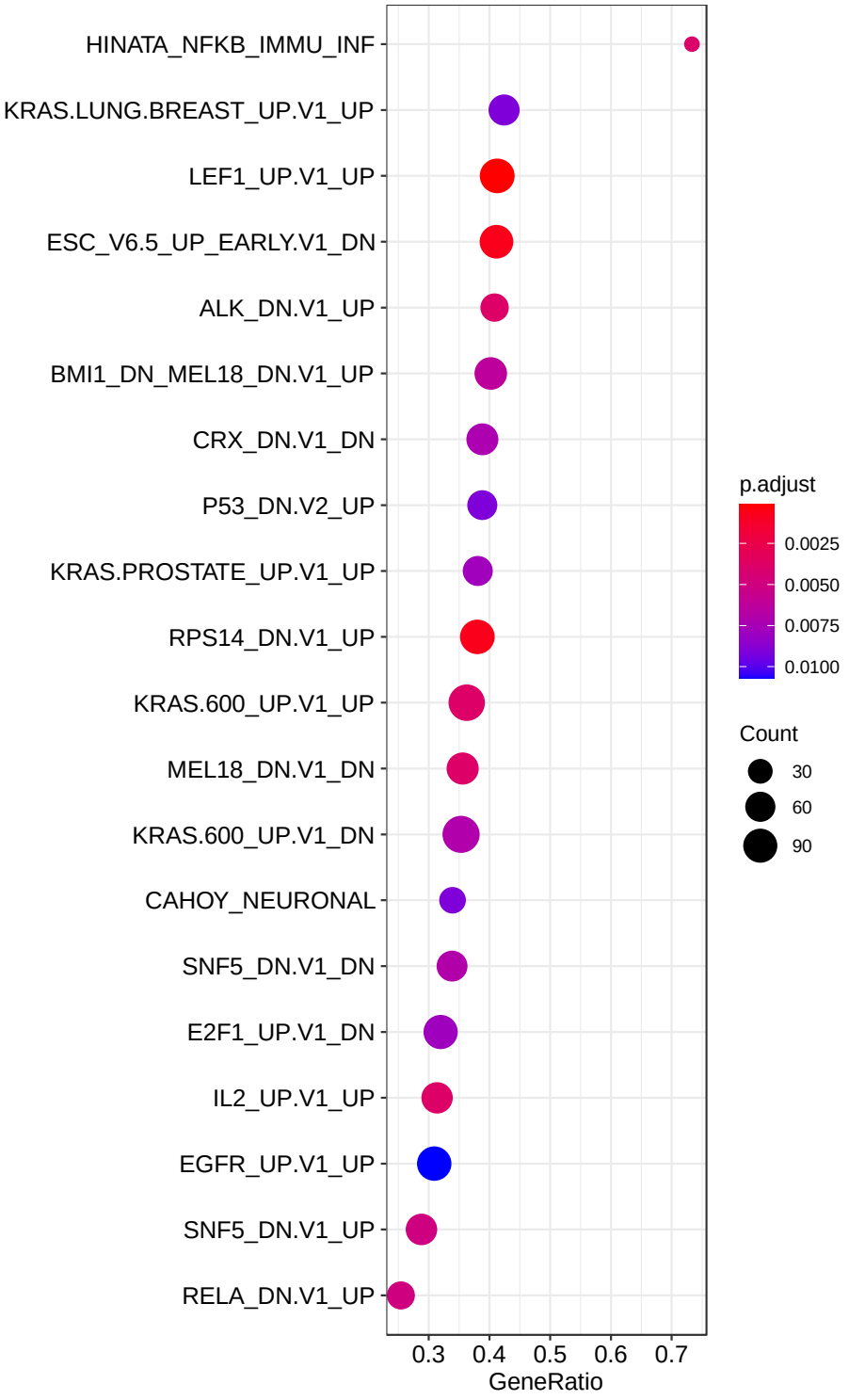

Figure 19

GSEA *Stk11*^{cko} vs Control.

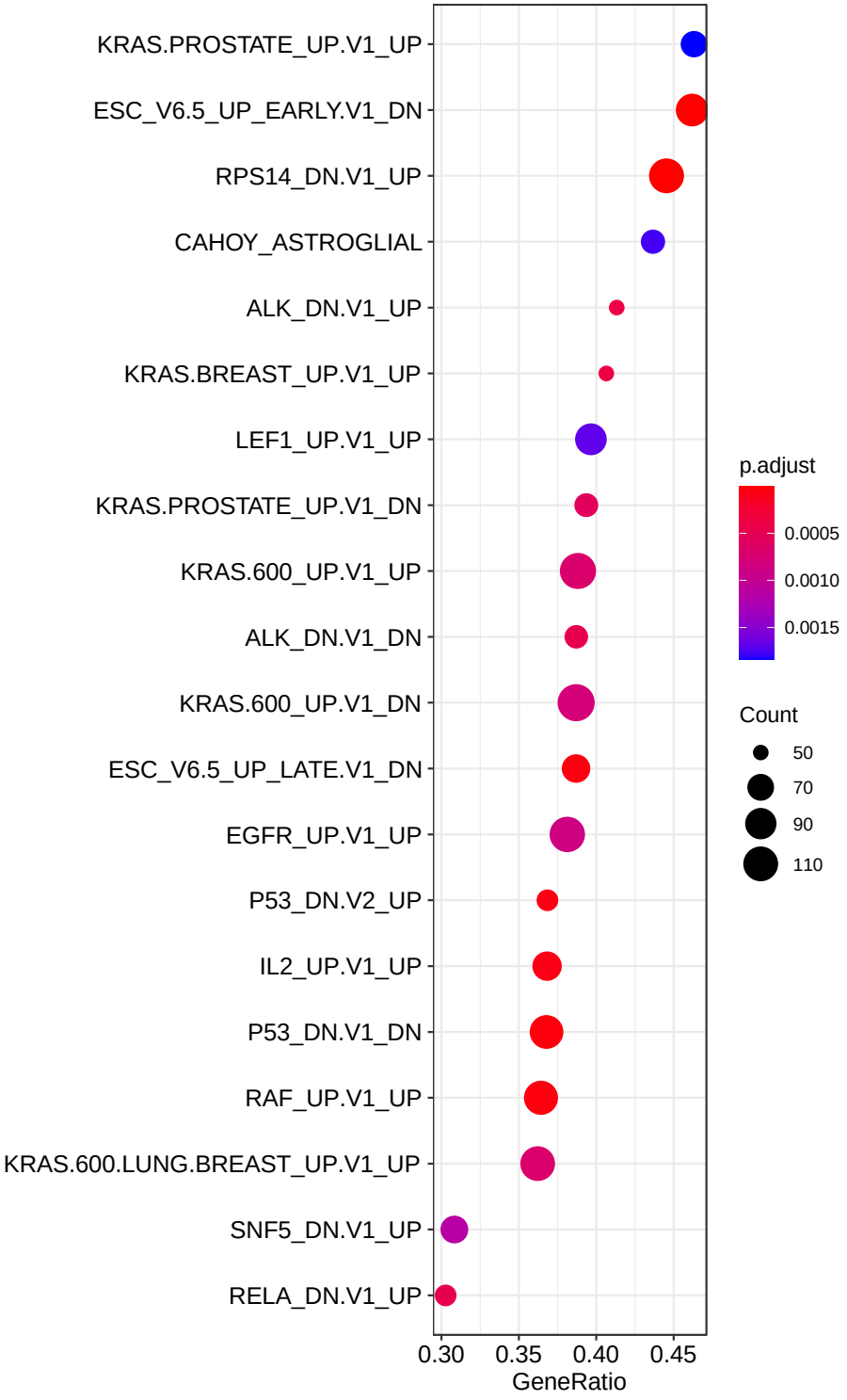

Figure 20

GSEA *Pten*^{cko} vs Control.

APPENDIX B

Roles of TSC2, PTEN, and P53 deletion in development of HGSOC

Previous studies discussed in Chapter 2, indicate that *Tsc2*^{cko}*Pten*^{cko} mice did not develop ovarian tumors up to 6 months of age. At 3 and 6 months, these mice only display abnormalities of the OSE such as papillae formation and cell shedding. However, we did find evidence of unilateral tumorigenesis in mice aged out to 8 months of age (Fig 12B). These tumors were large, but did not mimic any specific histotype of EOC (Fig 12 A). Since *Amhr2* drives *Cre* expression in both OSE and granulosa cells of the ovary, we stained for both CK8 and Inhibin Alpha. At this point normal ovarian development is severely disrupted and the normal structures of the ovary like follicles cannot be distinguished. A bulk of the tumor is necrotic as indicated by lack of hematoxylin staining on the right side, appearing pink (Fig 12 A). Another large portion of the tumor stains positive for CK8 indicating an epithelial cell origin (Fig 12 C, D). There is scattered expression of Inhibin Alpha indicating that these granulosa cells are not neatly organized surrounding the oocyte as we see in normal ovarian anatomy [155]. Because expression is sparse, it does not clearly indicate a granulosa cell origin. Without a clear association with an EOC histotype, we turned to other genetic combinations and mouse model strategies to pursue GEMMs of HGSOC.

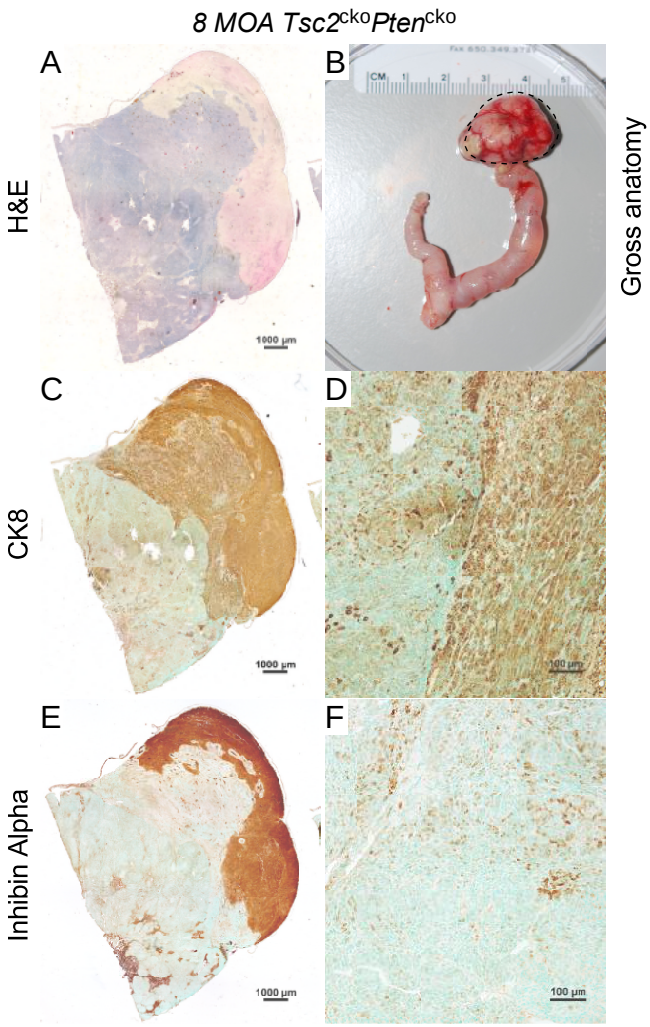

Figure 21

8MOA *Tsc2*^{cko}*Pten*^{cko} mice develop large, solid, unclassified ovarian tumors. When *Tsc2*^{cko}*Pten*^{cko} mice were aged out to 8 months of age, large, solid, unclassified ovarian tumors developed (B). These large ovarian tumors were sectioned and examined for histology (A), epithelial origin (C, D), and granulosa cell origin (E, F). Panels D and F are higher magnification images of boxed areas in C and E, respectively.

The unifying characteristic of HGSOC is the loss of function *TP53* mutation that is found in 96-100% of all HGSOC. It is thought to be an initial hit that can cause the widespread CNAs and subsequent carcinogenesis that occurs in the disease [12]. While our *Stk11*^{cko}*Pten*^{cko} mice develop papillary serous ovarian cancer and have been shown to express P53 [71], P53 mutation or deletion is not used to foundationally drive the tumorigenesis in those mice. With this in mind, we bred mice with conditional deletion of *Tp53* in the OSE in addition to *Tsc2* and *Pten*. *Tsc2*^{cko}*Pten*^{cko}*Tp53*^{cko} show promise of being a good model of HGSOC since they develop invasive papillary serous histology (Fig 13 C-D) by 3 months of age. Additionally, ascites fluid accumulates in the peritoneal cavity of these mice in a more frequent manner than our *Stk11*^{cko}*Pten*^{cko} mouse model (Fig 13 A). Solid tumors form along the reproductive tract from the stromal cells where Amhr2 drives CKO of these genes (Fig 13 B). *Tsc2*^{cko}*Pten*^{cko}*Tp53*^{cko} mice do not develop large cervical tumors unlike the adenoma malignum often causing our *Stk11*^{cko}*Pten*^{cko} mice to reach tumor burden.

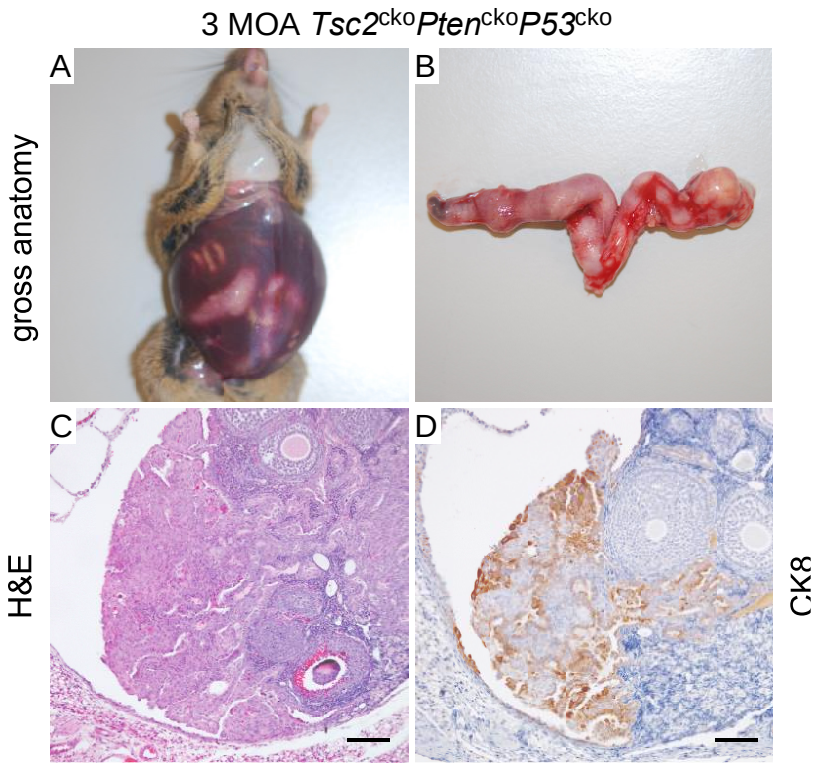

Figure 22

***Tsc2*^{cko}*Pten*^{cko}*P53*^{cko} mice develop papillary serous OvCA and ascites.** Representative mouse presents with bloated abdomen due to accumulation of 9mL of ascites in the peritoneal cavity (A). Tumors develop along the reproductive tract (B). Histology and CK8 staining show invasive papillary serous OvCa from epithelial origin (C, D).

Another drawback of our *Stk11*^{cko}*Pten*^{cko} mouse model is its inefficient breeding scheme. Both *Stk11*^{cko}*Pten*^{cko} males and females are infertile. Cre positive males with one wild type allele of *Stk11* but both *Pten* alleles conditionally deleted must be bred to Cre negative female with both alleles of both genes floxed. Since there is a 50% chance of having a Cre positive pup, a 50% chance that both alleles of *Stk11* are floxed, and a 50% chance of having a female, there is only a 1 in 8 chance of getting our desired genetic combination in each litter. To make this process more efficient and less costly, we wanted to introduce an Adenoviral *Cre* to a *Stk11*$^{fl/fl}$*Pten*$^{fl/fl}$ female. This strategy guarantees our desired genotype of *Stk11*^{cko}*Pten*^{cko} for every *Stk11*$^{fl/fl}$*Pten*$^{fl/fl}$ female we inject with Adenoviral-*Cre*.

6 mice were injected intrabursally with 3uL of Ad-*Cre* at $2.5*10^7$ plaque forming units (PFU) post superovulation. To test the effectiveness of this method of introducing *Cre* to OSE cells, Xgal staining was performed on one of the lacZ reporter mice 3 weeks post injection (Fig 14 B, E, H). In comparison to our negative (Fig 14 A, D, G) and positive (Fig 14 C, F, I) controls, we can see that the intrabursal injection of Ad-*Cre* successfully infected patches of OSE seen in blue in the gross anatomy of Fig 14 B and in the ovarian tissue sections of Fig 14 E and H. No abnormalities were found in the OSE layer at this early time point. While *Cre* was not introduced to 100% of the OSE as the *Amhr2-Cre* system does, it is also more specific to the OSE than the *Amhr2-Cre* system since it does not affect the rest of the reproductive tract.

.

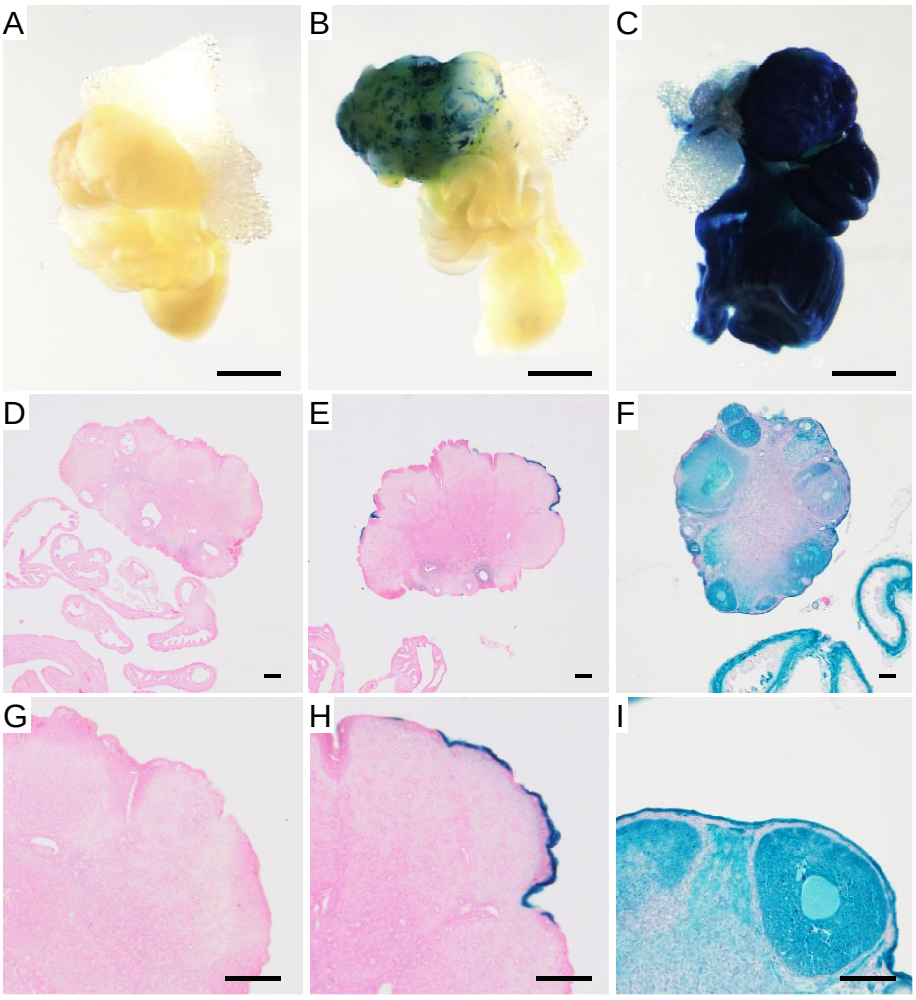

Figure 23

Intrabursal injection of Ad-*Cre* successfully infects a portion of OSE cells. X-gal staining protocol was performed on all ovaries 3 weeks post Ad-*Cre* injection. (A, D, G) Negative control ovary was not injected with Ad-Cre. (B, E, H) *Amhr2-Stk11*$^{fl/fl}$*Pten*$^{fl/fl}$*-Rosa26-Lacz*$^{fl/stop/fl}$ ovary was injected with Ad-*Cre*. (C, F, I) *Amhr2-Stk11*^{cko}*Pten*^{cko} *-Rosa26-Lacz*$^{+}$ ovary was our positive control reporter mouse and stained blue wherever *Amhr2* drives *Cre* expression. (Scale bars, 1mm (A-C), 100 um(G-I)).

After waiting over 12 months, one of my remaining mice had a distended abdomen and needed to be sacrificed. All other mice that were examined before 6 months of age yielded negative data: histologically normal appearing ovaries (data not shown). This mouse, however, yielded very exciting results. She had accumulated ascites fluid in her peritoneal cavity (Fig 15 A) which contained sheets of epithelial cells (Fig 15 B). The primary ovarian tumors (Fig 15 C, D) as well as the metastasis throughout the peritoneal cavity (Fig 15 E), including the omentum (Fig 3.4 F) and mesentery (Fig 15 G), had the cauliflower appearance characteristic of human HGSOC tumors (Fig 15 H). While these results more closely resembled human HGSOC, the largest drawback is the amount of waiting time necessary to produce these results.

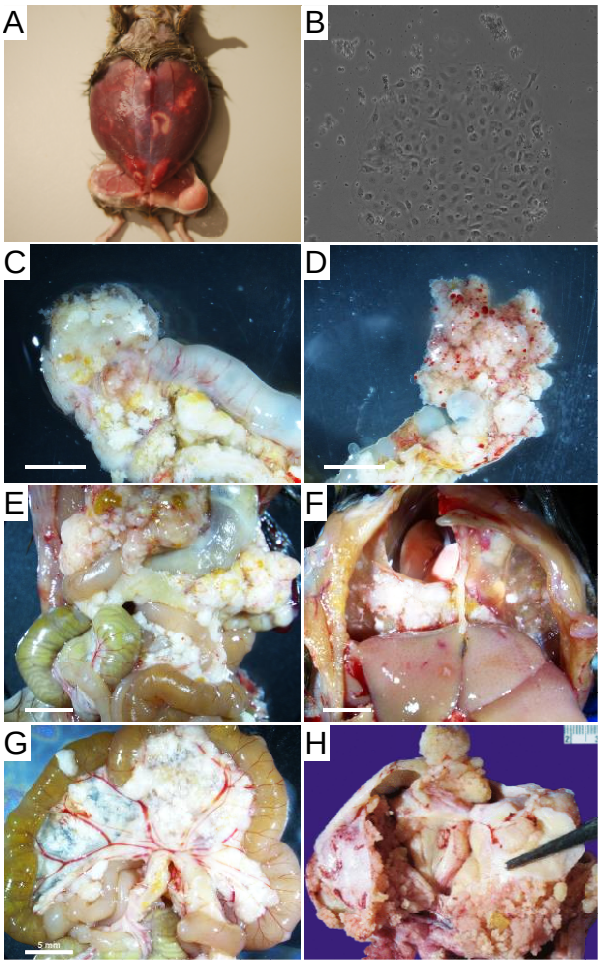

Figure 24

Ascites and metastatic papillary serous OvCa with characteristic cauliflower appearance was observed 1 year post Ad-*Cre* injection. (A) Gross anatomy before draining ascites fluid. (B) Ascites contained sheets of epithelial cells. (C, D) Gross anatomy of ovarian tumors and metastasis found along the reproductive tract. (E, F, G) Metastasis found throughout peritoneal cavity, omentum, and mesentery of the small intestine, respectively. (H) Human HGSOC tumor displaying the classic cauliflower appearance of HGSOC tumors. (Scale bars, 5mm)

While *Tsc2*^{cko}*Pten*^{cko} is not a good prospect for a mouse model for HGSOC, both the *Tsc2*^{cko}*Pten*^{cko}*Tp53*^{cko} and the Ad-Cre *Stk11*^{cko}*Pten*^{cko} show great promise for OSE GEMMs of HGSOC and may warrant further pursuit into HGSOC marker expression, pathway analysis, and differential gene expression. However, the heavy time and money investment may pose a significant barrier to those pursuits.

Methods

Mouse genetics and animal husbandry

All animal experimentation protocols used in this study were approved by the Michigan State University Institutional Animal Care and Use Committee and are in compliance with the NIH Guide for the Care and Use of Laboratory Animals. Mice used in this study were kept in standard housing conditions and were maintained on a mixed genetic background (C57BL/6;129/SvEv). These mice strains: *Amhr2-cre* [140], *Tsc2*$^{fl/fl}$ [142], *Pten*$^{fl/fl}$ [143], and *Trp53*$^{fl/fl}$ [156], were mated to produce *Cre*-null controls, *Amhr2-cre*/+;*Tsc2*$^{\Delta/\Delta}$;*Pten*$^{\Delta/\Delta}$ (referred to as *Tsc2*^{cko} *Pten*^{cko}), *Amhr2-cre*/+; *Tsc2*$^{\Delta/\Delta}$;*Pten*$^{\Delta/\Delta}$;*Trp53*$^{\Delta/\Delta}$, (referred to as *Tsc2*^{cko} *Pten*^{cko} *Trp53*^{cko}). Tail biopsies were collected for genotyping, and PCR conditions for *Tsc2*, *Pten*, and *Trp53* alleles have been described [141, 143-145]. Ovaries were collected postmortem for histological examination. Gross images of the tumors were taken using a Nikon D60 digital camera and macro lens.

Histology and immunohistochemistry

Tissues were fixed, processed and sectioned as previously described [144, 146]. 7-micron sections were cut from paraffin-embedded blocks for standard histological analysis with hematoxylin and eosin staining and for immunohistochemistry. The following primary and secondary antibodies were used for immunohistochemistry (IHC): cytokeratin 8 (TROMA-I AB_531826, Developmental Studies HybridomaBank, IA), Inhibin-α (ab47720 Cambridge, MA). Biotinylated secondary antibodies: donkey anti-mouse or anti-rabbit F_{ab2} (Jackson ImmunoResearch Laboratories, West Grove, PA). Images were taken with a Nikon Eclipse Ni microscope fitted with Nikon DSF12/DS-Q1MC cameras.

Intrabursal injection

6 mice were injected intraperitoneally with 2.0 IU of pregnant mare serum (PMS) on day 1, with 2.0 IU of human chorionic gonadotropin (HCG) on day 3. On day 4, *Stk11*$^{fl/fl}$;*Pten*$^{fl/fl}$ mice were injected intrabursally with 3uL of Ad-*Cre* at $2.5*10^7$ plaque forming units (PFU).

X-Gal Staining

Ovaries were rinsed in PBS, then fixed (for 50mL: 0.4mL 25% glutaraldehyde; 1.0mL 250mM EGTA pH7.3; 5.0mL 1M $MgCl_2$, 43.5mL 100mM sodium phosphate pH 7.3 or PBS) for 30 min shaking on ice, rinsed 3x for 30 min at 4 C in rinse buffer (for 500mL: 1.0mL 1 M $MgCl_2$; 5.0mL 1% sodium deoxycholate; 5.0mL 2% Nonidet P-40 in PBS pH 7.2; 489mL 100mM sodium phosphate pH 7.3), then stained overnight at 37C protected from light in X-gal staining solution (for 75mL: 72.0mL wash buffer, 3.0mL 25mg/mL X-gal (dissolved in DMSO), 0.159g potassium ferrocyanide; 0.123g potassium ferricyanide). Ovaries were then washed 3x for 10 minutes with 1x PBS. processed and sectioned as previously described [144, 146].

APPENDIX C

Alternative treatment options for patients with HGSOC: MIS project and gene therapy project

Current treatment options for women with HGSOC are largely limited to surgery and cytotoxic therapy, which is ineffective for a majority of women with metastatic HGSOC [34]. Misdiagnosis of gastrointestinal issues occurs frequently for women with HGSOC because their symptoms largely overlap: abdominal pain, bloating, nausea, acid reflux, lower back pain, fatigue, constipation or diarrhea, weight loss, tenesmus, increased urinary frequency, vaginal discharge, and sometimes dyspnea in more advanced disease [4, 11].

If EOC is suspected, women will receive a pelvic exam, imaging, and mucin16 (CA125) testing [10]. If EOC is diagnosed, women will undergo laparoscopic surgery to biopsy of the tumor as well as stage the disease [10]. For most women with metastatic HGSOC, debulking surgery is performed followed by cytotoxic therapy. Tragically, only 15% of these women will survive past 10 years [34].

To find better treatments, sometimes it is necessary to get creative. Through collaborations with Dr. Donahoe's and Dr. Manfredsson's labs, we were able to explore a couple of novel and creative avenues to better treat HGSOC.

Dr. Donahoe's lab has been studying MIS for many years. Early in male embryonic development, the testis-determining factor (SRY) causes the bipotential gonad to differentiate into the testes [51, 157]. MIS is one of the first hormones produced by the testes and causes apoptosis and disappearance of the female Mullerian duct by binding to its receptor: AMHR2 [51]. Perhaps it could be utilized for therapy against cancers of Mullerian origin including EOC. Studies in her lab have shown that MIS acts as a tumor suppressor in the ovary and fallopian tube and targets cells with stem characteristics that respond poorly to current chemotherapies. AMHR2 is expressed in most EOCs and MIS has been shown to inhibit their growth *in vitro* and *in vivo* [51, 157].

5 *Stk11*^{cko}*Pten*^{cko} mice received a 20uL intraperitoneal (IP) injection of AAV9-MIS at 6 weeks of age. An additional 5 *Stk11*^{cko}*Pten*^{cko} mice received a 20uL IP injection of EV at 6 weeks of age. Based on the preliminary data from Dr. Donahoe's lab, we hypothesized that mice injected with MIS would live longer and have less tumor burden than those injected with EV. Our survival curve shows that there appears to be a slight advantageous delay in tumor burden for mice injected with MIS, but ultimately all mice were sacrificed by 21 weeks of age (Fig 16 A). 2/10 ovaries in the control group grew to be quite large (Fig 16 E), but the average mass was not significantly greater than the MIS treated group (Fig 16 B). A similar non-significant trend can be seen in reproductive tract mass (Fig 16 C). Evidence of invasive papillary serous OvCa could be seen in both groups. 2/3 ovaries examined of MIS-injected mice only displayed minor surface papillae formations (Fig 16 F), while 3/4 ovaries examined of EV-injected mice had invasive papillary serous OvCa (Fig 16 G).

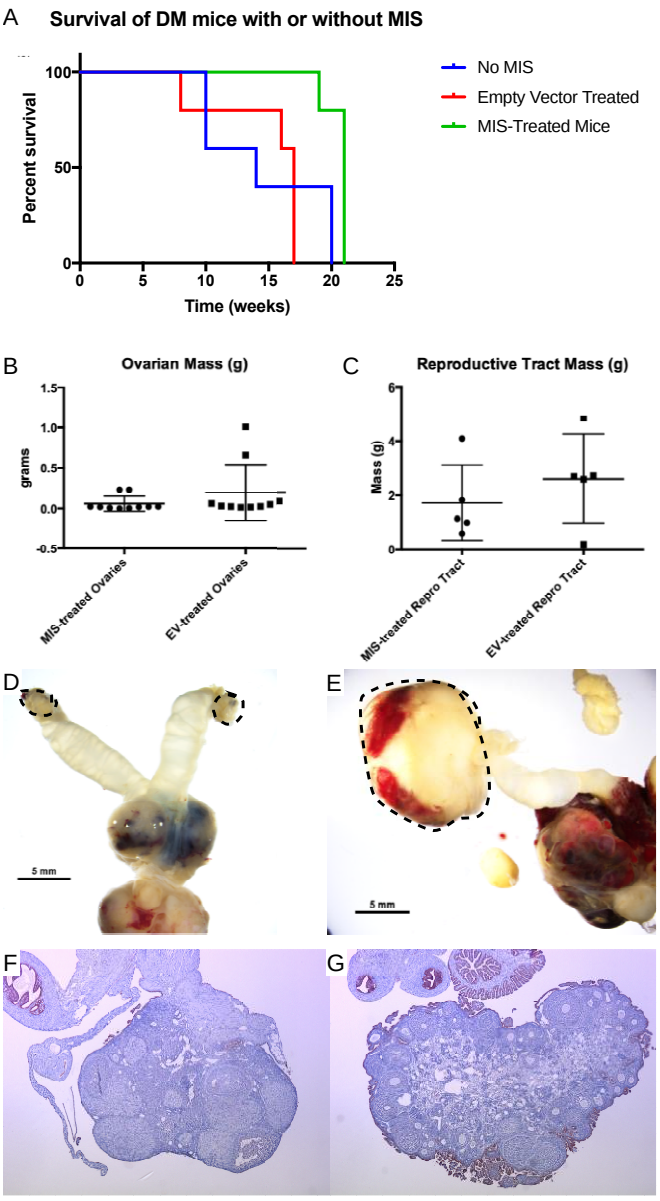

Figure 25

Treatment of *Stk11*^{cko}*Pten*^{cko} mice with MIS does not completely prevent tumorigenesis.

(A) Kaplan-Meier curve shows slight advantage of survival but all mice still reach tumor burden by 21 weeks. (B, C) There is no significant difference between MIS-treated and EV-treated mice in ovarian or reproductive tract weight. (D, E) Gross anatomy of the reproductive tracts of a MIS-treated mouse and an EV-treated mouse respectively. Dashed lines surround ovaries. (F, G) CK8 staining of a MIS-treated mouse and an EV-treated mouse respectively.

Dr. Manfredsson's expertise lies in a gene therapy treatment approach to treating neurogenerative diseases. In collaboration with our lab, we wanted to apply a similar approach to treating HGSOC. Gene therapy has shown success with one-gene diseases. Children with Leber's congenital amaurosis are blind because they are missing the vital enzyme in retinal cells: hRPE65 [158]. AAV2 was the viral vector used to deliver this missing gene, which was successful in restoring these children's eyesight [158]. HGSOC is far from a one gene disease and is known for widespread CNA [10]. Instead of using AAV to deliver a missing gene, we can use AAV to deliver a ubiquitous kill signal to ovarian cancer cells.

DNaseI is a waste-management nuclease that fragments DNA in late-stage apoptosis that can be engineered to trigger apoptosis in cells [159]. Normally it has limited access to the nucleus, but the signal peptide (SP) domain can be deleted and replaced with a nuclear localization signal (NLS) to better access the nucleus [159]. Normally it can be inhibited through the binding of actin, but that can be avoided by knocking down the actin binding site [159]. This modified enzyme, DNaseX can enter the nucleus and degrade DNA beyond repair causing apoptosis [159]. Since HGSOC expresses PAX8, we can use the PAX8 promoter to drive DNaseX expression so that it cannot kill PAX8 negative cells. The kidney is the only vital organ expressing PAX8 [122]. To prevent destruction of the kidney, kidney-specific microRNA binding sites could theoretically be included to de-target the kidney.

Our first goal of this project was to establish a method to track metastasis through live animal imaging. We were able to establish a ZsGreen-positive OVCAR3 cell line that could be used to image HGSOC metastasis *in vivo*. We transduced our OVCAR3 cells with lentivirus carrying our viral vector (Fig 17 A) at a multiplicity of infection of 1000. We then collected ZsGreen- positive cells through fluorescence activated cell sorting (FACS). Setting the gate

based on our control cells not expressing ZsGreen (Fig 17 B, C), we collected the 86.1% of cells that were ZsGreen positive (Fig 17 D, E).

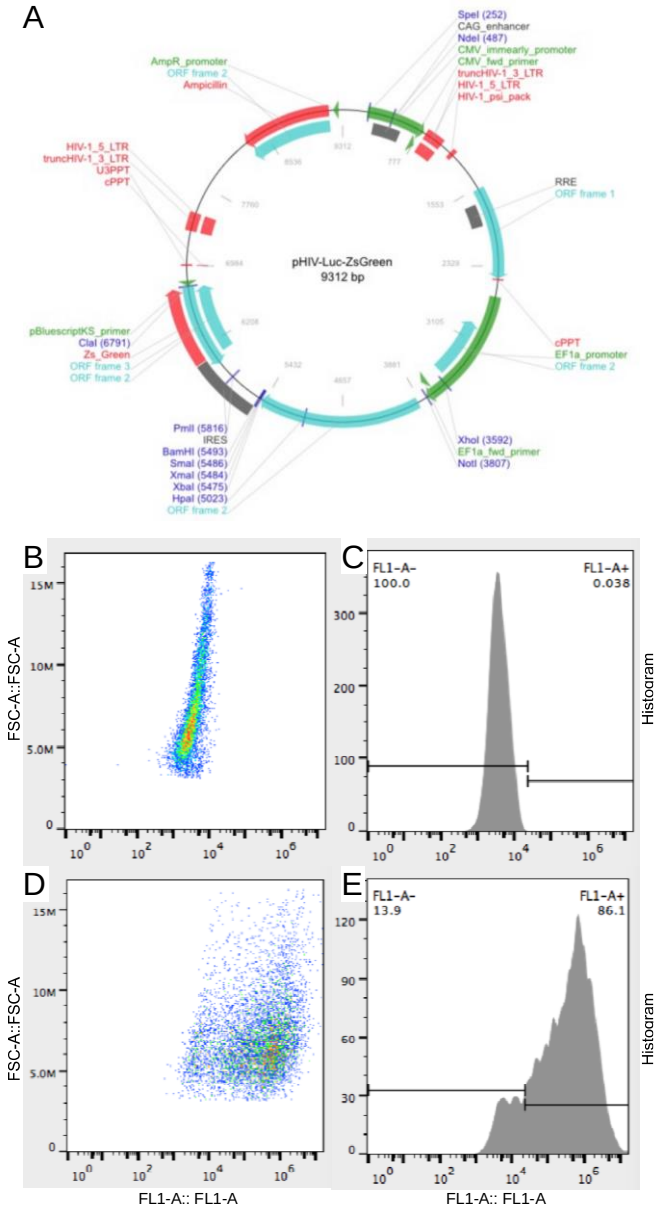

Figure 26

OVCAR3 cells were transfected at 1000 MOI with lentiviral vector containing ZsGreen.

ZsGreen positive cells were collected through FACS. (A) Map of viral vector used to transfect OVCAR3 cells. (B, C) Control OVCAR3 cells were not transduced with lentivirus and are ZsGreen negative. (D, E) Transduced OVCAR3 cells at 1000 MOI were gated based on control and 86% of the cells that were ZsGreen positive cells were collected.

3 control mice were injected IP with $1x10^6$ ZsGreen negative OVCAR3 cells and 3 mice were injected IP with $1x10^6$ ZsGreen positive OVCAR3 cells. Metastasis was tracked weekly through *in vivo* fluorescence imaging (Fig 18 A-C). ZsGreen positive OVCAR3 metastasis can be seen in the mesentery (Fig 18 D, E) and as small sheets of cells floating in the peritoneal cavity (Fig 18 F-I). This proof of concept shows the feasibility of being able to track metastasis over time in individual live mice. This could be widely utilized to show the efficacy of cancer treatments on established metastasis in mice. For this collaboration it could be used in the future to show the efficacy of AAV-DNaseX treatment on HGSOC metastasis.

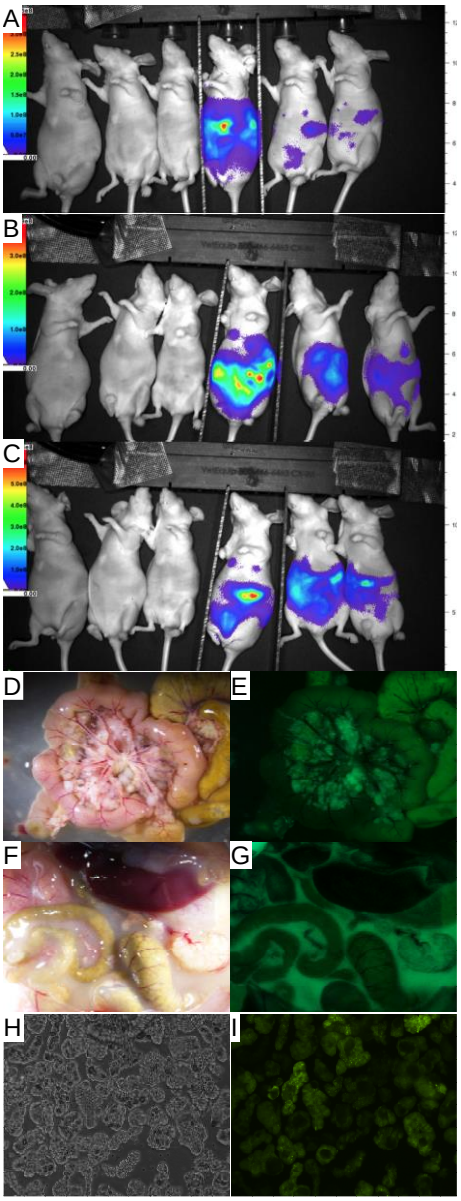

Figure 27

Mice injected with ZsGreen + OVCAR3 cells can be tracked for metastasis over time. (A-C) Progression of *in vivo* imaging of 3 control mice (on left) and 3 ZsGreen+ OVCAR3 injected mice (on right) over time. ZsGreen+ metastasis can be found in the mesentery (D, E) and floating throughout the abdominal cavity (F, G). Those free floating ZsGreen+ OVCAR3 cells were collected and examined (H, I).

The second goal of this collaboration was to test the efficacy of DNaseX on Ovarian cancer xenografts. Preliminary data (not shown) from Dr. Manfredssons lab showed that melanoma xenografts decreased in volume through treatment with AAV-DNaseX and had a lower final tumor weight at sacrifice compared to control. 5 nude mice received bilateral, subcutaneous (SC) injection of $2x10^6$ OVCAR3 cells in 200uL, 1:1 matrigel. After 14 weeks of tumor growth, tumors were injected with either control, AAV2-DNaseX, or AAV5-DNaseX. Tumor growth was then tracked over the subsequent 17 weeks (Fig 19 A). Average tumor volume at the end point showed no significant differences because of high variability, but AAV5-DNaseX treated tumors had the smallest final tumor volume. However, total tumor volume may not be an accurate way to measure the efficacy of DNaseX since it can cause cell death within the tumor not reflected in total tumor volume. Fig 19 D and E show a large discrepancy in percent necrosis between a control and AAV5-DNaseX treated tumor. While cell death occurs in control tumors as well, the percent necrosis of AAV5-DNaseX treated tumors is slightly higher. While DNaseX was not as clearly effective as it was in melanoma xenografts there does seem to be more cell death occurring in AAV5-DNaseX treated tumors compared to control.

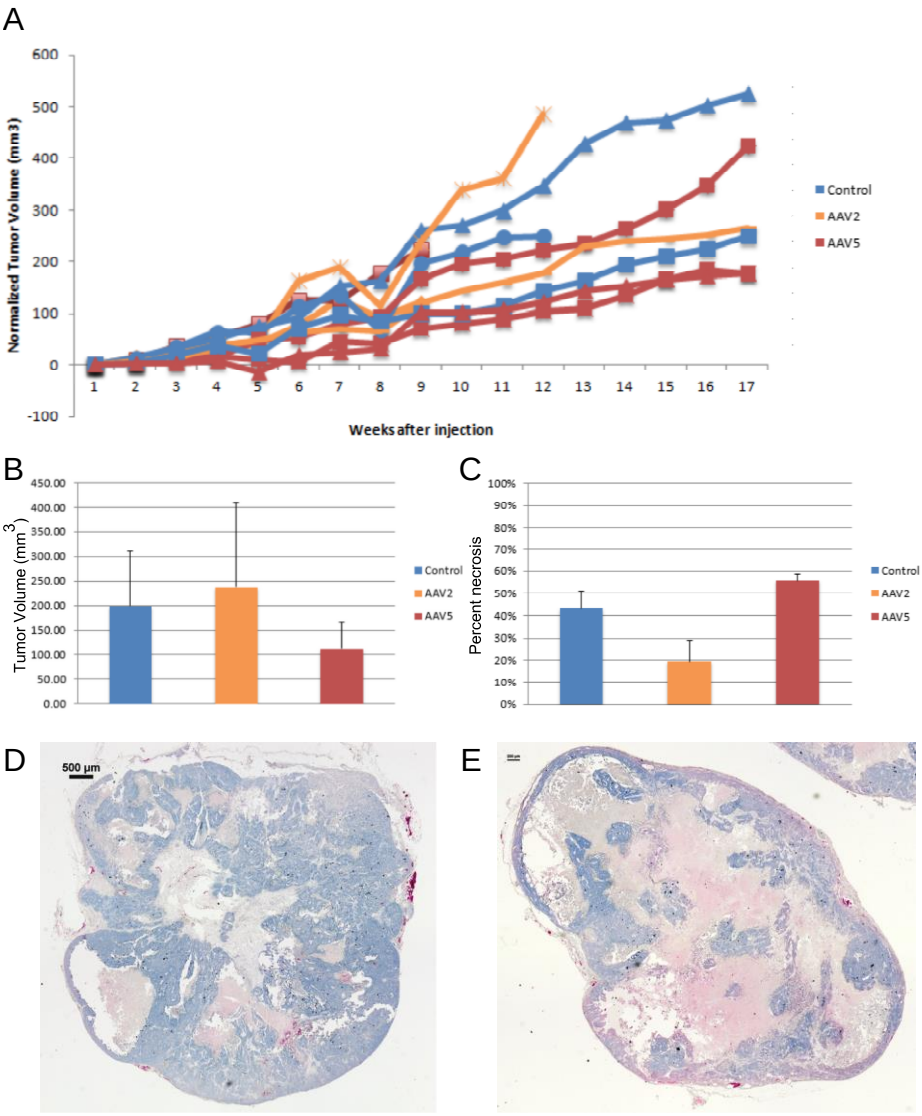

Figure 28

Tumor growth of OVCAR3 tumor xenografts injected with control, AAV2-DNaseX, or AAV5-DNaseX was not significantly different. (A) Tumor volume (mm^3) measured weekly post injection over 17 weeks. (B) Average tumor volume at end point. AAV5-DNaseX injected tumors were the smallest, but did not reach statistical significance. (D) An example of a control tumor showing 37.8% necrosis. (E) An example of an AAV5-DNaseX injected tumor showing 53.3% necrosis. (C) Average percent necrosis of tumors.

While neither MIS of DNaseX treatment gave us the robust results we were hoping for, there is still a lot of precedence and strong theory to continue thinking creatively when it comes to treatment of HGSOC.

Methods

Mouse genetics and animal husbandry

All animal experimentation protocols used in this study were approved by the Michigan State University Institutional Animal Care and Use Committee and are in compliance with the NIH Guide for the Care and Use of Laboratory Animals. Mice used in this study were kept in standard housing conditions and were maintained on a mixed genetic background (C57BL/6;129/SvEv). These mice strains: *Amhr2-cre* [140], $Stk11^{tm1Rdp}/Stk11^{fl/fl}$ [141] and $Pten^{fl/fl}$ [143] were mated to produce *Cre*-null controls, $Amhr2\text{-}cre/+;Stk11^{\Delta/\Delta};Pten^{\Delta/\Delta}$, (referred to as $Stk11^{cko}Pten^{cko}$). Tail biopsies were collected for genotyping, and PCR conditions for *Stk11* and *Pten* alleles have been described [141, 143-145]. Ovaries were collected postmortem for histological examination. Gross images of the tumors were taken using a Nikon D60 digital camera and macro lens.

Histology and immunohistochemistry

Tissues were fixed, processed and sectioned as previously described [144, 146]. 7-micron sections were cut from paraffin-embedded blocks for standard histological analysis with hematoxylin and eosin staining and for immunohistochemistry. The following primary and secondary antibodies were used for immunohistochemistry (IHC): cytokeratin 8 (TROMA-I AB_531826, Developmental Studies HybridomaBank, IA). Biotinylated secondary antibodies: donkey anti-mouse or anti-rabbit F_{ab2} (Jackson ImmunoResearch Laboratories, West Grove, PA).

Images were taken with a Nikon Eclipse Ni microscope fitted with Nikon DSF12/DS-Q1MC cameras.

Zs-green induction, Fluorescence Activated Cell Sorting, and imaging

OVCAR3 cells were transduced with lentivirus carrying our viral vector at a multiplicity of infection of 1000. Cell suspensions were strained though 100- and 40-μm meshes, and resuspended in PBS on ice. Samples were sorted on a MoFLo Astrios Flow Cytometer (Beckman Coulter, Brea, CA). Cells were gated by forward and side scatter to exclude our zs-green negative control cells and zs-green positive cells were subsequently collected. 3 control mice were injected IP with $1x10^6$ ZsGreen negative OVCAR3 cells and 3 mice were injected IP with $1x10^6$ ZsGreen positive OVCAR3 cells. Metastasis was tracked weekly through *in vivo* fluorescence imaging (Spectral Instruments AMI-1000) at the small animal imaging facility (SAIF) at Van Andel Research Institute (VARI).

DNAseX treatment of OVCAR3 Xenograft model

5 BALB/c (nu/nu) mice received bilateral, subcutaneous (SC) injection of $2x10^6$ OVCAR3 cells in 200uL, 1:1 matrigel. Tumors were injected with either control, AAV2-DNaseX, or AAV5-DNaseX after 14 weeks of tumor growth. Tumors were measured weekly with calipers.

REFERENCES

REFERENCES

1. Bray, F., et al., *Global cancer statistics 2018: GLOBOCAN estimates of incidence and mortality worldwide for 36 cancers in 185 countries.* CA Cancer J Clin, 2018. **68**(6): p. 394-424.

2. Siegel, R.L., K.D. Miller, and A. Jemal, *Cancer statistics, 2019.* CA Cancer J Clin, 2019. **69**(1): p. 7-34.

3. Scully, R.E., L.H. Sobin, and S.F. Serov, *Histological typing of ovarian tumours*. 2nd ed. Histological classification of tumours. 1999, Berlin ; New York: Springer. 136 p.

4. Matulonis, U.A., et al., *Ovarian cancer.* Nat Rev Dis Primers, 2016. **2**: p. 16061.

5. Perets, R., et al., *Transformation of the fallopian tube secretory epithelium leads to high-grade serous ovarian cancer in Brca;Tp53;Pten models.* Cancer Cell, 2013. **24**(6): p. 751-65.

6. Dubeau, L., *The cell of origin of ovarian epithelial tumors and the ovarian surface epithelium dogma: does the emperor have no clothes?* Gynecol Oncol, 1999. **72**(3): p. 437-42.

7. Pentheroudakis, G. and N. Pavlidis, *Serous papillary peritoneal carcinoma: unknown primary tumour, ovarian cancer counterpart or a distinct entity? A systematic review.* Crit Rev Oncol Hematol, 2010. **75**(1): p. 27-42.

8. Shih Ie, M. and R.J. Kurman, *Ovarian tumorigenesis: a proposed model based on morphological and molecular genetic analysis.* Am J Pathol, 2004. **164**(5): p. 1511-8.

9. Kurman, R.J. and M. Shih Ie, *The Dualistic Model of Ovarian Carcinogenesis: Revisited, Revised, and Expanded.* Am J Pathol, 2016. **186**(4): p. 733-47.

10. Lisio, M.A., et al., *High-Grade Serous Ovarian Cancer: Basic Sciences, Clinical and Therapeutic Standpoints.* Int J Mol Sci, 2019. **20**(4).

11. Kurman, R.J., International Agency for Research on Cancer., and World Health Organization., *WHO classification of tumours of female reproductive organs*. 4th ed. World Health Organization classification of tumours. 2014, Lyon: International Agency for Research on Cancer. 307 p.

12. Cancer Genome Atlas Research, N., *Integrated genomic analyses of ovarian carcinoma.* Nature, 2011. **474**(7353): p. 609-15.

13. Kurman, R.J., *Origin and molecular pathogenesis of ovarian high-grade serous carcinoma.* Ann Oncol, 2013. **24 Suppl 10**: p. x16-21.

14. Webb, P.M. and S.J. Jordan, *Epidemiology of epithelial ovarian cancer.* Best Pract Res Clin Obstet Gynaecol, 2017. **41**: p. 3-14.

15. Stratton, J.F., et al., *A systematic review and meta-analysis of family history and risk of ovarian cancer.* Br J Obstet Gynaecol, 1998. **105**(5): p. 493-9.

16. Cunningham, J.M., et al., *Clinical characteristics of ovarian cancer classified by BRCA1, BRCA2, and RAD51C status.* Sci Rep, 2014. **4**: p. 4026.

17. Testa, U., et al., *Ovarian Cancers: Genetic Abnormalities, Tumor Heterogeneity and Progression, Clonal Evolution and Cancer Stem Cells.* Medicines (Basel), 2018. **5**(1).

18. Ford, D., et al., *Genetic heterogeneity and penetrance analysis of the BRCA1 and BRCA2 genes in breast cancer families. The Breast Cancer Linkage Consortium.* Am J Hum Genet, 1998. **62**(3): p. 676-89.

19. Neff, R.T., L. Senter, and R. Salani, *BRCA mutation in ovarian cancer: testing, implications and treatment considerations.* Ther Adv Med Oncol, 2017. **9**(8): p. 519-531.

20. Savage, K.I., et al., *BRCA1 deficiency exacerbates estrogen-induced DNA damage and genomic instability.* Cancer Res, 2014. **74**(10): p. 2773-2784.

21. Hamada, J., et al., *Increased oxidative DNA damage in mammary tumor cells by continuous epidermal growth factor stimulation.* J Natl Cancer Inst, 2001. **93**(3): p. 214-9.

22. Taylor, K.N. and R.N. Eskander, *PARP Inhibitors in Epithelial Ovarian Cancer.* Recent Pat Anticancer Drug Discov, 2018. **13**(2): p. 145-158.

23. Ketabi, Z., et al., *Ovarian cancer linked to Lynch syndrome typically presents as early-onset, non-serous epithelial tumors.* Gynecol Oncol, 2011. **121**(3): p. 462-5.

24. Song, H., et al., *Contribution of Germline Mutations in the RAD51B, RAD51C, and RAD51D Genes to Ovarian Cancer in the Population.* J Clin Oncol, 2015. **33**(26): p. 2901-7.

25. Ramus, S.J., et al., *Germline Mutations in the BRIP1, BARD1, PALB2, and NBN Genes in Women With Ovarian Cancer.* J Natl Cancer Inst, 2015. **107**(11).

26. Norquist, B.M., et al., *Inherited Mutations in Women With Ovarian Carcinoma.* JAMA Oncol, 2016. **2**(4): p. 482-90.

27. Klotz, D.M. and P. Wimberger, *Cells of origin of ovarian cancer: ovarian surface epithelium or fallopian tube?* Arch Gynecol Obstet, 2017. **296**(6): p. 1055-1062.

28. Ahmed, N., et al., *Cancerous ovarian stem cells: obscure targets for therapy but relevant to chemoresistance.* J Cell Biochem, 2013. **114**(1): p. 21-34.

29. Kurman, R.J. and M. Shih Ie, *The origin and pathogenesis of epithelial ovarian cancer: a proposed unifying theory.* Am J Surg Pathol, 2010. **34**(3): p. 433-43.

30. Wentzensen, N., et al., *Ovarian Cancer Risk Factors by Histologic Subtype: An Analysis From the Ovarian Cancer Cohort Consortium.* J Clin Oncol, 2016. **34**(24): p. 2888-98.

31. Gong, T.T., et al., *Age at menarche and risk of ovarian cancer: a meta-analysis of epidemiological studies.* Int J Cancer, 2013. **132**(12): p. 2894-900.

32. Luan, N.N., et al., *Breastfeeding and ovarian cancer risk: a meta-analysis of epidemiologic studies.* Am J Clin Nutr, 2013. **98**(4): p. 1020-31.

33. Collaborative Group on Epidemiological Studies of Ovarian, C., et al., *Ovarian cancer and oral contraceptives: collaborative reanalysis of data from 45 epidemiological studies including 23,257 women with ovarian cancer and 87,303 controls.* Lancet, 2008. **371**(9609): p. 303-14.

34. Narod, S., *Can advanced-stage ovarian cancer be cured?* Nat Rev Clin Oncol, 2016. **13**(4): p. 255-61.

35. Jacobs, I.J., et al., *Ovarian cancer screening and mortality in the UK Collaborative Trial of Ovarian Cancer Screening (UKCTOCS): a randomised controlled trial.* Lancet, 2016. **387**(10022): p. 945-956.

36. Menon, U., et al., *Risk Algorithm Using Serial Biomarker Measurements Doubles the Number of Screen-Detected Cancers Compared With a Single-Threshold Rule in the United Kingdom Collaborative Trial of Ovarian Cancer Screening.* J Clin Oncol, 2015. **33**(18): p. 2062-71.

37. Walker, J.L., et al., *Society of Gynecologic Oncology recommendations for the prevention of ovarian cancer.* Cancer, 2015. **121**(13): p. 2108-20.

38. Wang, Y., et al., *Evaluation of liquid from the Papanicolaou test and other liquid biopsies for the detection of endometrial and ovarian cancers.* Sci Transl Med, 2018. **10**(433).

39. Ahmed, N. and K.L. Stenvers, *Getting to know ovarian cancer ascites: opportunities for targeted therapy-based translational research.* Front Oncol, 2013. **3**: p. 256.

40. Bast, R.C., Jr., B. Hennessy, and G.B. Mills, *The biology of ovarian cancer: new opportunities for translation.* Nat Rev Cancer, 2009. **9**(6): p. 415-28.

41. Vang, R., et al., *Molecular Alterations of TP53 are a Defining Feature of Ovarian High-Grade Serous Carcinoma: A Rereview of Cases Lacking TP53 Mutations in The Cancer Genome Atlas Ovarian Study.* Int J Gynecol Pathol, 2016. **35**(1): p. 48-55.

42. Kuhn, E., et al., *TP53 mutations in serous tubal intraepithelial carcinoma and concurrent pelvic high-grade serous carcinoma--evidence supporting the clonal relationship of the two lesions.* J Pathol, 2012. **226**(3): p. 421-6.

43. Ahmed, A.A., et al., *Driver mutations in TP53 are ubiquitous in high grade serous carcinoma of the ovary.* J Pathol, 2010. **221**(1): p. 49-56.

44. Zhang, Y., et al., *TP53 mutations in epithelial ovarian cancer.* Transl Cancer Res, 2016. **5**(6): p. 650-663.

45. Verhaak, R.G., et al., *Prognostically relevant gene signatures of high-grade serous ovarian carcinoma.* J Clin Invest, 2013. **123**(1): p. 517-25.

46. Konecny, G.E., et al., *Prognostic and therapeutic relevance of molecular subtypes in high-grade serous ovarian cancer.* J Natl Cancer Inst, 2014. **106**(10).

47. Fathalla, M.F., *Incessant ovulation--a factor in ovarian neoplasia?* Lancet, 1971. **2**(7716): p. 163.

48. Wang, C., et al., *Pooled Clustering of High-Grade Serous Ovarian Cancer Gene Expression Leads to Novel Consensus Subtypes Associated with Survival and Surgical Outcomes.* Clin Cancer Res, 2017. **23**(15): p. 4077-4085.

49. Murakami, R., et al., *Establishment of a Novel Histopathological Classification of High-Grade Serous Ovarian Carcinoma Correlated with Prognostically Distinct Gene Expression Subtypes.* Am J Pathol, 2016. **186**(5): p. 1103-13.

50. Lengyel, E., *Ovarian cancer development and metastasis.* Am J Pathol, 2010. **177**(3): p. 1053-64.

51. Fuller, A.F., Jr., et al., *Mullerian inhibiting substance reduction of colony growth of human gynecologic cancers in a stem cell assay.* Gynecol Oncol, 1985. **22**(2): p. 135-48.

52. Arnold, A.G., et al., *Assessment of individuals with BRCA1 and BRCA2 large rearrangements in high-risk breast and ovarian cancer families.* Breast Cancer Res Treat, 2014. **145**(3): p. 625-34.

53. Piek, J.M., et al., *Dysplastic changes in prophylactically removed Fallopian tubes of women predisposed to developing ovarian cancer.* J Pathol, 2001. **195**(4): p. 451-6.

54. R Vang, R.K., K Visvanathan, P Shaw, R Soslow, V Parkash, I Shih, *Ovarian Cancer Prevention, Detection, and Treatment: Diagnosis of Tubal Intraepithelial Lesions Definition and Algorithm* in *Johns Hopkins Medicine*.

55. Medeiros, F., et al., *The tubal fimbria is a preferred site for early adenocarcinoma in women with familial ovarian cancer syndrome.* Am J Surg Pathol, 2006. **30**(2): p. 230-6.

56. Kindelberger, D.W., et al., *Intraepithelial carcinoma of the fimbria and pelvic serous carcinoma: Evidence for a causal relationship.* Am J Surg Pathol, 2007. **31**(2): p. 161-9.

57. Kuhn, E., et al., *CCNE1 amplification and centrosome number abnormality in serous tubal intraepithelial carcinoma: further evidence supporting its role as a precursor of ovarian high-grade serous carcinoma.* Mod Pathol, 2016. **29**(10): p. 1254-61.

58. Kuhn, E., et al., *Shortened telomeres in serous tubal intraepithelial carcinoma: an early event in ovarian high-grade serous carcinogenesis.* Am J Surg Pathol, 2010. **34**(6): p. 829-36.

59. Hansel, D.E., et al., *Telomere length variation in biliary tract metaplasia, dysplasia, and carcinoma.* Mod Pathol, 2006. **19**(6): p. 772-9.

60. Kawai, T., et al., *Telomere length and telomerase expression in atypical adenomatous hyperplasia and small bronchioloalveolar carcinoma of the lung.* Am J Clin Pathol, 2007. **127**(2): p. 254-62.

61. Meeker, A.K. and P. Argani, *Telomere shortening occurs early during breast tumorigenesis: a cause of chromosome destabilization underlying malignant transformation?* J Mammary Gland Biol Neoplasia, 2004. **9**(3): p. 285-96.

62. Meeker, A.K., et al., *Telomere length abnormalities occur early in the initiation of epithelial carcinogenesis.* Clin Cancer Res, 2004. **10**(10): p. 3317-26.

63. Murdoch, W.J., *Carcinogenic potential of ovulatory genotoxicity.* Biol Reprod, 2005. **73**(4): p. 586-90.

64. Murdoch, W.J. and J.F. Martinchick, *Oxidative damage to DNA of ovarian surface epithelial cells affected by ovulation: carcinogenic implication and chemoprevention.* Exp Biol Med (Maywood), 2004. **229**(6): p. 546-52.

65. von Zglinicki, T., *Oxidative stress shortens telomeres.* Trends Biochem Sci, 2002. **27**(7): p. 339-44.

66. Bowtell, D.D., et al., *Rethinking ovarian cancer II: reducing mortality from high-grade serous ovarian cancer.* Nat Rev Cancer, 2015. **15**(11): p. 668-79.

67. Mitra, A.K., et al., *In vivo tumor growth of high-grade serous ovarian cancer cell lines.* Gynecol Oncol, 2015. **138**(2): p. 372-7.

68. Domcke, S., et al., *Evaluating cell lines as tumour models by comparison of genomic profiles.* Nat Commun, 2013. **4**: p. 2126.

69. McCloskey, C.W., et al., *A new spontaneously transformed syngeneic model of high-grade serous ovarian cancer with a tumor-initiating cell population.* Front Oncol, 2014. **4**: p. 53.

70. Kim, J., et al., *High-grade serous ovarian cancer arises from fallopian tube in a mouse model.* Proc Natl Acad Sci U S A, 2012. **109**(10): p. 3921-6.

71. Tanwar, P.S., et al., *Loss of LKB1 and PTEN tumor suppressor genes in the ovarian surface epithelium induces papillary serous ovarian cancer.* Carcinogenesis, 2014. **35**(3): p. 546-53.

72. Sherman-Baust, C.A., et al., *A genetically engineered ovarian cancer mouse model based on fallopian tube transformation mimics human high-grade serous carcinoma development.* J Pathol, 2014. **233**(3): p. 228-37.

73. Zhai, Y., et al., *High-grade serous carcinomas arise in the mouse oviduct via defects linked to the human disease.* J Pathol, 2017. **243**(1): p. 16-25.

74. Szabova, L., et al., *Perturbation of Rb, p53, and Brca1 or Brca2 cooperate in inducing metastatic serous epithelial ovarian cancer.* Cancer Res, 2012. **72**(16): p. 4141-53.

75. Yang, Q. and K.L. Guan, *Expanding mTOR signaling.* Cell Res, 2007. **17**(8): p. 666-81.

76. Zoncu, R., A. Efeyan, and D.M. Sabatini, *mTOR: from growth signal integration to cancer, diabetes and ageing.* Nat Rev Mol Cell Biol, 2011. **12**(1): p. 21-35.

77. Dowling, R.J., et al., *Dissecting the role of mTOR: lessons from mTOR inhibitors.* Biochim Biophys Acta, 2010. **1804**(3): p. 433-9.

78. Sanchez-Cespedes, M., et al., *Inactivation of LKB1/STK11 is a common event in adenocarcinomas of the lung.* Cancer Res, 2002. **62**(13): p. 3659-62.

79. Carling, D., M.J. Sanders, and A. Woods, *The regulation of AMP-activated protein kinase by upstream kinases.* Int J Obes (Lond), 2008. **32 Suppl 4**: p. S55-9.

80. Alessi, D.R., K. Sakamoto, and J.R. Bayascas, *LKB1-dependent signaling pathways.* Annu Rev Biochem, 2006. **75**: p. 137-63.

81. Shackelford, D.B. and R.J. Shaw, *The LKB1-AMPK pathway: metabolism and growth control in tumour suppression.* Nat Rev Cancer, 2009. **9**(8): p. 563-75.

82. Lizcano, J.M., et al., *LKB1 is a master kinase that activates 13 kinases of the AMPK subfamily, including MARK/PAR-1.* EMBO J, 2004. **23**(4): p. 833-43.

83. Hemminki, A., et al., *A serine/threonine kinase gene defective in Peutz-Jeghers syndrome.* Nature, 1998. **391**(6663): p. 184-7.

84. Riegert-Johnson, D., et al., *Peutz-Jeghers Syndrome*, in *Cancer Syndromes*, D.L. Riegert-Johnson, et al., Editors. 2009: Bethesda (MD).

85. Huang, J. and B.D. Manning, *The TSC1-TSC2 complex: a molecular switchboard controlling cell growth.* Biochem J, 2008. **412**(2): p. 179-90.

86. Rosset, C., C.B.O. Netto, and P. Ashton-Prolla, *TSC1 and TSC2 gene mutations and their implications for treatment in Tuberous Sclerosis Complex: a review.* Genet Mol Biol, 2017. **40**(1): p. 69-79.

87. Maehama, T. and J.E. Dixon, *The tumor suppressor, PTEN/MMAC1, dephosphorylates the lipid second messenger, phosphatidylinositol 3,4,5-trisphosphate.* J Biol Chem, 1998. **273**(22): p. 13375-8.

88. Zhang, S. and D. Yu, *PI(3)king apart PTEN's role in cancer.* Clin Cancer Res, 2010. **16**(17): p. 4325-30.

89. Shen, W.H., et al., *Essential role for nuclear PTEN in maintaining chromosomal integrity.* Cell, 2007. **128**(1): p. 157-70.

90. Chen, Z., et al., *Crucial role of p53-dependent cellular senescence in suppression of Pten-deficient tumorigenesis.* Nature, 2005. **436**(7051): p. 725-30.

91. Stambolic, V., et al., *Negative regulation of PKB/Akt-dependent cell survival by the tumor suppressor PTEN.* Cell, 1998. **95**(1): p. 29-39.

92. Zhang, J., et al., *PTEN maintains haematopoietic stem cells and acts in lineage choice and leukaemia prevention.* Nature, 2006. **441**(7092): p. 518-22.

93. Trimboli, A.J., et al., *Pten in stromal fibroblasts suppresses mammary epithelial tumours.* Nature, 2009. **461**(7267): p. 1084-91.

94. Vousden, K.H. and D.P. Lane, *p53 in health and disease.* Nat Rev Mol Cell Biol, 2007. **8**(4): p. 275-83.

95. Chaves-Moreira, D., P.J. Morin, and R. Drapkin, *Unraveling the Mysteries of PAX8 in Reproductive Tract Cancers.* Cancer Res, 2021. **81**(4): p. 806-810.

96. Macchia, P.E., et al., *PAX8 mutations associated with congenital hypothyroidism caused by thyroid dysgenesis.* Nat Genet, 1998. **19**(1): p. 83-6.

97. Friedrichsen, S., et al., *Expression of pituitary hormones in the Pax8-/- mouse model of congenital hypothyroidism.* Endocrinology, 2004. **145**(3): p. 1276-83.

98. Plachov, D., et al., *Pax8, a murine paired box gene expressed in the developing excretory system and thyroid gland.* Development, 1990. **110**(2): p. 643-51.

99. Wistuba, J., et al., *Male congenital hypothyroid Pax8-/- mice are infertile despite adequate treatment with thyroid hormone.* J Endocrinol, 2007. **192**(1): p. 99-109.

100. Magers, M.J., et al., *Comprehensive Immunophenotypic Characterization of Adult and Fetal Testes, the Excretory Duct System, and Testicular and Epididymal Appendages.* Appl Immunohistochem Mol Morphol, 2016. **24**(7): p. e50-68.

101. Chai, H.J., et al., *PAX8 is a potential marker for the diagnosis of primary epithelial ovarian cancer.* Oncol Lett, 2017. **14**(5): p. 5871-5875.

102. Di Palma, T., et al., *Pax8 has a critical role in epithelial cell survival and proliferation.* Cell Death Dis, 2013. **4**: p. e729.

103. Elias, K.M., et al., *Epigenetic remodeling regulates transcriptional changes between ovarian cancer and benign precursors.* JCI Insight, 2016. **1**(13).

104. Gao, J., et al., *Integrative analysis of complex cancer genomics and clinical profiles using the cBioPortal.* Sci Signal, 2013. **6**(269): p. pl1.

105. Haddadi, N., et al., *PTEN/PTENP1: 'Regulating the regulator of RTK-dependent PI3K/Akt signalling', new targets for cancer therapy.* Mol Cancer, 2018. **17**(1): p. 37.

106. Yang, L., S. Zhang, and G. Wang, *Keratin 17 in disease pathogenesis: from cancer to dermatoses.* J Pathol, 2019. **247**(2): p. 158-165.

107. Liu, J., et al., *Keratin 17 Promotes Lung Adenocarcinoma Progression by Enhancing Cell Proliferation and Invasion.* Med Sci Monit, 2018. **24**: p. 4782-4790.

108. Devor, E.J., et al., *p53 mutation status is a primary determinant of placenta-specific protein 1 expression in serous ovarian cancers.* Int J Oncol, 2017. **50**(5): p. 1721-1728.

109. Devor, E.J. and K.K. Leslie, *The oncoplacental gene placenta-specific protein 1 is highly expressed in endometrial tumors and cell lines.* Obstet Gynecol Int, 2013. **2013**: p. 807849.

110. Dong, X.Y., et al., *Plac1 is a tumor-specific antigen capable of eliciting spontaneous antibody responses in human cancer patients.* Int J Cancer, 2008. **122**(9): p. 2038-43.

111. Fant, M., et al., *PLAC1 (Placenta-specific 1): a novel, X-linked gene with roles in reproductive and cancer biology.* Prenat Diagn, 2010. **30**(6): p. 497-502.

112. Ghods, R., et al., *High placenta-specific 1/low prostate-specific antigen expression pattern in high-grade prostate adenocarcinoma.* Cancer Immunol Immunother, 2014. **63**(12): p. 1319-27.

113. Koslowski, M., et al., *A placenta-specific gene ectopically activated in many human cancers is essentially involved in malignant cell processes.* Cancer Res, 2007. **67**(19): p. 9528-34.

114. Li, Y., et al., *Cancer/testis antigen-Plac1 promotes invasion and metastasis of breast cancer through Furin/NICD/PTEN signaling pathway.* Mol Oncol, 2018. **12**(8): p. 1233-1248.

115. Satoh, K., et al., *Up-regulation of MSX2 enhances the malignant phenotype and is associated with twist 1 expression in human pancreatic cancer cells.* Am J Pathol, 2008. **172**(4): p. 926-39.

116. Kopczynska, E.K., *The potential therapeutic applications and prognostic significance of metastasis-associated in colon cancer-1 (MACC1) in cancers.* Contemp Oncol (Pozn), 2016. **20**(4): p. 273-80.

117. Sheng, X.J., et al., *MACC1 induces metastasis in ovarian carcinoma by upregulating hepatocyte growth factor receptor c-MET.* Oncol Lett, 2014. **8**(2): p. 891-897.

118. Zhang, R., et al., *Effects of metastasis-associated in colon cancer 1 inhibition by small hairpin RNA on ovarian carcinoma OVCAR-3 cells.* J Exp Clin Cancer Res, 2011. **30**: p. 83.

119. Zhang, R.T., F. Ren, and H.R. Shi, *[Expression of metastasis-associated in colon cancer-1 in different stages of epithelial ovarian cancer].* Zhongguo Yi Xue Ke Xue Yuan Xue Bao, 2014. **36**(1): p. 47-51.

120. Mundi, P.S., et al., *AKT in cancer: new molecular insights and advances in drug development.* Br J Clin Pharmacol, 2016. **82**(4): p. 943-56.

121. Bassi, C., et al., *Nuclear PTEN controls DNA repair and sensitivity to genotoxic stress.* Science, 2013. **341**(6144): p. 395-9.

122. Laury, A.R., et al., *A comprehensive analysis of PAX8 expression in human epithelial tumors.* Am J Surg Pathol, 2011. **35**(6): p. 816-26.

123. Colvin, E.K. and V.M. Howell, *Why the dual origins of high grade serous ovarian cancer matter.* Nat Commun, 2020. **11**(1): p. 1200.

124. Zhang, S., et al., *Both fallopian tube and ovarian surface epithelium are cells-of-origin for high-grade serous ovarian carcinoma.* Nat Commun, 2019. **10**(1): p. 5367.

125. Yuan, H., et al., *Plac1 Is a Key Regulator of the Inflammatory Response and Immune Tolerance In Mammary Tumorigenesis.* Sci Rep, 2018. **8**(1): p. 5717.

126. Grigoriadis, A., et al., *CT-X antigen expression in human breast cancer.* Proc Natl Acad Sci U S A, 2009. **106**(32): p. 13493-8.

127. Wang, X., M.C. Baddoo, and Q. Yin, *The placental specific gene, PLAC1, is induced by the Epstein-Barr virus and is expressed in human tumor cells.* Virol J, 2014. **11**: p. 107.

128. Liu, F., et al., *Identification of two new HLA-A*0201-restricted cytotoxic T lymphocyte epitopes from colorectal carcinoma-associated antigen PLAC1/CP1.* J Gastroenterol, 2014. **49**(3): p. 419-26.

129. Liu, F.F., et al., *The specific immune response to tumor antigen CP1 and its correlation with improved survival in colon cancer patients.* Gastroenterology, 2008. **134**(4): p. 998-1006.

130. Otsubo, T., et al., *MicroRNA-126 inhibits SOX2 expression and contributes to gastric carcinogenesis.* PLoS One, 2011. **6**(1): p. e16617.

131. Silva, W.A., Jr., et al., *PLAC1, a trophoblast-specific cell surface protein, is expressed in a range of human tumors and elicits spontaneous antibody responses.* Cancer Immun, 2007. **7**: p. 18.

132. Cheung, H.W., et al., *Systematic investigation of genetic vulnerabilities across cancer cell lines reveals lineage-specific dependencies in ovarian cancer.* Proc Natl Acad Sci U S A, 2011. **108**(30): p. 12372-7.

133. Tchabo, N.E., et al., *Expression and serum immunoreactivity of developmentally restricted differentiation antigens in epithelial ovarian cancer.* Cancer Immun, 2009. **9**: p. 6.

134. Chen, Y., D. Schlessinger, and R. Nagaraja, *T antigen transformation reveals Tp53/RB-dependent route to PLAC1 transcription activation in primary fibroblasts.* Oncogenesis, 2013. **2**: p. e67.

135. Suzuki, M., et al., *Over-expression of HOX-8, the human homologue of the mouse Hox-8 homeobox gene, in human tumors.* Biochem Biophys Res Commun, 1993. **194**(1): p. 187-93.

136. Russo, A., et al., *PTEN loss in the fallopian tube induces hyperplasia and ovarian tumor formation.* Oncogene, 2018. **37**(15): p. 1976-1990.

137. Planchon, S.M., K.A. Waite, and C. Eng, *The nuclear affairs of PTEN.* J Cell Sci, 2008. **121**(Pt 3): p. 249-53.

138. Mukherjee, A., et al., *Nuclear PTEN Localization Contributes to DNA Damage Response in Endometrial Adenocarcinoma and Could Have a Diagnostic Benefit for Therapeutic Management of the Disease.* Mol Cancer Ther, 2018. **17**(9): p. 1995-2003.

139. Povirk, L.F. and M.J. Austin, *Genotoxicity of bleomycin.* Mutat Res, 1991. **257**(2): p. 127-43.

140. Jamin, S.P., et al., *Requirement of Bmpr1a for Mullerian duct regression during male sexual development.* Nat Genet, 2002. **32**(3): p. 408-10.

141. Bardeesy, N., et al., *Loss of the Lkb1 tumour suppressor provokes intestinal polyposis but resistance to transformation.* Nature, 2002. **419**(6903): p. 162-7.

142. Hernandez, O., et al., *Generation of a conditional disruption of the Tsc2 gene.* Genesis, 2007. **45**(2): p. 101-6.

143. Lesche, R., et al., *Cre/loxP-mediated inactivation of the murine Pten tumor suppressor gene.* Genesis, 2002. **32**(2): p. 148-9.

144. Tanwar, P.S., et al., *Mammalian target of rapamycin is a therapeutic target for murine ovarian endometrioid adenocarcinomas with dysregulated Wnt/beta-catenin and PTEN.* PLoS One, 2011. **6**(6): p. e20715.

145. Tanaka, Y., et al., *Deletion of tuberous sclerosis 1 in somatic cells of the murine reproductive tract causes female infertility.* Endocrinology, 2012. **153**(1): p. 404-16.

146. Tanwar, P.S., et al., *Stromal deletion of the APC tumor suppressor in mice triggers development of endometrial cancer.* Cancer Res, 2011. **71**(5): p. 1584-96.

147. Gamwell, L.F., O. Collins, and B.C. Vanderhyden, *The mouse ovarian surface epithelium contains a population of LY6A (SCA-1) expressing progenitor cells that are regulated by ovulation-associated factors.* Biol Reprod, 2012. **87**(4): p. 80.

148. Pinheiro J, B.D., DebRoy S, Sarkar D, R Core Team, *_nlme: Linear and Nonlinear Mixed Effects Models_*. 2020: R package version 3.1-147, <URL: https://CRAN.R-project.org/package=nlme>.

149. Pinheiro, J.C. and D.M. Bates, *Mixed-effects models in S and S-PLUS*. Statistics and computing. 2000, New York: Springer. xvi, 528 p.

150. Beyene, J. and R. Moineddin, *Methods for confidence interval estimation of a ratio parameter with application to location quotients.* BMC Med Res Methodol, 2005. **5**: p. 32.

151. Di Palma, T., et al., *A role for PAX8 in the tumorigenic phenotype of ovarian cancer cells.* BMC Cancer, 2014. **14**: p. 292.

152. Rodgers, L.H., et al., *Loss of PAX8 in high-grade serous ovarian cancer reduces cell survival despite unique modes of action in the fallopian tube and ovarian surface epithelium.* Oncotarget, 2016. **7**(22): p. 32785-95.

153. Hardy, L.R., et al., *Proteomic analysis reveals a role for PAX8 in peritoneal colonization of high grade serous ovarian cancer that can be targeted with micelle encapsulated thiostrepton.* Oncogene, 2019. **38**(32): p. 6003-6016.

154. Ozcan, A., et al., *PAX 8 expression in non-neoplastic tissues, primary tumors, and metastatic tumors: a comprehensive immunohistochemical study.* Mod Pathol, 2011. **24**(6): p. 751-64.

155. Satoh, M., *Histogenesis and organogenesis of the gonad in human embryos.* J Anat, 1991. **177**: p. 85-107.

156. Marino, S., et al., *Induction of medulloblastomas in p53-null mutant mice by somatic inactivation of Rb in the external granular layer cells of the cerebellum.* Genes Dev, 2000. **14**(8): p. 994-1004.

157. Kim, J.H., D.T. MacLaughlin, and P.K. Donahoe, *Mullerian inhibiting substance/anti-Mullerian hormone: A novel treatment for gynecologic tumors.* Obstet Gynecol Sci, 2014. **57**(5): p. 343-57.

158. Wright, J.F., J. Wellman, and K.A. High, *Manufacturing and regulatory strategies for clinical AAV2-hRPE65.* Curr Gene Ther, 2010. **10**(5): p. 341-9.

159. Rosner, K., et al., *Engineering a waste management enzyme to overcome cancer resistance to apoptosis: adding DNase1 to the anti-cancer toolbox.* Cancer Gene Ther, 2011. **18**(5): p. 346-57.